Optimal Design of Magnetorheological Dampers Constrained in a Specific Volume Using Response Surface Method

Armin Hadadian

A Thesis

In

The Department Of Mechanical and Industrial Engineering

Presented in Partial Fulfillment of the Requirements

For the Degree of Master of Applied Science (Mechanical Engineering) at

Concordia University

Montreal, Quebec, Canada

2011

CONCORDIA UNIVERSITY

SCHOOL OF GRADUATE STUDIES

This is to certify that the Thesis prepared,

By: **Armin Hadadian**

Entitled: **"Optimal Design of Magnetorheological Dampers Constrained in a Specific Volume using Response Surface Method"**

and submitted in partial fulfillment of the requirements for the Degree of

Master of Applied Science (Mechanical Engineering)

complies with the regulations of this University and meets the accepted standards with respect to originality and quality.

Signed by the Final Examining Committee:

_____ Chair
Dr. M. Chen

_____ Examiner
Dr. I. Stiharu

_____ Examiner
Dr. L. Tirca   External
Building, Civil & Environmental Engineering

_____ Co-Supervisor
Dr. R. Sedaghati

_____ Co-Supervisor
Dr. E. Esmailzadeh

Approved by: _____
Dr. A.K.W. Ahmed, MASc Program Director
Department of Mechanical and Industrial Engineering

_____
Dean Robin Drew
Faculty of Engineering & Computer Science

Date: _____

Abstract

Optimal Design of Magnetorheological Dampers Constrained in a Specific
Volume Using Response Surface Method

Armin Hadadian

In recent years, semi-active magnetorheological (MR) and electrorheological (ER) fluid
technology based devices and systems have been developed and successfully utilized in
many applications as valves, shock absorbers, dampers and clutch/brake systems. These
promising devices have the adaptivity of the fully active systems to accommodate
varying external excitations while maintaining the reliability and fail-safe features of the
passive systems. Compared with ER based devices or systems, MR based devices have
recently received special attention due to their high performance with minimal power
requirements. Moreover MR fluids have significantly higher yield strength and are less
sensitive to contaminants and temperature compared with the ER fluids.

The geometric optimal design of MR valves/dampers is an important issue to improve the
damper performance, such as damping force, valve ratio and inductive time constant.
Considering this, the primary purpose of this study is to establish a general design
optimization methodology to optimally design single–coil annular MR valves constrained
in a specific volume in MR damper. To accomplish this, first the damping force of MR
damper has been modeled using Bingham plastic model. The magnetic circuit of MR

damper has been analyzed using finite element method in ANSYS environment to obtain magnetic field intensity which can be subsequently used to obtain the yield stress of the MR fluid in the active volume where the magnetic flux crosses. Then the developed finite element model of the MR valve is effectively used to construct an approximate response function relating the magnetic field intensity to the identified design parameters in the selected design space using response surface method and design of experiment methodology.

Using the derived approximate relation for the magnetic field intensity in the MR damper model, the design optimization problem has been formulated using gradient based nonlinear mathematical programming technique based on the Sequential Quadratic Programming (SQP) technique and also stochastic optimization technique based on the Genetic Algorithm (GA) to find optimal geometrical parameters of the MR valve in order to maximize the damping performance under given constrained volume.

Finally a PID controller has been designed to evaluate the close-loop performance of the optimally designed MR damper in a quarter-car suspension model.

Acknowledgement

I would like to take this opportunity to express my gratitude to my thesis supervisors, Dr. Ramin Sedaghati and Dr. Ebrahim Esmailzadeh, for their supports, help, encouragement, and guidance through my graduate studies at Concordia University.

Thanks are due to my fellow students and friends, Mr. Amin Changizi, Mr. Khodabakhsh Saeedi, Mr. Ali Fellah Jahromi, and Mr. Mostafa Mirzaee. I feel really fortune to have had such quality time with those nice peers.

I am extremely appreciative to my parents, Nasrin and Freidoun, for their continuous and endless love and support.

Finally, I would also like to thank my brother, Arash, who has provided me a brotherly encouragement to finish my education at Concordia University.

Table of Contents

List of Figures

List of Tables

Nomenclatures

Roman Symbols:

A   coil area

A the matrix of dynamic properties

A_k cross-sectional area of the kth magnetic link

A_p piston effective cross sectional areas

A_s piston shaft effective cross sectional areas

A_w the cross sectional area of the coil wire

A_c the cross sectional area of the coil

B   the matrix of actuator property

B magnetic flux density

B_x magnetic flux density components along the x axis

B_y magnetic flux density components along the y axis

Bi Bingham number

$B_{MR}(s)$ magnetic flux density of MR fluid along the pole length

c coefficient of the flow velocity profile

C matrix of sensor position

C_s	passive damping coefficient
C_t	tire damping coefficient
C_{eq}	equivalent damping coefficient
$C_i(x)$	constraint functions
C_0, C_1, C_2, and C_3	coefficients of the function of developed yield stress
d	MR valve orifice gap
d_h	MR valve housing thickness
$\bar{d}$	average diameter of the coil
D	matrix of constant force effect
D_0	displacement overshoot
F_{MR}	force due to the yield stress of the MR fluid
$F_{MR,r}$,	reference force due to the yield stress of the MR fluid
$f(x)$	objective function
f_i	penalty function value for a constrained problems
f_{max}	the largest recorded cost
G	the complex shear modulus
H	magnetic field intensity
H_{mr}	magnetic field intensity of MR fluid
H_x	magnetic field intensity components along the x axis
H_y	magnetic field intensity components along the y axis
I	the electric current applied to the valve

$\tilde{J}$	index sets of inequality constraints
K_p	proportional gain of PID controller
K_t	tire stiffness
K_s	car spring stiffness
J	current density
k	consistency index
l	the overall effective length of a magnetic link
L	MR valve height
$\mathcal{L}$	the Lagrangian function
L_A	active length
L_{in}	the inductance of the valve coil
L_P	length of the passive volume
L_W	the length of the coil wire
MAE	mean absolute error
M_{us}	unsprung mass
M_s	sprung mass
n	power-low index
N_c	the number of coil turns
Np	population size in genetic algorithms
p	the number of experiments
P_0	the initial pressure of the gas chamber

P_1	pressure in the upper chamber of MR damper
P_2	pressure in the lower chamber of MR damper
P_a	pressure in the gas chamber
p_k	search direction
q	the number of unknown model coefficients
Q	volumetric rate of flow
r	the resistivity of the coil wire
R	MR valve radius
R_n	design domain subset
R_w	the resistance of the coil wire
R_1	average radius of the annular duct
R^2	the coefficient of multiple determination
SSE	sum of squared errors defined
SST	sum of total squares
t	the pole length of MR valve
T	the inductive time constant of the valves
T_i	integral time of PID controller
T_d	derivative time of PID controller
T_r	reference inductive time constant of the damper
t_s	settling time of sprung mass
V	velocity of the sprung mass

V_0	initial volume of the gas chamber
v_0	the mean fluid velocity though the fluid annulus
v_p	the velocity of the piston
W	work done by the damper during one cycle
w	coil width
x	design point
X	represents the amplitude of displacement
X	the design matrix
y	accurate response
$\hat{y}$	approximate response
$\bar{y}$	average of real response

Greek Symbols:

α_d	weight factor for dynamic range
α_F	weight factor for the damping force
α_T	weight factor for inductive time constant
β	model coefficients
γ	the coefficient of thermal expansion
$\dot{\gamma}$	fluid shear strain rate
$\bar{\delta}$	non-dimensional plug thickness of MR fluid
ΔP	the pressure drop of MR fluid

ΔP_y	the yield stress of MR damper
ΔP_η	field independent pressure drop of MR fluid
ΔP_τ	field dependent pressure drop of MR fluid
ε	finite index sets of equality constrain
ε	error
η	the plastic viscosity of MR fluid with no applied magnetic field
λ	valve ratio
λ_d	dynamic range
$\lambda_{d,r,}$	reference dynamic range
λ_i	Lagrange multiplier
λ_r	reference valve ratio
μ	relative magnetic permeability
μ_0	magnetic permeability of free space
τ	fluid shear stress
τ_y	field dependent yield stress
φ	the magnetic flux of the valve coil
ω	angular frequency

Chapter 1 Introduction

1.1. Motivation and Objectives

Vehicle suspension is normally used to attenuate unwanted vibration due to various road conditions. A successful and effective suppression of the vibration is necessary for improvement of vehicle components' life, and the ride comfort, as well as steering stability.

One of the recent and promising technologies in design of vehicle dampers is implementing Magnetorological (MR) fluids. These smart fluids have the capability to continuously and rapidly change their rheological behavior (viscosity) under applied magnetic field. Due to this unique characteristics, MR based dampers can provide variable damping force semi-actively by varying the applied magnetic field (varying current) and thus have the capability to control vibration in a wide range of road conditions. Reports about commercial use of semi-active MR dampers have been increased in recent years. This is mainly due to the fact that semi-active MR dampers have demonstrated the fail-safe feature and reliability of conventional passive dampers and the adaptivity of fully active dampers while demanding minimal power requirements. Compared with their Electrorheological (ER) counterparts, MR dampers can generate higher damping force and they are less sensitive to external contaminants and

temperature. Also compared with other conventional semi-active dampers, MR dampers have less moving parts, thus they are subjected to less wear.

Most of the previous works on MR dampers have mainly focused on the quasi-static [1, 2] and dynamic modeling [3-6] of the MR dampers or development of control strategies based on various MR damper models [7-14]. However, few works have been done on optimal design of MR dampers to improve their performance [15-20]. Considering today's competitive markets, it is very important to establish a general design methodology to optimally design the geometry of the MR damper to further improve their damping performance while not increasing the cost. Considering this, the main objective of this research study is to establish a general and efficient design optimization methodology to improve the damping performance of MR dampers.

1.2. Overview and Literature Survey (State of the Art)

Various suspension methods have been developed and applied to the vibration control of vehicles. Basically, based on the amount of required external power for the system, vehicle suspension systems may be classified into three categories namely passive, active, and semi-active [17].

The passive suspension system, which usually includes fixed springs and shock absorbers, provides design simplicity, but performance limitations are inevitable in the relatively high frequency range. Since in the passive system the values of stiffness and damping are tuned for a specific design condition, thus a passive system cannot provide optimal vibration isolation for various road conditions.

2

In order to overcome these limitations, active suspension systems have been employed [17]. With an additional active force introduced as a part of the suspension unit, the system then can be actively controlled using appropriate control algorithms to attenuate external disturbances. Generally, an active suspension system provides high controllability in a wide frequency range, but on the other hand, it requires high power sources, complicated components such as sensors, servo valves, and a sophisticated control algorithm [17, 21].

The semi-active (also known as adaptive–passive) suspension system addresses these drawbacks by effectively integrating a tuning control scheme with tunable passive devices. In this suspension configuration, active force generators are replaced by modulated variable damping and stiffness compartments. Therefore, semi-active suspension can be utilized to generate desirable performance without requiring large power sources and expensive hardware [17]. The main feature of semi-active suspension systems is their ability to vary damping for a wide range of input motion. Comparing with typical passive suspension systems, semi-active shock absorbers provide softer damping when needed, and harder damping in demanded situations. Thus, faster operational speeds over similar terrain and better vibration isolation for sensitive payloads are the main benefits of this technology for ground vehicles [22].

Over the past decade, the usage of Magnetorheological (MR) and Electrorheological (ER) fluids in smart damping devices has been received much consideration because they allow controllable performance with no moving parts. In fact, they are controllable fluids that respond to an exposed magnetic or electric field with an impressive change in their rheological behavior. MR and ER fluids are similar in that they develop a controllable

yield stress in the existence of magnetic and electric fields, respectively. While MR fluids are actuated by applying a magnetic field perpendicular to the fluid flow direction, ER fluids are actuated by guiding an electric field perpendicular to the fluid flow direction [19]. ER and MR fluids have been successfully employed in controllable valves, clutches, brakes, suspensions, and engine mounts [1]. However, It has been proved that MR valves have comparable or superior range of operating conditions and less power requirements compared with the ER valves which makes MR technology more attractive for volume-constrained conditions [19].

In MR fluids, rheological properties can be rapidly (in an order of milliseconds) changed by applying a magnetic field to the fluid domain [10, 15, 23]. In the absence of the applied field, the fluid exhibits a Newtonian-like behavior, however when it is subjected to the magnetic field, the induced dipoles create a chain-like structure which restrict the flow of the fluid, thus increases the apparent viscosity of the fluid [15].

The important distinctive of MR fluids is their ability to reversibly change from free flowing, linear viscous liquids to semi-solids behavior with a controllable yield strength in milliseconds when exposed to magnetic field. This feature develops a very large change in the resisting force of dampers in which MR fluid is manipulated [24]. The process is fully variable and reversible.

Among other applications of MR fluid, MR dampers have been considered significantly in applications where rapid response time is critical [25]. Because of mechanical simplicity, high dynamic range, low power requirements, large force capacity and robustness, MR based dampers have been used in many industrial applications specially in vehicle dynamic suspension systems [8, 10, 17, 18, 21, 26], vibration reduction of

4

home appliance [12] as well as civil infrastructure damping systems against severe earthquake and wind loading [24]. Generally outstanding features like the fast response and the contactless nature of controlling system make MR fluid technology attractive for various control devices [27].

Gordaninejad and Kelso [22] also proposed MR fluid based dampers to enhance the cross-country mobility of combat vehicles, such as high mobility multi-purpose wheeled vehicles.

Essentially, to model MR valves and dampers, there are two approaches namely quasi-static modeling and dynamic modeling. Although the quasi-static models can describe the behavior of MR dampers rationally well, they are not sufficient to model the nonlinear force–velocity behavior of the MR damper especially in high frequency excitations [6, 16, 24]. Some dynamic models considering the hysteresis behavior of MR damper have been proposed to overcome this drawback [3-6]. However, these dynamic models are experiment based models where experimental results of a real damper are used to derive parameters.

While great amount of works have been dedicated to the modeling of MR based devices mainly based on the Bingham model of MR fluid [16-20, 24, 27-29], a few research has been reported in the literature using the nonlinear Bingham or Herschel–Bulkley model based on quasi-static modeling [2, 30].

In one of the most fundamental works in this field, Wereley and Pang [1], derived equations to explain the rheological behaviors of ER and MR dampers by means of non-dimensional groups. In their solutions, they assumed quasi-steady models and idealized Bingham plastic shear flow mechanism.

In a steady fully developed flow, ER and MR fluids almost behave like idealized Bingham plastic shear flows [1] and as a result the modeling and design of MR dampers has been conducted at early stages of design based on this assumptions [15, 17-20]. Thus, in practice, MR valves and dampers are designed using quasi static Bingham plastic model. Then, the dynamic models are developed by experimental results of the manufactured MR valve and damper.

Many research works have addressed control strategies for semi-active vehicle suspension systems featured by MR dampers. Turnip et al. [13] studied controlled MR dampers by skyhook control and proposed a sensitivity control and compared the response of the active system featured by these controllers with the same passive system. Their results show the great improvement in handling performance of vehicle. Nonetheless, for modeling MR damper they used a fitted polynomial on the experimental results. Although this approach of modeling can explain the hysteresis behavior of the damper reasonably well but the result is only valid for a specific damper and cannot be used in design.

Georgiou et al. [31] performed a study with emphasizing on finding of an optimum values of suspension damping and stiffness parameters to optimize ride comfort, suspension travel and road holding by introducing a multi objective function.

Tusset et al. [32] utilized linear feedback and fuzzy logic damper controllers for the semi-active control of the quarter-car suspension and proved the effectiveness of this method. The control problem is formulated and determined by assuming linear feedback damping force controller for a nonlinear suspension system. Frequency shaped LQ control [33], Proportional–integral–derivative(PID), fuzzy logic, and hybrid controllers [34] , neuro-

6

fuzzy control [35], adaptive fuzzy sliding mode control [7] and adaptive fuzzy-neural network control [9] have also been applied for semi-active vibration control of the car suspension systems.

Wang et al. [14] implemented H-infinity method to control vehicle active suspension with MR damper. After deriving mathematical equations to model a car-quarter featured by a nonlinear MR damper, they implemented a linear piecewise function to linearize the MR damper Model.

Dong et al. [36] studied and compared five semi-active control algorithms including skyhook control, the hybrid control, the LQG, the sliding mode control and the fuzzy logic control. They used quarter car model with a MR damper which was modeled by a polynomial formulated through the experimental data. They demonstrated that the performances of the resulting controlled system are highly dependent on the employed control algorithm. But each of controllers performs noticeably better than the passive system. According to their results, the sliding mode control algorithm is found to be the most appropriate for use with MR dampers in the vibration control of MR suspension system. In reality assuming linear control systems can cause some errors in industrial applications. Thus to study the control of the system, nonlinear methods or non-model based methods should be used. Thus PID controller which is easy to design and have acceptable precision has been employed [37].

As mentioned before, there have been a large number of research works presented on modeling and design of MR valves and dampers [15-19, 38]. In design problems, due to the complexity of the magnetic field problem in the MR valve, finite element method (FEM) is usually employed to model and design of MR valves and dampers [15-20, 39,

40]. Optimal design of MR dampers has been recently received a special attention to improve their performances. Although there are a large number of presented research articles on modeling of MR fluid dampers using quasi-static and dynamic models and developing appropriate control strategies for them, there are few studies which mainly focus on the design optimization of MR valves to improve the damping performance of the MR dampers. It is worth noting that as the main operating part of a MR damper is MR valve, the optimization of the MR damper is basically conducted through the optimization of the MR valve.

The major damping performances of a MR damper are damping force, valve ratio, dynamic range and inductive time constant of the MR valve. The valve ratio is the ratio of the viscous pressure drop to the field-dependent pressure drop of the MR valve. Also dynamic range is defined as the ratio of the peak force with a maximum current input to the minimum force with zero current input. So in practice, valve ratio and dynamic range convey the same concept and so optimal design of one of them will lead to the optimal design of the other one.

Optimization of MR valves which are constrained in a specific cylindrical volume defined by its radius and height is typically conducted to optimize the mentioned damping performances.

The optimization problem typically identifies the geometric dimensions of the damper that minimize an objective function. The objective function can be damping force and dynamic range [17], damping coefficient [19], a multi objective function of damping force, dynamic range and the inductive time constant of the shock absorber [18], valve

ratio [15, 16], control energy, time response and pressure drop [20] or power consumption [40].

In all the above mentioned references [15-20, 40], the damping force and dynamic range are derived based on quasi static Bingham plastic model of MR fluid. The finite element solution of the magnetic circuit is typically used to determine the objective functions for the optimization problems and then optimization procedure is conducted by a golden-section algorithm and a local quadratic fitting technique which is constructed in ANSYS parametric design language (APDL) [15-20, 40].

Rosenfield and Wereley [19], presented some design guidelines for volume-constrained MR valves with assumption of constant magnetic flux density throughout the magnetic circuit. Additionally, they compared the performance of volume-constrained MR valves against similarly constrained ER valves. Their results show that optimized MR valve provides a greater range of controllable damping than a geometrically similar ER valve. Their studies established that, MR valves have comparable or superior range of operating conditions, power requirements, and response characteristics comparing to the ER valve which makes MR technology more attractive for volume-constrained conditions.

In the most of above mentioned work, the magnetic circuit in the MR valves has been solved by finite element method using ANSYS. Also golden-section algorithm and a local quadratic fitting technique constructed in parametric design language of ANSYS have been typically utilized for optimization.

Based on the proposed methodology in Ref. [19], Nguyen et al. [16] presented an analytical methodology for the optimal design of a MR valve constrained in a specific volume to maximize the damping force of a MR damper. They analyzed magnetic circuit

using the magnetic Kirchoff's law and for that purpose they assumed that the magnetic field intensity along the effective length of each link of the magnetic circuit is constant. Utilizing finite element method to analyze the magnetic circuit is mainly due to the variation of the magnetic field along every links. Nevertheless their results proved to be more optimal than the results presented in Ref. [15] which uses only ANSYS software to solve both the FEM and optimization problems. This is mainly due to the fact that the proposed analytical method in Ref. [16] provides smoother objective function compared with noisy objective function formulated by finite element method. Therefore, employing the same linear optimization methods led to better answers.

As mentioned before, most of the previous studies mainly rely on first order optimization procedure in ANSYS. Due to the inherent nonlinearity and complexity of the problem, the first-order optimization may not generate a reliable optimal design or may easily trap in a local optimum. To the best of our knowledge, no work has been done on the formal design optimization of MR dampers and related design sensitivity analysis. Moreover closed loop performance evaluation of the optimal designed valve for vehicle suspension application is also extremely rare.

1.3. MR Valves Configurations

According to the fluid flow modes, all devices that use MR fluids can be classified as having either (a) a valve mode (flow mode); (b) a direct shear mode (clutch mode); (c) a squeeze film compression mode; or (d) a combination of these modes [41]. The schematic of the operational modes are shown in Figure 1-1 .
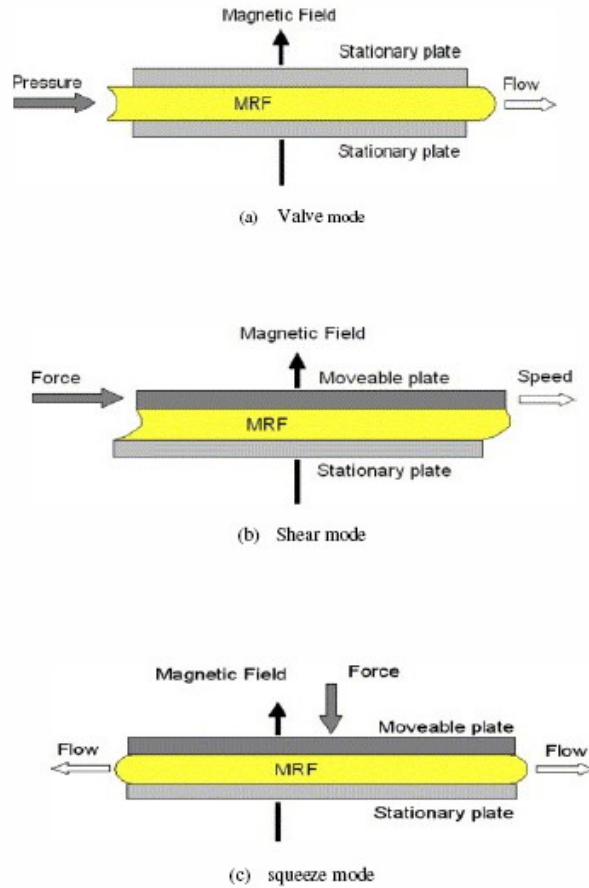
Figure 1-1: MRF operational modes [30]

Valve mode as an operational mode is employed in servo valves, dampers, shock absorbers and actuators [41]. In this mode the magnetic field is perpendicular to the flow of the MR Fluid while the two plates which are electrodes of the magnetic circuit are stationary plates. Since, the size of the gap is significantly smaller than the radius of the valve, the fluid flow is typically modeled by the parallel plate assumption [1]. The developed pressure drop in this mode (for example in a damper) is the summation of the viscous (pure rheological) component due to MR fluid viscosity and the yield stress dependant component due to yield stress of the MR fluid. More details will be discussed in next chapter.

Shear mode is typically used in clutches, brakes, chuckling and locking tools [30]. In this mode the electrode plates have relative motion and the magnetic field is perpendicular to the flow of the MR Fluid. In this operational mode, the total force has also two parts namely viscous and yield stress dependant component.

The third operational mode is called squeeze mode which is less well studied than the other modes. Since, it offers the possibility of very large forces; it is used for small amplitude vibration and impact dampers [30, 41].

As mentioned before, the magnetic field lines are typically perpendicular to the fluid flow direction in all modes. The areas where MR fluid is exposed to magnetic flux lines are referred to as "activation regions".

Among these, valve mode is the most widely utilized operational mode. In fact, MR valve is a fixed-size orifice valve with the ability of exposing magnetic field using an electromagnet. As the MR fluid passes through the orifice (duct), magnetic field is imposed on the MR fluid and as a result the rheological property of MR fluid in this region is changed. Without the external magnetic field, the MR fluid behaves like Newtonian fluid while the magnetic field causes a change in the viscosity of fluid in the orifice volume. As a result, the damping characteristic of MR damper is a function of the applied electrical current. This allows controlling the MR damper in real time.

As the magnetic field's strength increases, the resistance to fluid flow at the activation regions increases until the saturation current has been reached. Further increase in the electric current beyond the saturation current does not change the magnetic field intensity and hence the MR damper force for a given velocity.

Several configurations of MR valves have been proposed by many researchers such as single coil annular duct, two-coil annular duct and annular-radial duct [15]. However, among different configuration of MR valves, the single-coil annular MR valve structure, shown in Figure 1-2 (a), is typically adopted in many engineering applications such as MR relief valve, and specially in MR dampers [15, 20]. The MR fluid flow is shown with green line in this figure. The magnetic field developed in the gap area is also shown in detailed view in Figure 1-2 (b).

(a)   (b)
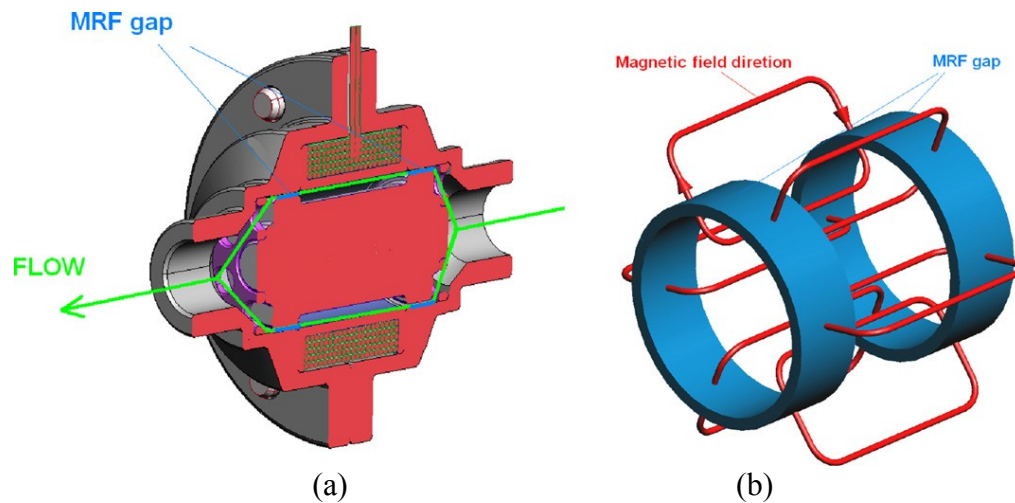
Figure 1-2: (a) Single-coil MR valve and fluid flow and (b) Magnetic field directions in the valve gap [27]

In this work, the design and optimization is basically conducted for this kind of valve. The schematic view of MR damper with embedded single-coil MR valve is shown in Figure 1-3.
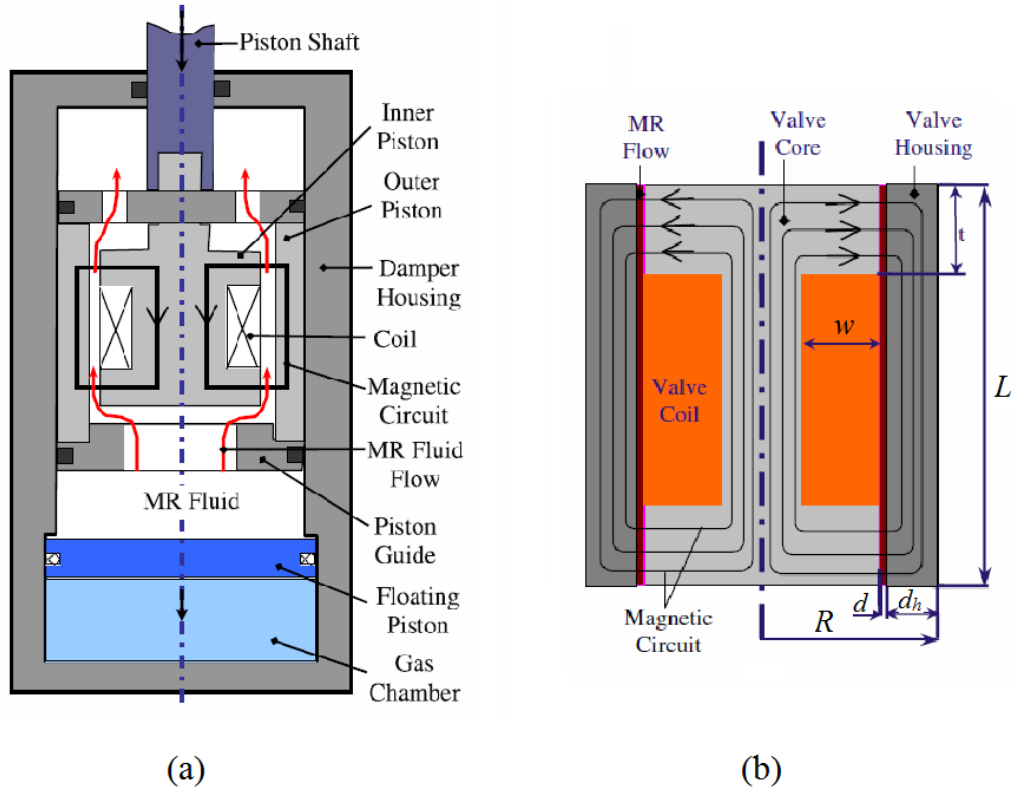
Figure 1-3: Schematic configuration of a single-coil MR valve and damper. (a) Single coil MR damper [18], (b) Single coil MR valve [15]

As shown in Figure 1-3, the MR valve structure includes the outer and inner pistons which divide the MR damper into upper and lower champers. Both champers are fully filled with MR fluids. As the inner piston moves, the MR fluid flows from one champers to the other one through the orifice of the valve. Significant geometrical parameters of the MR valve are the valve height L, the valve radius R, the coil width w, the valve housing thickness d_h, the valve orifice gap d and the pole length t, which are presented in Figure 1-3 (b).

1.4. Thesis Organization

The present thesis contains six chapters. In the first chapter, an introduction describing the general objectives, a literature survey, and general information about MR valves are presented.

The second chapter is devoted to mathematical modeling of MR valve and damper where the MR damper has been formulated and important operational parameters are explained.

In the third chapter, the magnetic field problem in MR valve is defined and solved by Finite Element Method (FEM) in ANSYS. Then Response Surface Methodology (RSM) is briefly explained. RSM is then combined with design of experiments to derive analytical functions of magnetic field intensity and magnetic flux density.

Chapter four is dedicated to optimization procedure. First a brief introduction of employed optimization methods in this study is presented. Then different constrained optimization problems of MR valve is defined and solved by both SQP and GA approaches. A sensitivity analysis has also been conducted for a selected optimal design.

In chapter five, performance of a sample optimal design configuration obtained in Chapter 4 is studied as a case study. For this purpose a PID controller is designed and displacement and velocity response of the optimal shock absorbers are plotted and analyzed.

Finally, chapter six will present a summary of significant conclusions of current research. Some recommendations have also been suggested to extend the research work in this area in future.

Chapter 2 Mathematical Modeling of MR Dampers

2.1. Introduction

Having a good knowledge of functional requirements, design parameters and design objectives are prerequisite of any successful design of a mechanical system. Saturation phenomenon in the magnetic circuit and yield stress of the MR fluid, limit the performance of the MR valve [29]. In the first part of this chapter a brief review on characteristics of MR fluid is presented. The mathematical models, governing equations and the performance indexes that can be considered in optimal design of MR dampers are then presented and discussed.

2.2. MR fluid characteristics

Discovery of MR fluids and developing the idea of using them in controllable devices can be credited to Jacob Rabinow at the US National Bureau of Standards in the late 1940s [24, 41].

These fluids are suspensions of micron-sized (5μm), magnetizable particles in an appropriate carrier liquid which in the absence of an applied magnetic field, exhibit Newtonian-like behavior. In the presence of the field, the induced dipoles force particles aligned with the external field that causes particles forming chain-like structures which restrict the flow of the fluid as schematically shown in Figure 2.1. This will cause a

16

sudden and significant change in the rheological behavior of MR fluid which is mainly manifested as a increase in the dynamic yield stress or the apparent viscosity of the fluid [15, 40]. This capability of MR fluids to develop a controllable yield stress which is drastically related to the applied magnetic field provides a unique feature to interface mechanical systems with electrical devices in order to control vibration. The change in the yield stress due to the applied magnetic field is very fast and typically is in the order of milliseconds. It should be noted that compared with their Electro-rheological fluid counterparts, MR fluids can exhibit an order of magnitude higher yield stress (ranging between 50-100 KPa) and a wider operational temperature range (typically between -40 ^{o}C to 150 ^{o}C). Moreover MR fluids are much less sensitive to external contaminants.
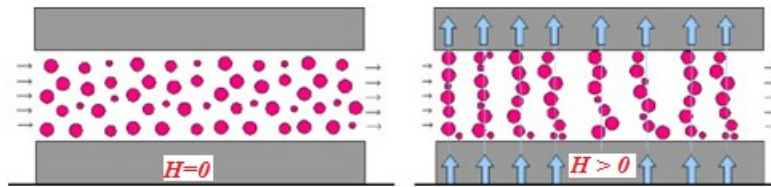
Figure 2-1: Schematic of "MR"-effect

The behavior of controllable fluids under applied magnetic field is mainly modeled by quasi-static Bingham plastic model. This model which is shown by straight red lines in Figure 2-2 is mathematically described as [15, 23] $\tau = \tau_y(H) + \eta;$ $\tau \geq \tau_y$

$$\tau = \tau_y(H) + \eta\,\dot{\gamma} \qquad\qquad \tau \geq \tau_y \qquad\qquad\qquad (2.1)$$

$$\tau = 0 \qquad\qquad\qquad \tau < \tau_y \qquad\qquad\qquad\qquad (2.2)$$

where τ is the fluid stress, τ_y is the field dependent yield stress, H represents the magnetic field intensity, $\dot{\gamma}$ is the fluid shear strain rate, and η is the plastic viscosity which is the same as the viscosity of the fluid in the absence of the magnetic field. It is noted that the Eq. (2.1) describes the behavior of MR fluid under the presence of magnetic field while

Eq. (2.2) governs the viscoelastic behavior of the material in which G represents the complex shear modulus [23].
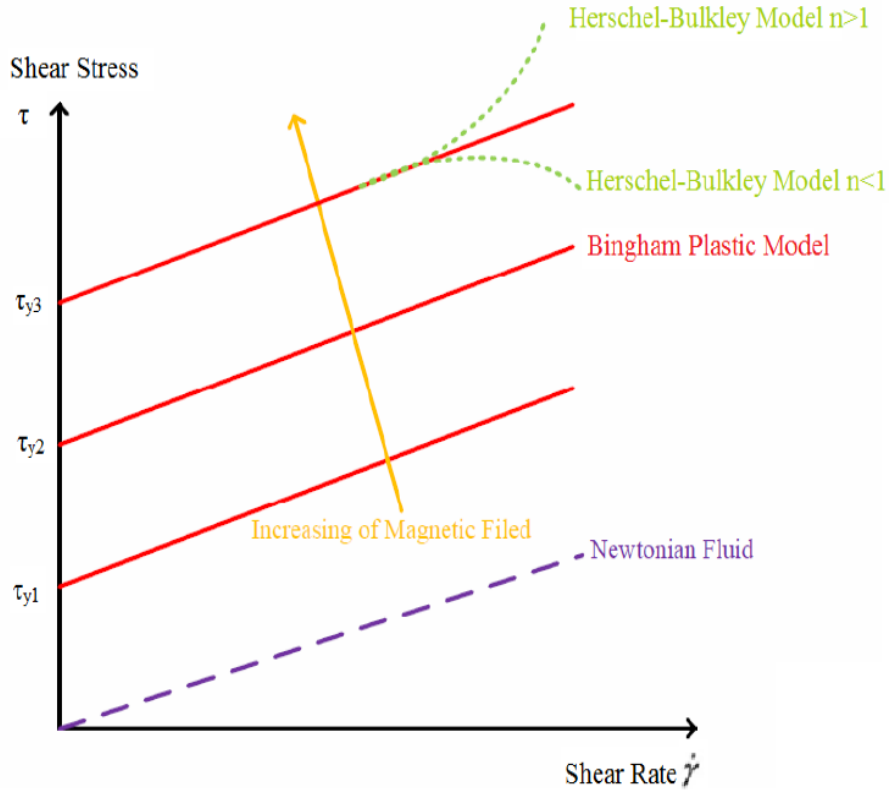
Figure 2-2: Simple models of MR fluids

As shown in Figure 2-2 and also realized from Eq. (2.1) the dynamic yield strength of the MR fluid has strong dependency to the applied magnetic field (stronger magnetic field results in higher value of yield stress), however the viscosity of the fluid does not change according to Bingham plastic model. The variation of viscosity of MR fluid in post-yield has been described by Herschel-Bulkley model [4, 30]. This model is depicted in

Figure 2-2 by green curves. In this model the shear stress in MR fluid is expressed by [23, 42, 43]

$$\tau = \tau_y(H) + \eta\,\dot{\gamma}^n \qquad\qquad \tau \geq \tau_y \tag{2.3}$$

$$\tau = 0 \qquad\qquad\qquad \tau < \tau_y$$

in which k and n are regarded as consistency index and power-low index, respectively. The post yield region can be described either as shear thickening ($n<1$) or shear thinning ($n>1$) shown in Figure 2-2. It can be realized that the Bingham model is a linear form (when $n=1$) of Herschel-Bulkley model [2]. Although Herschel-Bulkley results in more accurate model of rheological behavior when adequate experimental data are available, due to simplicity of Bingham plasticity model, it is most often used for design of MR dampers [4].

2.3. Mathematical Modeling of MR valves

In this section, the quasi-static model of MR valves is presented. The equations are derived based on the assumption that the MR fluid exhibits Bingham plastic behavior and the flow is fully developed in the ducts [15, 23]. The effects of geometry of MR valve on the damper performance, controllable force, and dynamic range are also discussed. Schematic representation of single-coil valve with annular duct is again shown in Figure 2-3 for the sake of clarity.
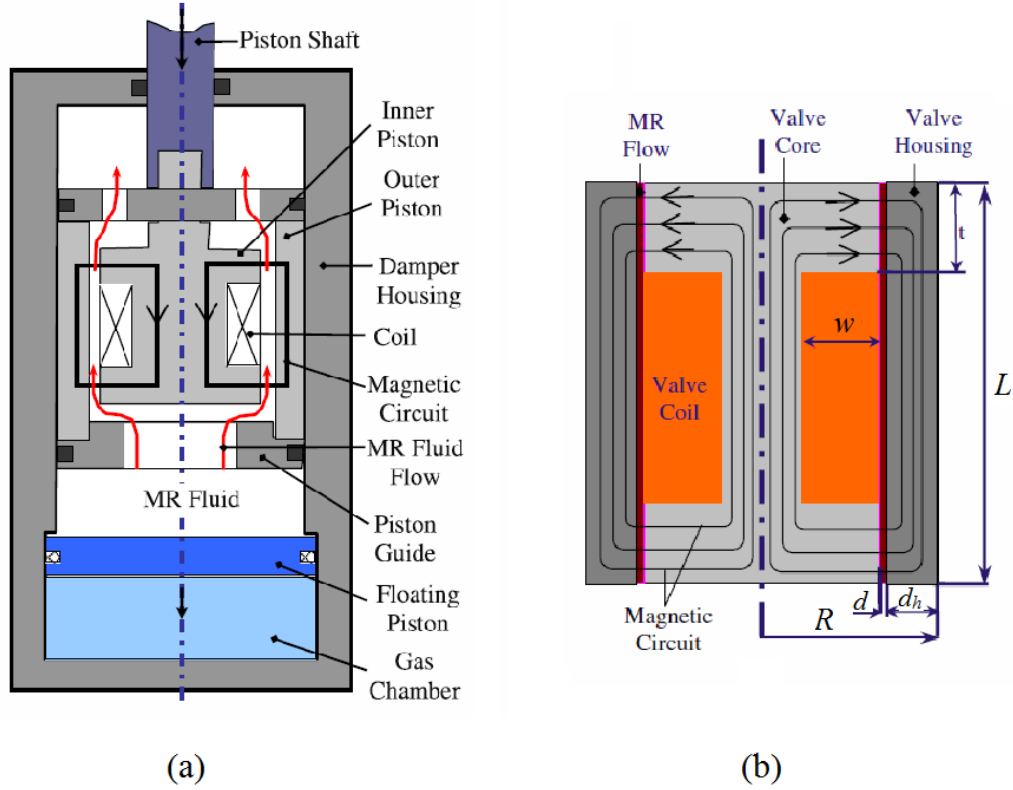
Figure 2-3: Schematic configuration of a single-coil MR valve and damper. (a) Single
coil MR damper [18], (b) single coil MR valve [15]

When the coil is electrified, a magnetic circuit appears as shown in the figure. At the two
end flanges, flux lines are perpendicular to the flow direction which causes a field-
dependent resistance on the flow. The pressure drop developed in such kind of MR valve
is given by [15, 16, 20]

$$\Delta P = \Delta P_\eta + \Delta P_\tau = \frac{6\eta L}{\pi d^3 R_1} Q + 2c \frac{t}{d} \tau_y \tag{2.4}$$

According to Eq. (2.4), the pressure drop can be divided into a filed independent viscous
component ΔP_η and an applied filed dependent induced yield stress component ΔP_τ . In
the above equation, Q is volumetric rate of flow, η is the viscosity with no applied
magnetic field and τ is the yield stress developed as result of applied filed. L, d and w are

also length, fluid gap and the pole length of the MR valve, respectively as shown in Figure 2-3. R_1 is the average radius of the annular duct given by $R_1 = R - d_h - 0.5d$.

The parameter c is a coefficient which depends on the flow velocity profile, and it has a value varying from 2.07 to 3.07. The coefficient c can be approximately estimated as follows [16, 17]

$$c = 2.07 + \frac{12Q\eta}{12Q\eta + 0.8\pi R_1 d^2 \tau_y} \tag{2.5}$$

As it can be realized, the second term in Eq. (2.4) can be continuously controlled by the intensity of the magnetic field through the MR valve ducts. This is the dominant term of the damping force, which is expected to have a significant influence on MR damper design [17].

The developed yield stress τ_y in the MR fluid due to the applied magnetic field has been typically characterized for different MR fluids. In this research study, the commercial MR fluid (MRF132-LD) from Lord Corporation [30] has been used.

The experimentally generated yield stress (τ_y) in this kind of MR fluid as a function of the applied magnetic field intensity (H_{MR}) is analytically expressed as [17, 18]:

$$\tau_y = C_0 + C_1 H_{MR} + C_2 H_{MR}^2 + C_3 H_{MR}^3 \tag{2.6}$$

in which the unit of the yield stress is kPa, and the unit of magnetic field intensity is kAm^{-1}. The coefficients C_0, C_1, C_2, and C_3 are respectively identified as 0.3, 0.42, −0.001 16, and 1.0513×10^{-6} [17, 18]. It should be noted that the least square curve fitting method has been employed on experimental data to obtain the approximate polynomial function. The variation of yield stress versus the magnetic field intensity according to Eq. (2.6) is also plotted in Figure 2-4.
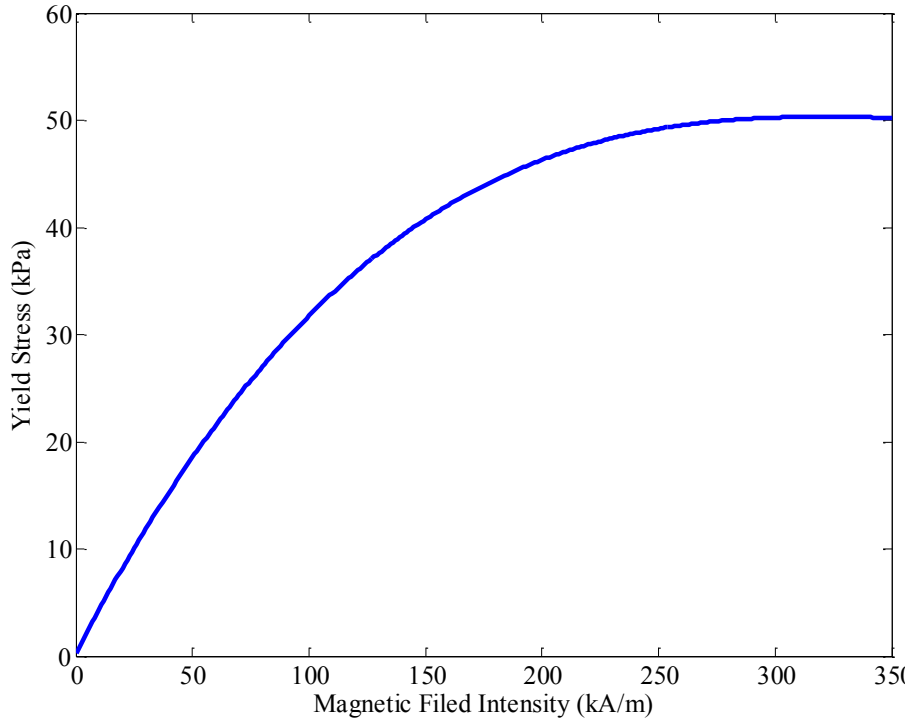
Figure 2-4: Yield stress of the MR fluid as a function of magnetic field intensity

It is noted that in order to calculate the pressure drop of the MR valves, first its magnetic circuit should be analyzed to calculate the magnetic field intensity in the activation region. Then, from the magnetic circuit solution, the yield stress of MR fluid in the active volume (the volume of the MR fluid where the magnetic flux crosses) can be determined by Eq. (2.6) , and consequently the pressure drop can be obtained using Eq. (2.4).

2.4. Performance Indexes

In this section, operational and performance functions of MR damper/valve which can be considered as objective functions in optimization problem are systematically introduced and formulated.

2.4.1. Damping Force

The pressure drop and damping force of MR dampers are the most important operating parameters. Generally in design optimization of MR valve one of the main objectives is to identify the optimal geometry of valve in order to maximize the damping force.

The damping force of a MR damper is governed by the damper's geometry, input electrical current to the electromagnet, the characteristics of MR fluids and the motion of the damper. By assuming a quasi-static behavior of the shock absorber and neglecting the frictional force, the damping force of the MR damper can be obtained as

$$F_d = P_2 A_p - P_1(A_p - A_s) \tag{2.7}$$

Where A_p and A_s are, respectively, piston and piston shaft effective cross sectional areas. P_1 and P_2 are the pressure in the upper and lower chamber of MR damper, respectively. The pressure in the gas chamber, P_a is approximated equal to the pressure in the lower chamber, P_2. Thus, we may write

$$\begin{aligned} P_1 &= P_a - \Delta P \\ P_2 &= P_a \end{aligned} \tag{2.8}$$

in which the ΔP is the pressure drop of the MR fluid flows through passing the orifice gap of the valve. The pressure drop ΔP can be calculated by Eq. (2.4). The pressure in the gas chamber can be obtained by [18]:

$$P_a = P_0 \left(\frac{V_0}{V_0 + A_s x_p} \right)^\gamma \tag{2.9}$$

in which P_0 and V_0 are the initial pressure and volume of the gas chamber, respectively. The parameter γ represents the coefficient of thermal expansion which varies between 1.4 and 1.7. Now considering Eqs. (2.7) and (2.8), the damping force can be described as:

$$F_d = P_a A_s + \Delta P(A_p - A_s) \tag{2.10}$$

Now by substituting Eq. (2.4) in Eq. (2.10) and considering that and $Q = (A_p - A_s)\dot{:}$

separating the viscous and filed dependent parts, one may write

$$F_d = P_a A_s + C_{vis}\dot{x}_p + F_{MR}sgn(\dot{x}_p) \tag{2.11}$$

where

$$C_{vis} = \frac{6\eta L}{\pi\left(R - d_h - d/2\right)d^3}\left(A_p - A_s\right)^2 \tag{2.12}$$

and

$$F_{MR} = \left(A_p - A_s\right)\frac{2ct}{d}\tau_y \tag{2.13}$$

The first term in Eq. (2.11) represents the elastic force due to the gas compliance; the second term is the damping force due to MR fluid viscosity and the third term represents the force due to the yield stress of the MR fluid [18]. As it can be realized, the yield dependant term in Eq. (2.13) can be easily controlled by the applied magnetic field and as mentioned before, it is expected to have a large effect on the damping force [17].

2.4.2. Dynamic Range

The dynamic range of the damper is defined as the ratio of the peak force under maximum applied current to that under zero current input. Thus, the equation of dynamic range can be described as [17]:

$$\lambda_d = \frac{C_{vis}\dot{x}_p + F_{MR}}{C_{vis}\dot{x}_p} \tag{2.14}$$

Since the force term due to gas chamber ($P_a A_s$) is a constant term in both of numerator and denominator of Eq. (2.14), so it can be eliminated in optimization procedure and as a result, it has not been considered in Eq. (2.14).

It should be noted that the dynamic range is an important parameter in evaluating the overall performance of the MR damper. To provide a wide control range of the MR damper, a large value of the dynamic range is desired [17].

2.4.3. Valve Ratio

The valve ratio is defined as the ratio of the viscous pressure drop to the field-dependent pressure drop of the MR valve. This ratio has significant effect on the characteristics of the MR valve. In design of MR valve, it is desirable to have a small valve ratio as it indicates that the regulated pressure of the valve changes slightly with that of the fluid flow rate. For a single-coil annular MR valve and considering Eq. (2.4), the valve ratio is derived as [15]

$$\lambda = \frac{\Delta P_\eta}{\Delta P_\tau} = \frac{3\eta LQ}{\pi d^2 R_1 ct\tau_y} \tag{2.15}$$

As it can be realized, by minimizing the valve ratio, the field-dependent pressure drop of MR valve improves significantly [15]. It is clear that valve ratio and dynamic range convey the same feature, and as a result only one of them is considered in optimization problem.

2.4.4. Damping Coefficient

An equivalent viscous damping coefficient can be defined as [44]:

$$C_{eq} = \frac{W}{\pi X^2 \omega} \tag{2.16}$$

where C_{eq} is the equivalent damping coefficient, W is the work done by the damper during one cycle, X represents the amplitude of displacement, and ω is the frequency in

radians per second. The equivalent damping coefficient is utilized in calculation of the energy dissipation by using MR damper in the system.

The same theory used for deriving Eq. (2.16); which is based on the energy dissipation of the system in one cycle, is employed to derive the equation of equivalent damping coefficient of the MR damper. The yield stress of the MR fluid modeled by Bingham plastic model described as Eq. (2.1) allows to define the non-dimensional Bingham number, Bi, introduced as [1]:

$$Bi = \frac{\tau_y}{\mu \frac{v_0}{d}} \tag{2.17}$$

where

$$v_0 = \frac{A_p}{A_d} v_p \tag{2.18}$$

Here A_p is the area of the piston face (i.e., πR^2), A_d is the cross-sectional area of the fluid annulus, v_0 is the mean fluid velocity though the fluid annulus, and v_p is the velocity of the piston. A_p and A_d are typically found once when the geometries of the valve are defined.

The Bingham number in Eq. (2.17) is used to determine non-dimensional plug thickness. The non-dimensional plug thickness expresses the ratio of the gap width in which the MR fluid behaves as a solid due to MR effect. Wereley and Pang [1] showed that the non-dimensional plug thickness, $\bar{\delta}$, is solved by the following cubic equation:

$$\frac{1}{2}\bar{\delta}^3 - (\frac{3}{2} + \frac{A_p}{A_d}\frac{6}{Bi})\bar{\delta} + 1 = 0 \qquad 0 \le \bar{\delta} \le 1 \tag{2.19}$$

To derive the equivalent viscous damping coefficient of the MR valve, the duct in the valve; which the MR fluid passes, is divided to three regions as shown in Figure 2-5. These regions are active volume at either end of the valve described as regions 1 and 3, respectively, and the central passive volume identified as region 2 in Figure 2-5.
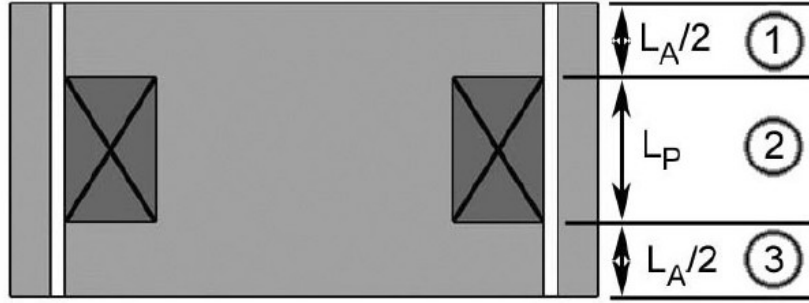
Figure 2-5: Active and passive volume regions in MR valve [19]

The length of region 1 and 3 are each half the active length L_A and the length of the passive region is assumed to be L_P. With assuming to have constant annular cross section, the volumetric flow rate through these defined regions can be calculated as [19]:

$$Q_1 = \frac{A_d d^2 \Delta P_1}{12\mu(\frac{1}{2}L_A)}(1-\bar{\delta})^2(1+\frac{1}{2}\bar{\delta})$$
(2.20)

$$Q_2 = \frac{A_d d^2 \Delta P_2}{12\mu L_p}$$
(2.21)

$$Q_3 = \frac{A_d d^2 \Delta P_3}{12\mu(\frac{1}{2}L_A)}(1-\bar{\delta})^2(1+\frac{1}{2}\bar{\delta})$$
(2.22)

In all above equations ΔP is the pressure drop along the length of each volume. It is noted that A_d is for the approximation of the rectangular duct. Continuity dictates the same volume flux trough all the defined volumes. Thus,

$$Q_1 = Q_2 = Q_3 = A_p v_p$$
(2.23)

27

By substituting Eq. (2.23) into Eqs. (2.20)-(2.22), one may calculate the pressure drops in the volumes as:

$$\Delta P_1 = \frac{12\mu(\frac{1}{2}L_A)}{2A_d\, d^2} A_p v_p \frac{1}{(1-\bar{\delta})^2(1+\frac{1}{2}\bar{\delta})} \tag{2.24}$$

$$\Delta P_2 = \frac{12\mu L_p}{A_d\, d^2} A_p v_p \tag{2.25}$$

$$\Delta P_3 = \frac{12\mu(\frac{1}{2}L_A)}{2A_d\, d^2} A_p v_p \frac{1}{(1-\bar{\delta})^2(1+\frac{1}{2}\bar{\delta})} \tag{2.26}$$

The total pressure drop for the valve is the summation of the individual pressure drops. Also the damping force over the piston area is equal to the total pressure drop. Thus

$$\Delta P = \sum_{i=1}^{3} \Delta P_i = \frac{F}{A_p} \tag{2.27}$$

Considering that the damping force is the multiplication of equivalent damping coefficient with the velocity of the piston as $F=C_{eq}v_p$, equivalent damping coefficient of an active MR damper can be derived as [19]:

$$C_{eq} = \frac{12\mu L A_p^2}{A_d\, d^2} \left\{ 1 + \frac{L_A}{L}\left[\frac{1}{\left(1-\bar{\delta}\right)^2\left(1+0.5\bar{\delta}\right)} - 1 \right] \right\} \tag{2.28}$$

In Eq. (2.28), the term $\dfrac{12\mu L A_p^2}{A_d\, d^2}$ beside the brackets is the damping C for off-mode configuration. Dividing Eq. (2.28), by this term one may write

$$\frac{C_{eq}}{C} = 1 + \frac{L_A}{L}\left[\frac{1}{\left(1-\bar{\delta}\right)^2\left(1+0.5\bar{\delta}\right)} - 1 \right] \tag{2.29}$$

Rosenfield and Wereley [19], introduced the damping coefficient (C_{eq} /C) as objective function. The damping coefficient is defined as equivalent damping of an active mode MR valve compared to off-mode of MR damper (zero current).

2.4.5. Inductive Time Constant of the Valves

For real-time control applications, fast time response of the system is desired. Therefore, in MR valve design, the inductive time constant of the valve is an important factor to implement MR damper in practical application. The inductive time constant of the valves, can be stated as

$$T = \frac{L_{in}}{R_w} \tag{2.29}$$

where L_{in} is the inductance of the valve coil given by $L_{in} = \frac{N_c \varphi}{I}$ and R_w is the resistance of the coil wire which can be described as [16] :

$$R_w = L_w r_w = N_c \pi \bar{d} \frac{r}{A_w} \tag{2.30}$$

in which L_w is the length of the coil wire and I is the electric current applied to the valve, A_w is the cross sectional area of the coil wire, A_c is the cross sectional area of the coil; and $N_c = A_c/A_w$ is the number of coil turns [20]. r also represents the resistivity of the coil wire which is equal to 0.01726×10^{-6} Ωm for copper wire. The term $\bar{d} = R - d_h - d - \frac{w}{2}$ is the average diameter of the coil and φ represents the magnetic flux of the valve coil and is given by

$$\varphi = 2\pi R_1 B_{MR} \tag{2.31}$$

where $R_1 = R - d_h - \frac{d}{2}$ and

$$B_{MR} = \frac{1}{t}\int_0^t B_{MR}(s)\,ds \qquad\qquad (2.32)$$

in which B_{MR} (s) is the magnetic flux density of MR fluid along the pole length at active area in each nodal point. In current work, we rewrite and simplify the equation of inductive time constant of the MR valve which has been derived as follows

$$T = \frac{2 r_1 A_w \int_0^t B_{MR}(s)\,ds}{R_w \bar{d}\ I\,t} \qquad\qquad (2.33)$$

It should be noted the magnetic flux density is not constant along the pole length. Thus in order to calculate the time constant the average magnetic flux density (B) passing across the MR ducts is used as given in Eq. (2.32) in which the flux density is integrated along the defined path and then dividing by the path length.

Higher pressure drop and the smaller time constant require the higher applied current to the coil. However, the maximum electrical current is limited by the coil wire to resist the current. In case that the required pressure drop and time constant cannot be satisfied, it is necessary to increase the constrained volume of the valve. Koo et al. [25] provided a comprehensive review on the response time of magnetorheological (MR) dampers. They evaluated various electrical currents, piston velocities and system compliance and time response of driving electronics and their effect on the response time of MR dampers.

Chapter 3 Finite Element and Response Surface Modeling

3.1. Introduction

As discussed in chapter 2, in order to evaluate the MR damping force, valve ratio and inductive time constant of the MR valve, it is necessary to calculate magnetic field intensity across the duct as developed yield stress directly depends on the applied magnetic filed in the activation region. Due to the geometrical complexity of the valve, it is very difficult to analyze the magnetic circuit in the MR valve analytically [17, 18, 20]. Thus in general numerical technique mainly based on the finite element method is employed. Here we have developed a parametric design language (APDL) code to parametrically construct the finite element model of the MR valve in the ANSYS environment.

Design of experiments (DOE) techniques [45] are utilized to build up design variables sets which are the geometrical input data of ANSYS file. After finding the output results (average field intensity and average flux density) for each set of design variables, response surface method (RSM) is used to fit polynomial functions to the output results. The derived RSM functions will be tested to evaluate their accuracy to effectively predict the magnetic field intensity and magnetic flux density in the entire design space. These

analytical functions are subsequently used to calculate the resultant yield stress from the available fitted polynomial yield stress–flux density curve of the MR fluid.

3.2. Magnetic Field Analysis

To analyze the magnetic circuits the Kirchoff's law can be employed as follows:

$$\sum H_k l_k = N_c I \tag{3.1}$$

where H_k is the magnetic field intensity in the kth link of the circuit and l_k is the overall effective length of that link. N_c is the number of turns of the valve coil and I is the applied current in the coil wire. The magnetic flux conservation rule of the circuit can be sated as

$$\varphi = B_k A_k \tag{3.2}$$

where φ is the magnetic flux of the circuit, and A_k and B_k are the cross-sectional area and magnetic flux density of the kth link, respectively. At low magnetic field, the magnetic flux density, B_k, increases in proportion to the magnetic filed intensity H_k as follows:

$$B_k = \mu_0 \mu_k H_k \tag{3.3}$$

where μ_0 is the magnetic permeability of free space ($\mu_0 = 4\pi \times 10^{-7}$ T m A^{-1}) and μ_k is the relative permeability of the kth link material. As the magnetic field increases, its capability to polarize the magnetic material reduces and the material becomes nearly magnetically saturated. Basically, a nonlinear B–H curve is used to express the magnetic property of a material.

As mentioned in the introduction, since the magnetic circuit of the valve is too complicated to be analyzed analytically, an approximate analytical based solution of the magnetic circuit may be used in general [17, 20]. Using the Kirchoff's law, magnetic flux conservation rule of the magnetic circuit, and assuming that the magnetic field intensity

32

along the effective length of each link of the magnetic circuit is constant, the relation between filed intensity in the MR fluid, H_{MR} , and the applied current I can be approximated as [16, 18] :

$$H_{MR} = \frac{N_c I}{2d} \tag{3.4}$$

In which N_c, d and I represent the number of coil turns, the gap size of the valve and electrical current to the coil of the valve, respectively. So it can be concluded that the relationship between I and H_{MR} is linear.

However, due to many simplified assumptions these approximate solutions may not render accurate distribution of magnetic filed in the activation region. Considering this, in order to find the accurate distribution of the magnetic field intensity across the active length which the MR fluid is exposed to magnetic field, the finite element method (FEM) has been recently employed [15, 17, 18, 39].

3.3. Finite Element Analysis

In the current study, commercial FEM software ANSYS is used to analyze the magnetic circuit problem in the MR valve. Because the geometry of MR valve structure is axisymmetric, to reduce the computational cost a 2-D axisymmetric model is used to develop the finite element modeling of the valve for the purpose of electromagnetic analysis. The magnetic flux density (B) and magnetic field intensity (H) in the MR fluid under applied current of 1 Amp are determined in a few geometrical dimensions well-chosen by DOE.

A log file in the ANSYS has been developed in which the design variables (DVs) such as the coil width (w), the pole length (t), the MR orifice gap (d), and the housing thickness

(d_h) are coded as parametric variables. These design variables are clearly shown in Figure 1-3, in chapter 1. As the geometric dimensions of the valve structure are varied during the optimization process, the meshing size has been specified by number of elements per line rather than by element size. Figure 3-1 shows a schematic of a 2-D axisymmetric MR damper piston and its components.
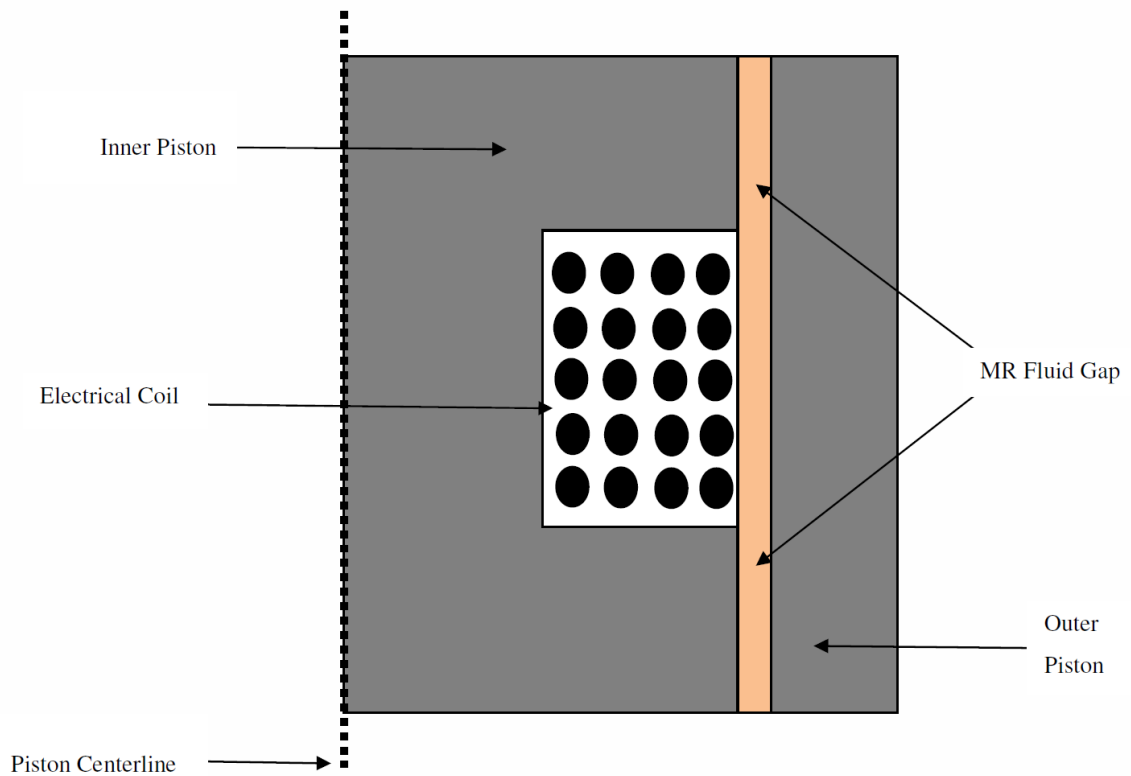
Figure 3-1: 2-D Axisymmetric MR damper valve

3.3.1. Approach and Assumptions

In modeling of an electromagnetic problem in ANSYS environment, static (DC) current is applied as a current density shown by J which is given by the number of turns (N_c), the current (I), and the coil area (A) as [46] :

$$J = \frac{N_c I}{A}$$
(3.5)

From the Kirchoff's law as presented in Eq. (3.1), it can be concluded that the relationship between electrical current and magnetic field intensity of MR fluid in the valve is linear. Therefore, without losing any generality, the FEM problem is solved for $I = 1$ Amp.

In the modeling, it is assumed that the flux leakage out of the perimeter of the inner and outer piston, shown in Figure 3-1, is small enough to be negligible. This assumption is applicable when flux is contained in an iron circuit [39, 46]. The assumption of no leakage at the perimeter of the model means that the flux will be acting parallel to this surface and it is imposed by the "flux parallel" boundary condition placed around the model.

The magnetic field intensities are calculated in nodal points for the inner piston, MR fluid and the outer piston, by means of Maxwell stress tensor and a virtual work calculation [39].

As mentioned before, since in this study, during the optimization process the geometry of the problem may be changed, the mesh size is specified by the number of elements per line rather than by element size. The number of element on the lines across the MR fluid orifice is specified as a parameter called the basic meshing number. The number of elements of other lines in the model is selected as a product of the basic meshing number and an appropriate scalar.

As it is well known, using fine meshes results in more accurate result. However, a small meshing size increases computational cost. Here, we have conducted several simulations

with different mesh size in order to find optimum mesh size which generates accurate results efficiently. It has been found that the basic meshing number 10 is accurately sufficient to ensure the convergence of the finite element solution. This basic meshing size is also reported in some previous works [17, 18, 20]. Thus, the basic meshing number of 10 is used in this study. Figure 3-2 shows the finite element model of the MR valve.
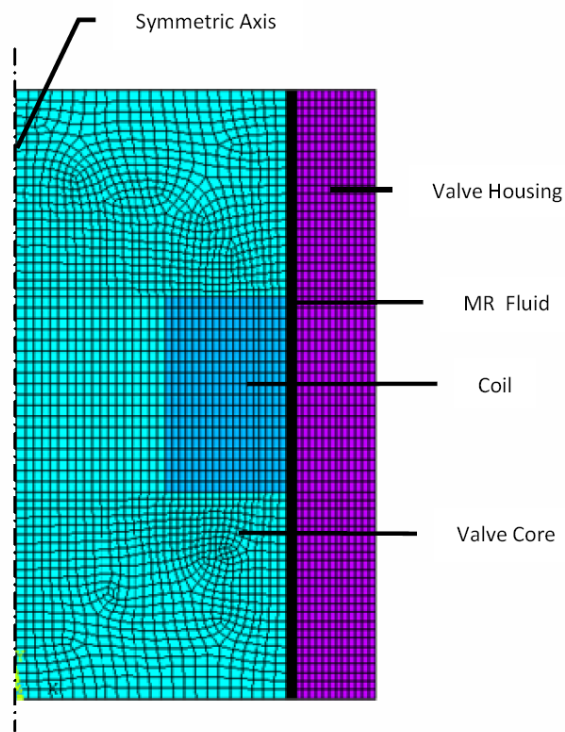
Figure 3-2: Finite element model of the Single-coil MR valve

3.3.2. Element description

For solving coupled problems of 2-D magnetic, thermal, electrical, piezoelectric, and structural both PLANE 53 and PLANE 13 can be utilized as candidate elements. To keep the model size small, the lower-order element PLANE 13 is usually used [15]. Here, the 4-node quadrilateral element PLANE 13 as shown in Figure 3-3 is used for the finite

36

element model. It is noted that this element has nonlinear magnetic capability for modeling *B-H* curves.
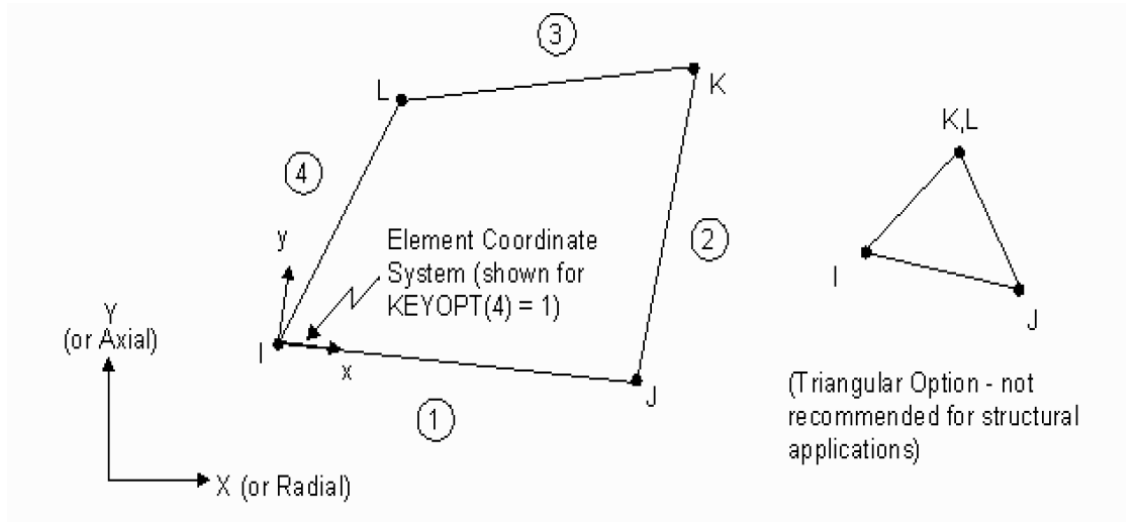
Figure 3-3: Geometry of element PLANE 13 [46]

3.3.3. Input Data

In electromagnetic problems, defining the system of unit is very important. Since the metric unit is used, the software assigns the value of $\mu_0 = 4\pi \times 10^{-7}$ H/m as the magnetic permeability of free space. For the elements representing the MR fluid and also the steel used for housing, *B-H* curves shown in Figure 3-4 are assigned. These properties are taken from other published works [15, 16].
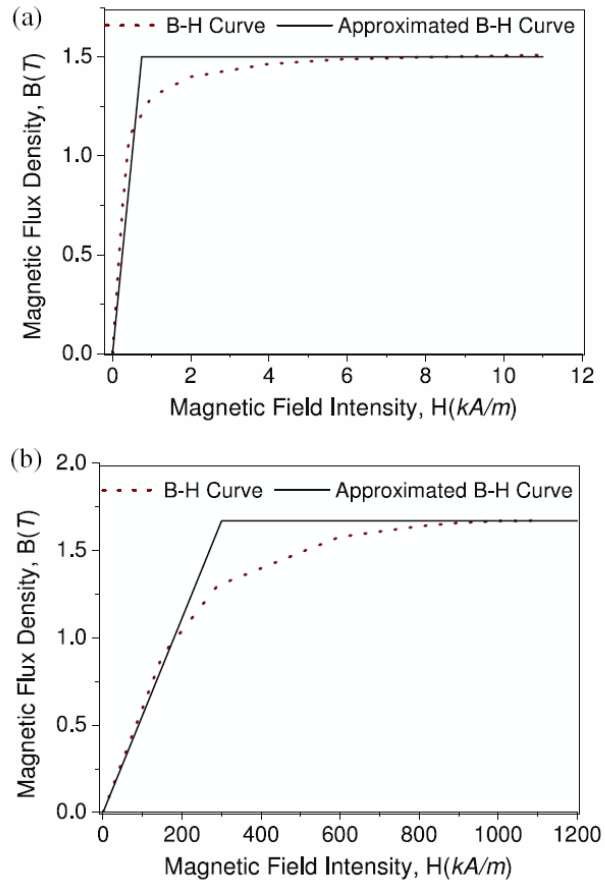
Figure 3-4: Magnetic properties of silicon steel and MR fluid. (a) *B–H* curve of silicon steel, (b) *B–H* curve of MR fluid [15, 16]

According to Figure 3-4, the equivalent relative permeability of the material can be estimated to be $\mu = 1600$ and the magnetic saturation is $B_s = 1.5$ T for the silicon steel; and the equivalent permeability and magnetic saturation of MR fluid can be estimated to be $\mu_{mr} = 4.5$ and $B_{s,mr} = 1.7$ T, respectively [15, 16]. It should be mentioned that relative permeability can be calculated by the slope of the straight lines in the *B-H* graphs and Eq.(3.3).

Magnetic properties of the valve components used in the FEM analysis and optimization are provided in Table 3-1. The base viscosity of the MR fluid, flow rate of the MR valves

38

and piston velocity are assumed to be $\eta = 0.092$ Pa.s , $Q = 3 \times 10^{-4}$ m^3 s^{-1} and $v_p = 0.4$ m s^{-1}, respectively [15].

Table 3-1: Magnetic Properties of the valve components

Valve Components	Material	Relative Permeability	Saturation Flux
Valve Core	Silicon Steel	2000	1.5 T
Valve Housing	Silicon Steel	1600	1.5T
Coil	Copper	1	-
MR fluid	MRF 132-DG	*B-H* curve (Figure 3-4)	1.7 T

According to Figure 3-4, at a specific electrical current value the valve performance reaches saturation due to the magnetic saturation of the valve components especially in MR fluid region. In addition, the power consumption is almost linearly increased with the applied current. Therefore, it is really important to be aware of the maximum of the applied current in the optimal design of the MR valve for its effective application (high performance and low power consumption), and also to avoid magnetic saturation of MR fluid.

3.3.4. Output data

The primary output of the written code in ANSYS is magnitude of magnetic field intensity H which is the vector magnitude of **H**, defined by

$$H = \sqrt{H_x^2 + H_y^2} \tag{3.6}$$

where H_x and H_y are magnetic field intensity components along the x and y axes. The same as for magnetic field intensity, the vector magnitude of magnetic flux density, B, is defined as

$$B = \sqrt{B_x^2 + B_y^2} \qquad\qquad (3.7)$$

where B_x and B_y are magnetic flux density components along the x and y axes [46]. The magnetic flux density has been evaluated for the initial design of ($t=15$ mm, $w=8$ mm, $d_h=5$ mm, $d=1$ mm) at applied current 1 Amp. Figure 3-5 shows a 3-D view of vector magnitude of magnetic flux in the valve. The 2-D presentation of the magnetic flux density and magnetic flux lines are respectively shown in Figure 3-6 and Figure 3-7.
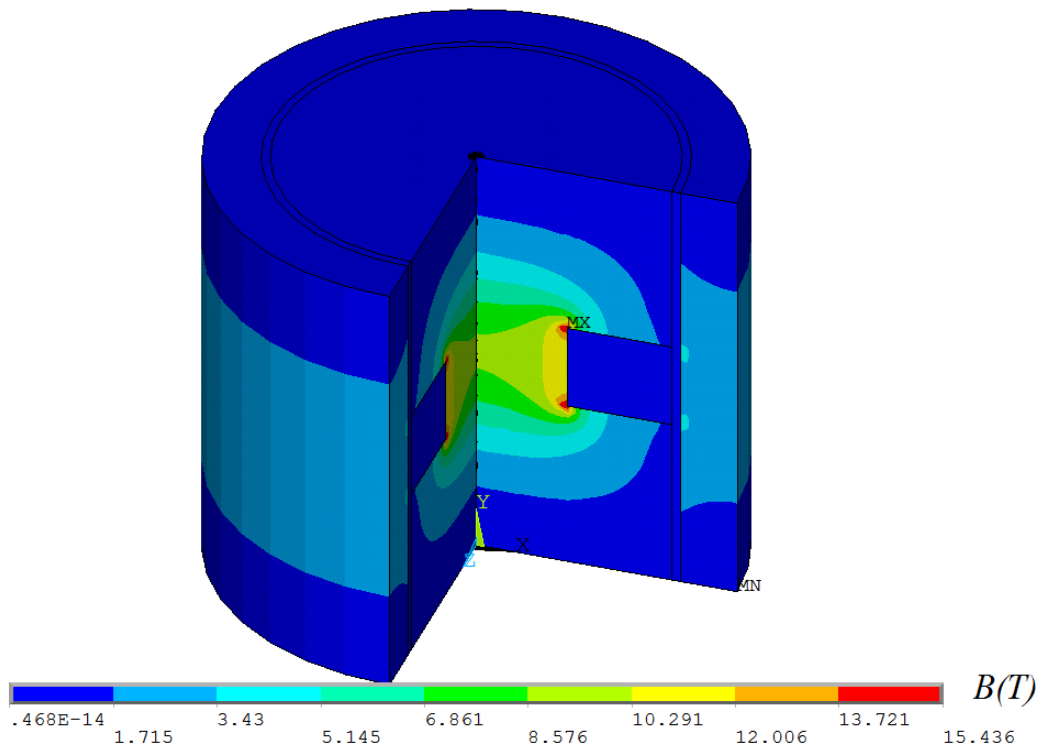
Figure 3-5: Magnetic flux density with 3-D view in the valve
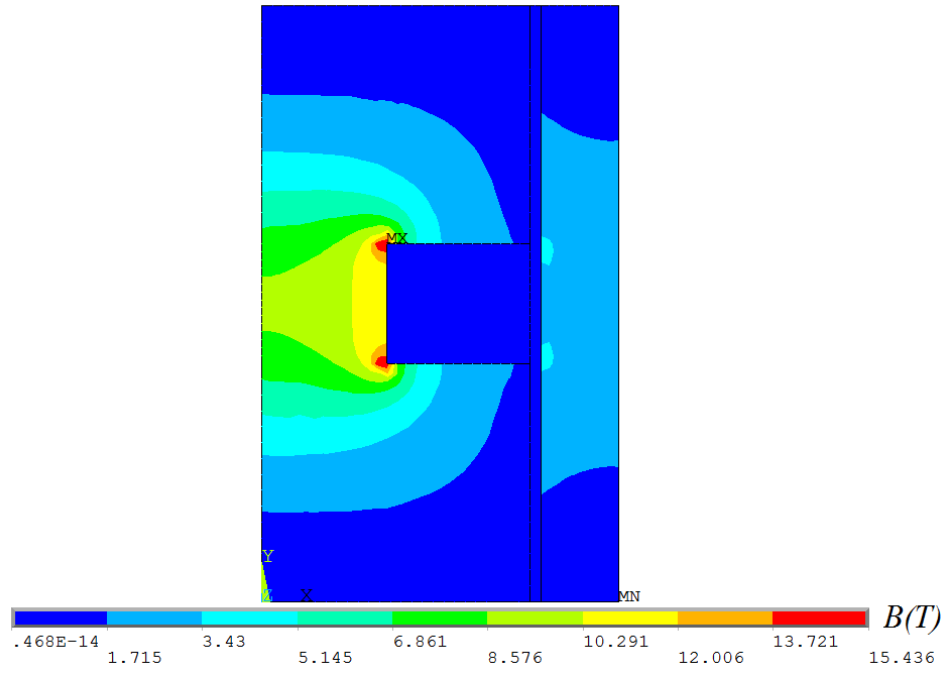
Figure 3-6: Finite element solution of magnetic flux density in the valve magnetic circuit at initial design variables
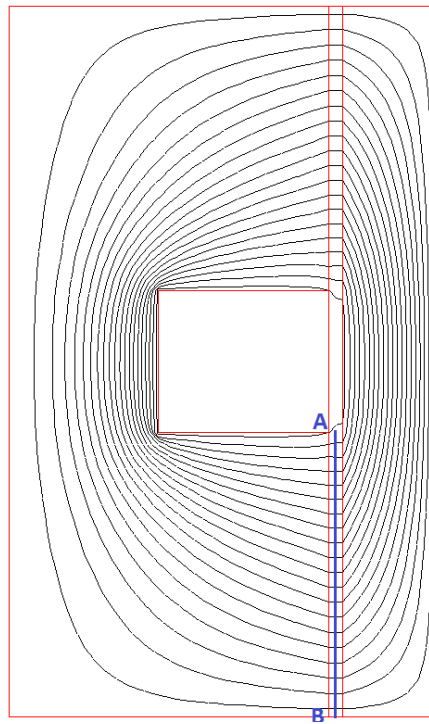
Figure 3-7: Magnetic flux lines in the MR valve

The variation magnitude of magnetic flux density vector along the effective length (line AB in Figure 3-7) is demonstrated in Figure 3-8.
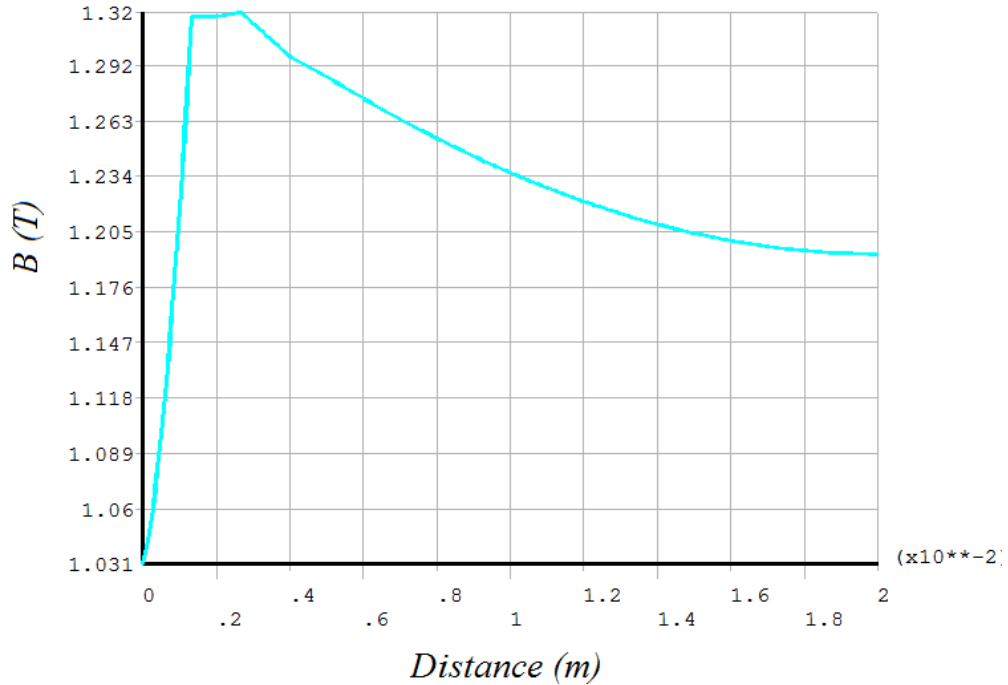
Figure 3-8: Magnetic flux density *B* along line AB at initial design variable

As it can be seen from Figure 3-8, the maximum magnetic flux density in the MR fluid along the orifice of the valve is about 1.32 T. This flux density is less than 1.7 T, which is the saturation flux density of MR fluid. It can also be realized from the Figure 3-8 that *B* and *H* are not constant along the pole length. Therefore, for the purpose of design optimization, the average values across the MR valve ducts have been used. To achieve this, a path is defined along the MR active volume where the magnetic flux crosses. Then the averages are determined by integrating the magnetic field intensity along the defined path and then dividing it by the path length. Thus, the magnetic flux density and magnetic field intensity are calculated as follows [17, 18] :

42

$$B_{mr} = \frac{\int_0^t B_{mr}(s)\,ds}{t} \tag{3.8}$$

$$H_{mr} = \frac{\int_0^t H_{mr}(s)\,ds}{t} \tag{3.9}$$

where $B_{mr}(s)$ and $H_{mr}(s)$ are the magnetic flux density and magnetic field intensity at each nodal points located on the defined path. The yield stress of the MR fluid caused by the magnetic circuit is then calculated from the polynomial curve of the yield stress, given by Eq. (2.6). As discussed in chapter 2, once the yield stress of the MR fluid in the duct is obtained, the magnetic field dependent damping force and valve ratio can be calculated by using Eqs. (2.13) and (2.15) in Chapter 2, respectively.

3.4. Response Surface Method (RSM)

In this section, response surface methodology (RSM) is introduced. The optimal sets of design variables are designed by "Design of Experiments" techniques. Then, finite element analysis will be conducted on these sets of design variables. RSM is basically employed to map analytical functions to the finite element based values of magnetic flux density and magnetic field intensity corresponding to design variable sets. The accuracy of the assigned functions will then be evaluated.

The objective here is mainly to find approximate response functions which can accurately model the magnetic flux density and magnetic field intensity across the entire design region. This will allow doing optimization outside the ANSYS environment by combining the developed response functions with high-fidelity optimization algorithms. It was mentioned that in most of the previous works, the design optimization of MR valve or dampers has been directly conducted in ANSYS environment. This is not only

43

computationally expensive as each optimization run may call the analysis of the model several times, but also may render an inaccurate optimum solution due to low order optimization method implemented in ANSYS. On the other hand, since output responses generated by finite element method are typically noisy, direct using of a higher order gradient based optimization algorithm on the finite element results is not possible as the gradient may not be obtainable. In addition, numerical calculation of the gradients may also spurious due to the noisy nature of the responses. Moreover, in case of non-gradient based algorithms such as genetic algorithms, a higher number of iteration is required to obtain the results which makes the procedure highly computationally expensive. As a result, here an alternative method is used which is based on approximation techniques [47]. For this purpose meta-models are used to develop the approximate function of the actual model. Meta models are constructed from sample data of an experiments or computer simulation like FEM. Therefore, a more practical approach is to perform FEM at a few well-selected points in the design domain and fit an analytical function to the results by the use of RSM. The RSM based responses are smooth and thus they can be effectively used in any gradient based or non gradient based optimization algorithms [45].

3.4.1. RSM Model Building

Response surface method (RSM) is a methodology to quantify the relationships between one or more measured or calculated responses and predictors (here design variables). They are typically used with the design of experiments where a set of design variables are established to minimize the error of the approximation. RSM is employed to generate the best fitted polynomial function to model of phenomenon under investigation over the

entire design region based on the defined set of design variables. A detail review of RSM is presented in Ref. [48].

Regression analysis is usually used in RSM to formulate a polynomial function. The approximated RSM based response can be written as

$$\hat{y} = X\beta \tag{3.10}$$

where X is the design matrix with size $p \times q$, in which p is the number of experiments and q is the number of unknown model coefficients β. The exact output response (in our case the direct results of FEM) can be written as

$$y = \hat{y}(x_1, x_2, ..., x_p) + \varepsilon \tag{3.11}$$

in which x_1, x_2, ..., x_p are the design variables and ε is the error between the accurate response y and its approximation $\hat{y}$. The approximate function $\hat{y}$ should be defined in a way that minimizes the error ε for all points in the design space. The types of regression model between the approximated function and design variables are generally in form of polynomial functions as follows:

$$y = \beta_0 + \sum_{i=0}^{N}\beta_i x_i + \sum_{i<j}^{N}\beta_{ij} x_i x_j + \sum_{i=0}^{N}\beta_{ii} x_i^2 + ... \tag{3.12}$$

The model includes an intercept, linear terms, quadratic interaction terms, and squared terms from left to right. Higher order terms would be also considered, as necessary. The model parameters can be determined most effectively if proper experimental design is utilized to collect the data. The main objective of regression methods is to find the best unbiased estimator of coefficients β which minimize the error ε. To achieve this, a function L, which is the summation of error squared, is typically defined as:

$$L = \sum_{i=1}^{n} \varepsilon_i^2 = \varepsilon^T \varepsilon = (y - X\beta)^T (y - X\beta) \tag{3.13}$$

To minimize L, we can differentiate L with respect to β and equate it to zero to find β as:

$$\beta = \left(X^T X\right)^{-1} X^T y \tag{3.14}$$

It should be noted that in the derivation of the above equation, it is assumed that $X^T X$ is nonsingular.

Model types

There are different types of regression models used to build a RSM response. For a model with four design variables (x_1, x_2, x_3, x_4); which will be used later in Sections 3.4.4. and 3.4.6. , linear, quadratic or cubic models can be used as follows:

(1) A linear model with interaction that includes constants, linear, and interaction terms in the following form

$$\begin{aligned}
\hat{y} &= a_0 + a_1 x_1 + a_2 x_2 + a_3 x_3 + a_4 x_4 + a_{12} x_1 x_2 + a_{13} x_1 x_2 \\
&\quad + a_{14} x_1 x_4 + a_{23} x_2 x_3 + a_{24} x_2 x_4 + a_{34} x_3 x_4
\end{aligned} \tag{3.15}$$

(2) A quadratic model with constant, linear, interactions and squared terms as follows

$$\begin{aligned}
\hat{y} &= a_0 + a_1 x_1 + a_2 x_2 + a_3 x_3 + a_4 x_4 + a_{12} x_1 x_2 + a_{13} x_1 x_2 + a_{14} x_1 x_4 \\
&\quad + a_{23} x_2 x_3 + a_{24} x_2 x_4 + a_{34} x_3 x_4 + a_1 x_1^2 + a_2 x_2^2 + a_3 x_3^2 + a_4 x_4^2
\end{aligned} \tag{3.16}$$

(3) A cubic form includes constant, linear, interactions, squared and cubic terms as follows

46

$$\hat{y} = a_0 + a_1 x_1 + a_2 x_2 + a_3 x_3 + a_4 x_4 + a_{12} x_1 x_2 + a_{13} x_1 x_2 + a_{14} x_1 x_4$$
$$+ a_{23} x_2 x_3 + a_{24} x_2 x_4 + a_{34} x_3 x_4 + b_1 x_1^2 + b_2 x_2^2 + b_3 x_3^2 + b_4 x_4^2$$
$$+ a_{123} x_1 x_2 x_3 + a_{134} x_1 x_3 x_4 + a_{234} x_2 x_3 x_4$$
$$+ b_{12} x_1^2 x_2 + b_{13} x_1^2 x_3 + b_{14} x_1^2 x_4 + b_{21} x_2^2 x_1 \qquad (3.17)$$
$$+ b_{21} x_2^2 x_1 + b_{31} x_3^2 x_1 + b_{41} x_4^2 x_1 + b_{32} x_3^2 x_2$$
$$+ b_{34} x_3^2 x_4 + b_{41} x_4^2 x_1 + b_{42} x_4^2 x_2 + b_{43} x_4^2 x_3$$
$$+ b_{23} x_2^2 x_3 + b_{24} x_2^2 x_4 + c_1 x_1^3 + c_2 x_2^3 + c_3 x_3^3 + c_4 x_4^3$$

The model selection is the process that the designer tries to find the best polynomial that can approximate the true response. The knowledge about the type and level of interaction between variables will facilitate the formulation of the approximate model. So usually, different approximate polynomial functions are developed and evaluated based on their ability to estimate the results. Based on that, the model with highest accuracy is then chosen.

As it can be realized, meta-models (including the RSM) model the response based on the data which is sampled over the entire design space. For this purpose, the multi-dimensional design region is discretized to selected points. These points represent a combination of design variables with different levels which here we call them design sets. To minimize the number of required design sets (the selected points), Design of Experiments (DOE) is utilized.

3.4.2. Design of Experiments (DOE)

DOE is typically carried out to find the best location of points in the design space which experiments shall be conducted. In fact, the objective of DOE is to find a desirable location in the design space where the response is stable in a specified range of the factors. DOE refers to a collection of statistical techniques to select values for design

variables to obtain the more accurate response with using minimum number of experiments.

Proper choice of experimental design facilitates the fitting and analyzing response surfaces greatly. Some of the features of desirable designs are [45] :

- To provide a reasonable distribution of data point in design space

- To allow higher order designs

- To provide accurate estimations of the model coefficients

- To avoid a large number of runs

- To provide the investigation of model adequacy including the lack of fit

These features are conflicting and a kind of trade off must be done in design of experiments.

DOE has two main categories classified as classical DOE and computer based DOE. The first category deals with physical experiments which typically includes some stochastic noise component while the latter is computer simulation based in which repeated experiments with identical inputs result in the identical output [49].

Classical DOE includes methods such as full or fractional factorial designs, Box-Behnken designs, Central composite, randomize block design and Plackett-Burman design [50]. For the second category of DOE which is our concern here, different algorithms has been introduced and utilized in commercial software of DOE namely as "Point Exchange" , "Coordinate Exchange", "A-optimal", "D-optimal", "IV-optimal" design. Among these algorithms the last three techniques are frequently used and shown to provide the most accurate estimates of the model coefficients [50].

The A-optimal algorithm is used to minimize the average prediction variance around the model. This design minimizes the trace of the $(X^TX)^{-1}$ matrix. This leads to minimization of the average prediction variance of the polynomial model [50].

The D-optimal criteria selects design points in a way that minimizes the variance associated with the estimates of the specified model coefficients. A D-optimal design minimizes the determinant of the $(X^TX)^{-1}$ matrix. In other words, it maximizes the determinant of D=$|X^TX|$, where X is the design matrix of model terms evaluated at specific treatments in the design space [50].

The IV- optimal design selects design points to minimize the average prediction variance over the range of the design space [51]. An appropriate objective function for this purpose is presented as follows [49] :

$$\min_{\omega} \frac{1}{\Delta} \int_{x \in X} E\left\{\left[\hat{Y}(x) - Y(x)\right]^2\right\} d\mu(x) \tag{3.18}$$

where $\Delta = \int_{x \in X} d\mu(x)$ is a normalizing function and $\min_{\omega}$ defines that the experimental design ω ; which is the set of specified values of design variables $x \in X$; is obtained by minimizing the integral over the design domain. E represents expectation that is an average over the statistical distribution of the error ε, and the weighting of different regions of the response is done through differential $d\mu(x)$. Typically Gaussian distribution is selected as weighting function in which the weight reduces exponentially as the design variables moved away from a specific location in design space. In the simplest case that weighting function is unity, $d\mu(x)=d(x)$ which indicates the same weight over the entire design space [49]. IV-optimal designs are best used with RSM [52-54] in which the goal

is to model the true response surface with an appropriate function accurately. It should be noted that IV-optimal is known as I-optimal as well.

While D-optimal designs minimize the variance of coefficient estimates, IV-optimal design minimize the average prediction variance across the design space. As a result, IV-optimal designs are more effective for prediction [53, 54]. Detail explanations of variable selection algorithms and model building by use of these optimal models are presented by Adams [51, 55]. In this work, According to the survey which has been presented briefly, IV- optimal design is employed.

3.4.3. Implementation of RSM to Model Magnetic Responses in MR valve

In this study, as mentioned before, the design variable of MR valve are selected to be t, w, d_h and d as shown in Figure 1-3. The lower and upper bonds on these design variables are as follows:

$$
\begin{aligned}
8.5 \ mm \ &\leq \ t \ \leq \ 20 \ mm \\
5 \ mm \ &\leq \ w \ \leq \ 15 \ mm \\
3 \ mm \ &\leq \ dh \ \leq \ 8 \ mm \\
0.8 \ mm \ &\leq \ d \ \leq \ 1.2 \ mm
\end{aligned}
\tag{3.19}
$$

It should be noted that in all previous works [15-18, 20], the gap distance d has not been considered as a design variable while in the present work it is treated as a design variable.

It will be discussed later that cubic model estimates the results better and thus this model is used to approximate the magnetic field intensity and magnetic flux density in optimization process. As it can be realized from Eq.(3.17), a cubic model has 36 coefficient terms which requires the same number of design point to map a function to results. Table 3-2 and Table 3-3 show the design of experiments and FEM results at each run for quadratic and cubic models, respectively. As mentioned before, IV-optimal design

method has been employed to estimate the sets of design variables. These set points are

generated by trial version of *Design-Expert* [©] commercial software. The finite element

code which is built in ANSYS parametric design language (APDL) is run once for each

set of design variables. After finding the value of magnetic flux density and magnetic

field intensity for each set of design points, the analytical functions associated to the

magnetic results are derived by RSM approach.

Table 3-2: Design of Experiments for Quadratic RSM

t	w	d_h	d	B (T)	H (kA/m)
16.84	15	3	1.1	1.7	327.288
8.5	5.5	3	1.08	1.7	309.226
13.04	10.35	8	0.96	1.7	446.704
13.1	10.25	5.05	1.2	1.7	373.779
8.5	5.5	6.5	0.8	1.7	436.593
8.5	15	6.7	1.1	1.7	569.277
8.5	5	8	1.2	1.615656	285.942
20	5	8	0.8	0.66864	118.328
16.95	15	6.65	0.8	1.7	335.891
20	10.35	4.95	0.96	1.065573	188.545
8.5	13	3	0.8	1.7	823.063
16.59	5.5	3	0.8	1.032459	182.734
20	5	3	1.2	0.423869	74.989
15.92	5	6.22	1.05	0.946384	167.467
20	15	8	1.2	0.794079	140.484

Table 3-3 : Design of Experiments for Cubic RSM

t (mm)	w (mm)	d_h (mm)	d (mm)	B(T)	H (kA/m)
20	5	4.2	0.8	0.6	108.073
14.08	9.74	5.59	1.01	1.7	377.603
10.96	5	7.35	1.01	1.562991	276.629
13.27	5	6.35	0.87	1.438612	254.623
8.5	15	8	1.2	1.7	409.145
8.5	14.85	3	0.91	1.7	799.628
20	9.3	4.08	1.2	0.803483	142.149
19.6	6	5.85	1.07	0.659976	116.771
11.38	9.5	7.03	1.2	1.7	409.775
8.5	14.5	6.73	0.8	1.7	749.535
20	15	3.67	1.09	1.192041	210.901
20	15	7.88	0.8	1.0719	189.688
20	12.35	5.23	0.89	1.278796	226.285
8.5	5	6.98	1.17	1.642137	290.634
15.8	12	3.03	1.08	1.864868	329.989
9.31	5.95	8	0.8	1.7	448.577
8.5	10.1	7.68	0.98	1.7	623.355
17.53	8.45	6.9	0.8	1.568252	277.551
8.5	7.85	3	1.2	1.7	400.892
20	14.6	3	0.8	1.412086	249.894
17.36	14.05	6.75	1.19	1.496207	264.727
19.89	11	8	1.07	1.048701	185.546
15.29	6.1	8	1.09	1.208991	213.936
17.41	7	3	0.89	1.091523	193.165
11.38	10.55	3.6	0.8	1.7	575.423
8.5	12.7	4.8	1.13	1.7	651.259
20	5	8	0.87	0.62552	110.69
8.5	5	3	0.8	1.7	354.875
10.74	5.5	3.5	1.04	1.5588	275.884
15.63	5.65	4.5	1.2	0.952149	168.475
11.38	15	3.25	1.2	1.7	524.093
16.05	15	4.5	0.85	1.7	420.392
14.25	12.85	8	0.87	1.7	435.982
20	5	3	1.2	0.423869	74.989
11.55	15	6.72	1.03	1.7	461.615
8.5	7.35	4.84	0.88	1.7	514.323

3.4.4. The Response Surface Function (RSM) for Magnetic Field Intensity in the MR Valve

The function of magnetic field intensity (*H*) is required in optimization process to calculate the objective function. Therefore, developing a smooth analytical function of *H* in terms of design variables is desirable. Considering the design points presented in Table 3-2 and fitting the quadratic RSM model on these points, one may derive the following quadratic equation for magnetic field Intensity in the MR valve:

$$
\begin{aligned}
H_{mr} = &+1026.58308 - 51.32332t + 153.91542w - 34.83763d_h \\
&- 1414.78545d - 2.25740tw + 0.91123td_h + 43.71887td \\
&- 2.95229wd_h - 22.37401wd + 10.68398d_hd - 0.23797t^2 \\
&- 3.08801w^2 + 3.50658d_h^2 + 354.34617d^2
\end{aligned}
\tag{3.20}
$$

Considering Table 3-3 and fitting the cubic RSM model on these points, the following cubic function can be derived:

$$
\begin{aligned}
H_{mr} = &-3119.55547 + 158.50182t + 103.62799w - 65.16629d_h + 8551.36772d \\
&- 13.02691tw - 8.21118t\,d_h - 218.52291t\,d + 19.30581wd_h - 27.21718wd \\
&- 108.45565d_h\,d - 1.09511t^2 + 4.25117w^2 + 20.07344d_h^2 - 7288.56044d^2 \\
&+ 0.22715\,twd_h + 0.99053twd + 4.23481\,t\,d_h d - 5.74880\,wd_h\,d \\
&+ 0.061521t^2w + 0.12573t^2\,d_h + 1.74782t^2\,d + 0.34467tw^2 - 0.069413t\,d_h^2 \\
&+ 83.76980t\,d^2 - 0.67736w^2\,d_h + 1.37794w^2d - 0.63734wd_h^2 - 0.62263wd^2 \\
&- 8.94903d_h^2d + 101.98488d_h\,d^2 - 0.033824t^3 - 0.32121w^3 - 0.39758d_h^3 \\
&+ 1931.41029d^3
\end{aligned}
\tag{3.21}
$$

Figure 3-9 and Figure 3-10, show the cubic mapped surfaces to *H* response. Since there are four variables it is impossible to show the variation of *H* versus all the design variables simultaneously. So in each figure, two of factors are kept fixed and the responses are drawn versus the other two factors.
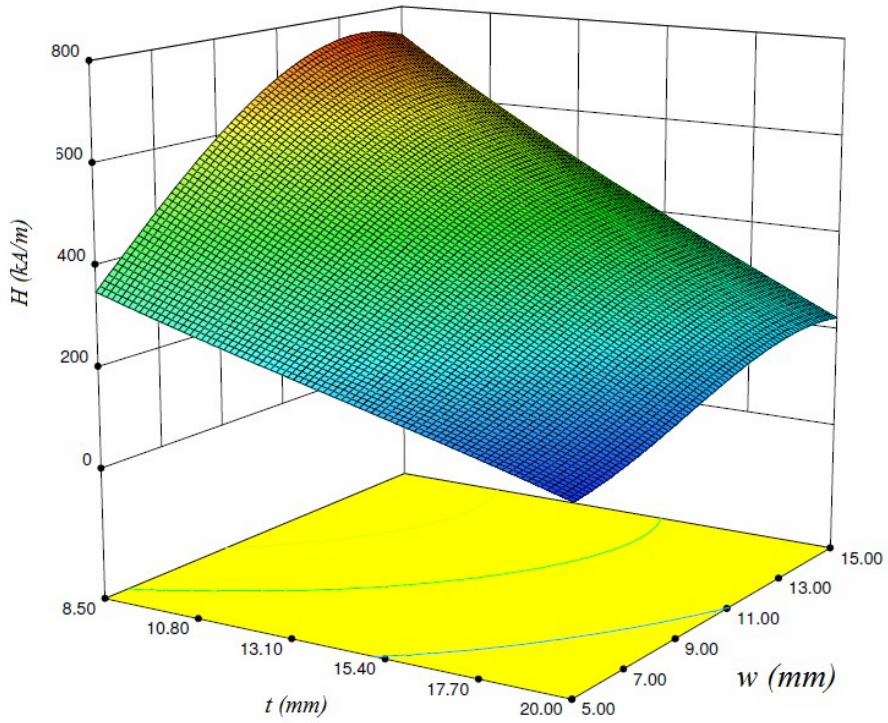
Figure 3-9: Surface of cubic model of H_{mr} for d=1 mm and d_h=7 mm
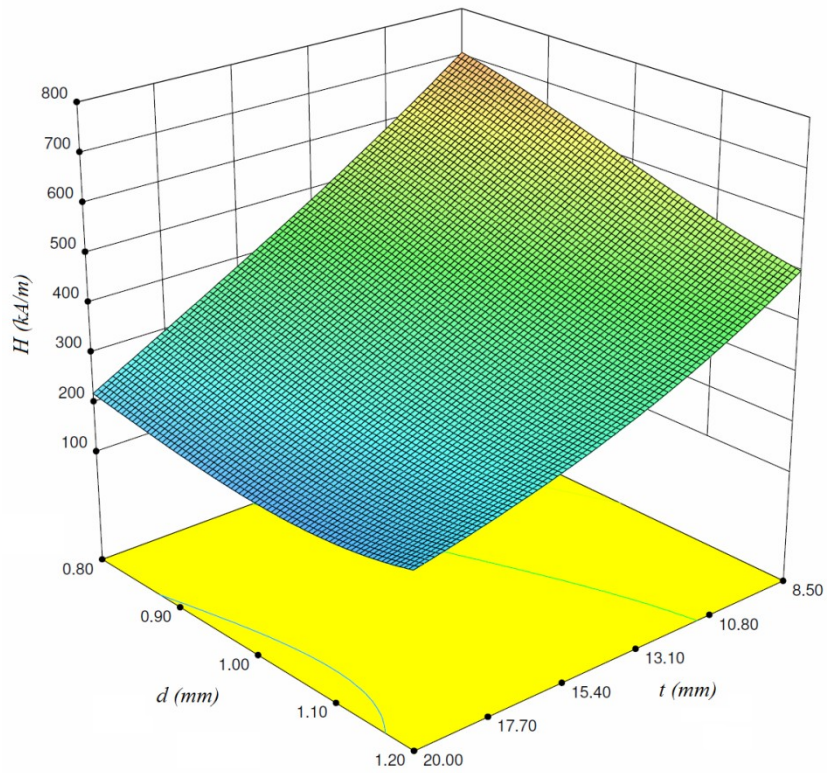
Figure 3-10: Surface of cubic model of H_{mr} for w=10 mm and d_h=8 mm

In design response method, sometimes the contour of the response is shown to explain the nature of the response. An example of this kind of contours is shown in Figure 3-11.
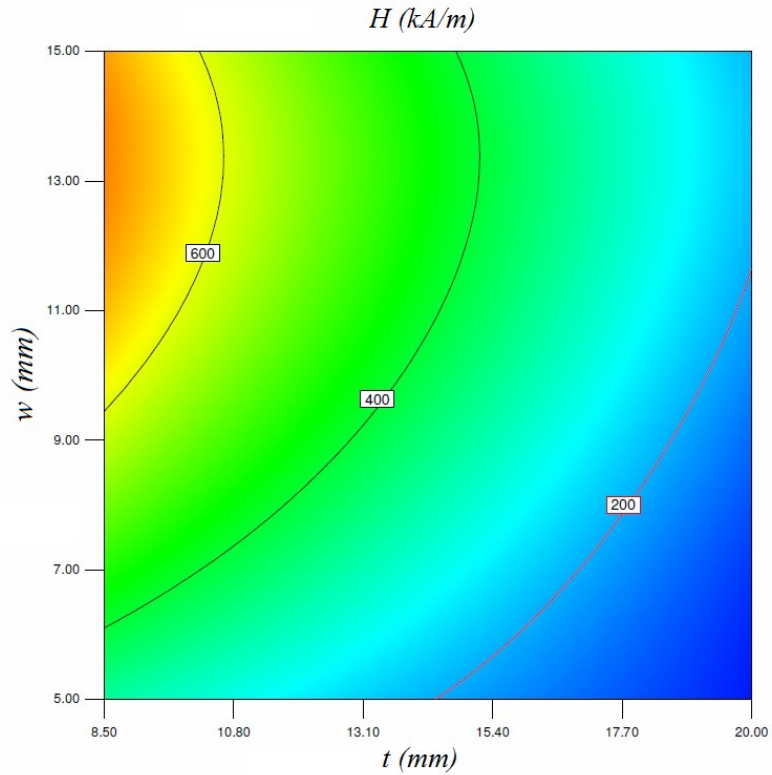
Figure 3-11: Contour of cubic H_{mr} for d_h=5.5mm and d=1mm

Since H_{mr} is the most dominant and important state variable that is utilized in other calculations, it is necessary to investigate the accuracy of the developed approximate function. It is noted that H_{mr} and B_{mr} are directly related and thus, the accuracy of one function is inferred from the accuracy of the other one.

3.4.5. Model Accuracy Checking

It is always necessary to examine the accuracy of developed model to ensure that it provides an adequate approximation of true response. One of the typically used quantity to check the ability of model to identify the variation within the output response is the coefficient of multiple determination R^2 [45] . It is defined as:

$$R^2 = 1 - \frac{SSE}{SST} \qquad (3.22)$$

where

$$SSE = \sum_{i=1}^{n}(y_i - \hat{y}_i)^2 \qquad (3.23)$$

and

$$SST = \sum_{i=1}^{n}(y_i - \bar{y})^2 \qquad (3.24)$$

in which y_i is the real output response, here calculated by FEM, $\hat{y}_i$ is the approximate response determined by RSM, $\bar{y}$ is the average of real response, and n is the number of design points to generate the model. R^2 values vary between 0 and 1, where values close to 1 mean that the approximate model has high ability to explain the response in the design space.

Also in statistic the mean absolute error (MAE) is a used quantity to measure the accuracy of the predicted results to true ones are. MAE is defined as follow:

$$MAE = \frac{\sum_{i=1}^{n}|y_i - \hat{y}_i|}{n} \qquad (3.25)$$

To check the accuracy of the developed models, R^2 and *MAE* has been calculated for both quadratic and cubic models and the results are summarized in Table 3-4.

Table 3-4: Accuracy of RSM models

RSM Model	R^2	MAE
Quadratic	0.9325	2.2%
Cubic	0.9955	1.4%

As it can be realized, the introduced RSM cubic function of H defined by Eq. (3.21) can describe the response very well as R^2 value is very close to 1. In addition, the calculated MAE is 1.4% which proves the ability of the developed model to estimate the true response across the entire design space.

To show the results graphically, the variation of the magnetic field intensity versus the coil width is shown in Figure 3-12. For this purpose the other design values are assumed to be constant.
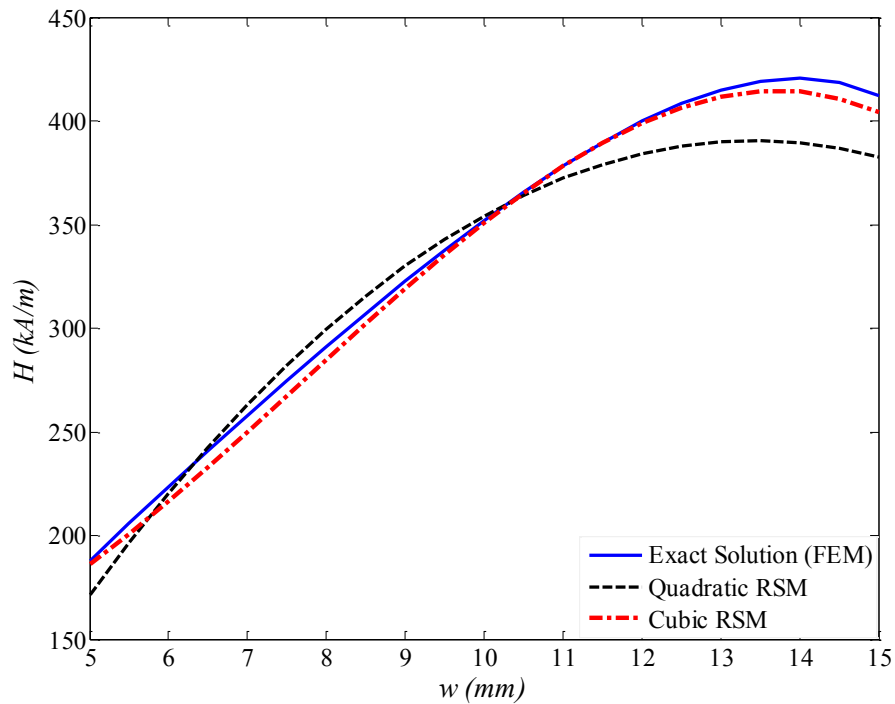
Figure 3-12: Variation of magnetic field intensity versus coil width (w) for t=15 mm, d_h=5 mm and d=1 mm

As Figure 3-12 shows, developed cubic function by RSM is able to model true response obtained from FEM precisely all over the design variable range. On the other hand, although the derived quadratic function by RSM can model the response (especially in the middle range of the design variable) properly, it is not as precise as the cubic

function. As a result, the cubic function has been selected to model the magnetic flux density and magnetic field intensity in the present work.

3.4.6. The Response Surface Function of Magnetic Flux Density in the MR valve

The magnetic flux density (B) in the MR fluid across the ducts is an important constrain in the optimization problem. In order to avoid saturation of MR fluid design, the designed geometrical dimensions of the valve and applied electric current should be in proper range. Therefore, having the value of magnetic flux density in terms of geometric parameters is highly desired to consider it as a constrain function. It is worth to point out that the B and H are related as stated with B-H curve of the MR fluid. Since the relationship between them is not a linear function, the same procedure has been performed to find the response function for B. Using the selected set of design variables presented in Table 3-2 and fitting the quadratic model of RSM, the following quadratic function can be derived for magnetic flux density in the valve:

$$
\begin{aligned}
B_{mr} = &-1.02710 + 0.15727t + 0.11020w + 0.31972d_h \\
&+ 1.22028d + 6.71014E - 3tw - 4.10390E - 3t\,d_h \\
&- 0.10492t\,d - 3.92556E - 3\,wd_h - 3.66430E - 3\,wd \\
&- 0.27166\,d_h d - 6.01490E - 3t^2 - 6.52254E - 3\,w^2 \\
&+ 2.35249E - 3d_h^{\,2} + 0.71551d^2
\end{aligned}
\tag{3.26}
$$

Considering Table 3-3 and fitting the cubic RSM model on these points, the following cubic functions can be derived for magnetic flux density of MR fluid in the valve:

58

$$
\begin{aligned}
B_{mr} =\ & +28.51542 - 1.66785\,t - 0.086247\,w + 0.53045\,d_h \\
& - 65.13746\,d \quad + 0.044206\,t\,w + 0.058094\,t\,d_h \\
& + 1.09356\,t\,d - 0.042874\,w d_h - 1.06463\,w\,d \\
& - 1.38816 d\,d_h + 0.059981 t^2 + 0.049999\,w^2 \\
& + 0.022876\,dh^2 \quad + 68.53221 d^2 - 3.42500e-005\,t\,w\,d_h \\
& + 5.51675e-003 t\,w\,d - 0.036275\,t\,d_h d + 0.051735\,w\,d_h d \\
& - 8.46256e-004\,t^2 w - 1.02580e-003\,t^2 d_h - 0.014880 t^2\,d \\
& - 9.26565e-004 t\,w^2 + 4.00368e-004 t\,d_h{}^2 - 0.30457\,t\,d^2 \\
& - 1.02122e-003\,w^2\,d_h - 9.18100e-003\,w^2\,d \\
& + 7.98899e-004\,w\,d_h{}^2 + 0.47047\,w\,d^2 + 0.085832\,d_h{}^2\,d \\
& + 0.15964\,d_h d^2 - 9.20378e-004\,t^3 - 1.00386e-003\,w^3 \\
& - 7.50709e-003\,d_h{}^3 - 23.56851\,d^3
\end{aligned}
\tag{3.27}
$$

Figure 3-13 shows the variation of response function of B with respect to selected design variables. Since there are four design variables, it is impossible to show the variation of B versus all the design variables in one plot simultaneously. So in the figure two of factors are kept fixed and the responses are drawn versus the other two factors.
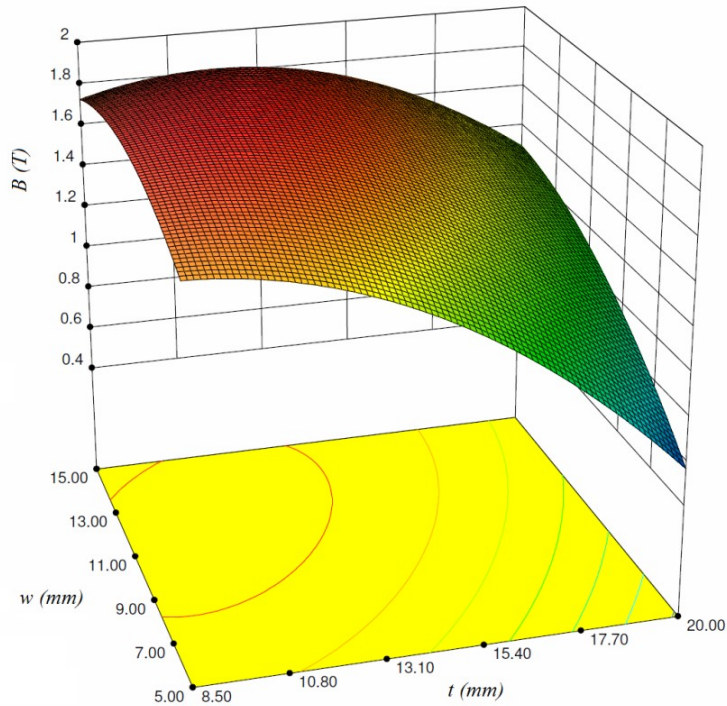
Figure 3-13 : Surface of cubic model of B_{mr} for d_h=5.5 mm and d=0.8 mm

59

As it can be seen in the figure, magnetic flux density has a high level of nonlinearity. The contours of constant magnetic flux density are also demonstrated in the base plane. As it can be realized, it is possible to have the same value for B in different MR valves while their geometrical dimensions are different. Moreover, the surface shows that the maximum value of B in valves is limited by the magnetic saturation of the employed MR fluid.

3.5. Conclusion

In this chapter a robust tool was introduced to make continuous analytical functions out of the finite element results. This chapter is a great step in optimal design of MR damper. It was discussed that all the previous published works which took the advantages of FEM to analysis the magnetic circuit of the MR valve, performed the optimization procedure in ANSYS environment. However, employing first order optimization methods in ANSYS optimization toolbox is not reliable enough to solve an optimization problem which has high order of nonlinearity in both of objective and constrained functions. Moreover, performing optimization process in ANSYS environment is computationally expensive and takes long time as at each optimization run the analysis of finite element model is recalled several times.

So as a practical approach, the finite element analysis has been performed at a few well-selected points using DOE techniques over the entire design space. Then, by taking advantages of RSM technique, continuous analytical function were built based on discrete results of ANSYS at the selected points. The developed functions are able to model the output result of FEM across the design space effectively. These functions are

polynomials in terms of design variables. Having these mapped polynomial functions will

facilitate the use of more advanced optimization methods.

Chapter 4 Optimization

4.1. Introduction

Performance functions of MR dampers which can be considered in optimal design of MR valves were introduced in Chapter 2. In vehicle suspension design, the suspension travel and the ride comfort are the two conflicting performance indices that should be considered in optimal design of MR dampers procedure. A high damping force is required to reduce the suspension travel. On the other hand, to improve the ride comfort, a low damping force is expected. Thus, a large dynamic range is required. Moreover, improving the controllability of the suspension system needs fast time response of the MR valve [18]. In evaluating the overall performance of MR dampers, the controllable force and dynamic range are the two most important parameters [24]. Considering the equation of the force due to the yield stress of the MR fluid which has been described by Eq. (2.13), it is realized that the controllable force range is inversely related to the gap size d. To maximize the efficiency of the MR damper, the controllable force should be as large as possible which demands a small gap size.

According to Eqs. (2.12) and (2.13), the viscous force increases faster than the controllable force with decreasing of the valve orifice gap size. Both the controllable

force and viscous force decrease as the gap size increases. In addition yield strength, τ_y , is also influenced by the gap size.

Also as discussed in Chapter 2, the valve ratio is inversely proportional to the square of the gap size, d^2. Thus, a small change of d can cause a large change of the valve ratio, especially at small values of d. It is noted that the lower value of the valve ratio, the better performance of the valve is. Therefore, there is a tradeoff between the pressure drop and the valve ratio.

Moreover, to decrease the response time, MR valve should be far from its saturation phase in the operational range of the valve which demands a design with a wide controllable region for the MR valve. But this is in contrary to having a higher damping force. In addition, a lower time constant needs higher resistance which leads to higher power consumption and lower useful power ratio. Thus to obtain any practical optimal design of MR valves, a multi-objective function shall be considered that includes all the performance functions of the MR damper. Considering the above mentioned requirements, the following multi-objective function has been proposed [17, 18],

$$OBJ = \alpha_F \frac{F_{MR,r}}{F_{MR}} + \alpha_d \frac{\lambda_{d,r}}{\lambda_d} + \alpha_T \frac{T}{T_r} \qquad (4.1)$$

where, F_{MR}, λ_d and T are the MR damping force, dynamic range, and inductive time constant of the damper, respectively. $F_{MR,r}$, $\lambda_{d,r}$, and T_r are the reference damping force, dynamic range, and inductive time constant of the damper, respectively.

It should be noted that, the reference damping force, dynamic range, and inductive time constant of the damper are obtained from the solution of the MR damper at initial values

of design parameters, in which the magnetic flux density throughout the magnetic circuit of the damper does not exceed the saturation magnetic flux density of the MR fluid.

α_F, α_d, and α_T respectively represent the weighting factors for the damping force, the dynamic range, and the inductive time constant ($\alpha_F + \alpha_d + \alpha_T = 1$). The values of these weighting factors are chosen according to desired application. For instance, for suspension systems designed for uneven or unpaved road, a large damping force is required. Thus, large values of α_F and α_T are chosen. On the other hand, in design of suspension systems for flat roads, a large value of α_d is selected as it provides better ride comfort.

4.2. Numerical Methods for Constrained Optimum Design

One may write the mathematical model of the optimization problem in this work as

$$Min\ f(x)\quad subjected\ to \qquad \begin{aligned} &C_i(x) = 0,\ i \in \varepsilon \\ &\\ &C_i(x) \geq 0,\ i \in \tilde{\mathcal{I}} \end{aligned} \qquad (4.2)$$

where the objective function $f(x)$ and the constraint functions $C_i(x)$ are all smooth and real-valued functions on a subset of R_n, and ε and $\tilde{\mathcal{I}}$ represent finite index sets of equality and inequality constraints, respectively.

For solving the optimization problem in form of Eq. (4.2), different algorithms have been proposed in which the most practical ones are [56]

- *quadratic programming*

- *penalty and augmented Lagrangian methods*

- *sequential quadratic programming (SQP)*

- *interior-point methods for nonlinear programming*

64

One of the most effective and popular methods for nonlinear constrained optimization problems is sequential quadratic programming (SQP) approach [56]. SQP generates steps by determining quadratic subproblems. This approach can be applied either in line search or trust-region frameworks, and is appropriate for both small and large problems. In contrast to linear constrained Lagrangian methods which are effective when the constraints are linear, SQP methods are effective and strong when there are significant nonlinearities in the constraints of problems. In SQP method the optimization problem defined by Eq. (4.2) is modeled by a quadratic programming subproblem at each iteration and the search direction is defined to be the solution of this subproblem.

Here, SQP method has been employed as gradient-based optimization algorithm. The method has been implemented through optimization toolbox of MATLAB® software.

4.3. Genetic Algorithms for Optimum Design

Genetic algorithms (GA) are stochastic search optimization methods that the decisions made are based on random number generation in most computational steps of the algorithms. The algorithms use only the function values in the search process to make progress toward an optimum solution without considering how the functions are evaluated.

The strong aspect of GA is that continuity or differentiability of the problem functions is neither required nor used in calculations. Thus, the algorithms are very general which can be employed to solve all kinds of problems (discrete, continuous, and nondifferentiable). Since genetic algorithms do not use the gradients of cost or constraint functions, the

methods are easy to apply and program. However they have two main drawbacks listed as follow [57]:

1-Even for reasonable size problems, they require a large amount of calculation.

2-There is no absolute guarantee that the obtained optimal answer is a global optimum.

The basic idea of *GA* is to start with a set of randomly generated designs in design space. By using the cost function for unconstrained problems or the penalty function for constrained problems, a fitness value is also assigned to each design. From the current set of designs, more fit members of the set are randomly selected as subset. Random processes are used to generate new designs using the selected subset of designs while keeping the size of sets fixed. The successive sets of designs have a higher probability of having better fitness values because more fit members of the set are employed to create new design set. This process is continued until a stopping criterion is satisfied [57]. Here, some important terminologies associated with the algorithm are briefly explained:

1-Population: Population is the set of design points at the current iteration. It stands for a group of designs as potential solution points. The number of designs in a population shown with N_p is also called the population size.

2-Generation: A generation is an iteration of the genetic algorithm which is performed to make progress toward an optimum solution. A generation has a population of size N_p which is referred to the number of randomly selected design points over a defined design range.

3-Chromosome: Chromosome represents a design point. Thus a chromosome is a design of the system; whether feasible or infeasible, which contains values for all the design variables of the system.

4-Gene: This term defines a scalar component of the design vector; i.e., it is the value of a particular design variable.

5- Fitness Function: The fitness function is used to represent the relative importance of a design. A higher fitness value means a better design. Although several methods have been used to define the fitness function, one may define it by using the cost function value as follows:

$$F_i = (1 + \varepsilon) f_{max} - f_i \qquad (4.3)$$

where f_i is the penalty function value for a constrained problems (cost function) for the i_{th} design, f_{max} represents the largest recorded cost (penalty) function value, and ε is a small value (here 10^{-6}) to prevent numerical difficulties when F_i becomes 0 [57].

The basic idea of a GA is to generate a new set of designs (population) from the current set in a way that the average fitness of the population is improved. The process is continued until meeting a stopping criterion or when the number of iterations exceeds a specified limit.

4.4. Optimal Design of MR Valves

The optimal solution for single-coil type of MR valves is accomplished in this section. The valve is constrained in a cylinder of radius $R = 30$ mm and height $L = 50$ mm and the bounds of design variables are assigned to be:

$$8.5mm \leq t \leq 20mm$$
$$5mm \leq w \leq 15mm$$
$$3mm \leq d_h \leq 8mm$$
$$0.8mm \leq d \leq 1.2mm$$

(4.4)

Since a small change in the valve gap size d would change the performance of the valve, a fixed gap size has been considered in previous works [15-18, 20] to simplify the optimization problem based on first order method. In the current study, the valve gap distance is treated as a design variable in all the optimization problems.

By applying RSM on FEM based results, the analytical functions (3.21) and (3.27) have been derived for H and B, respectively. Since H and B are determined by analytical functions in term of design variables, the objective and constrained functions are available in the design domain defined by Eq. (4.4). This means that it is not necessary to calculate field intensity and flux density by running FEM at each design point and they can be estimated directly by substituting design variables in their corresponding analytical functions. In current work, constrain function of the optimization problem is the magnetic flux density B in MR fluid which has to be less than 1.7 T to avoid magnetic saturation.

Although the wire diameter can be treated as a design variable but since the coil wire diameter effect is just imposed as current density in the FE modeling, and current density is defined by the applied current over the overall area of the coil, so changing the wire diameter does not change the result practically. Nonetheless, Nguyen et al. [20] proved that optimal solution does not depend on the wire diameter and it is not necessary to consider the wire diameter as a design variable in optimal design of the MR valve.

Considering this, here the coil wires is not taken as design variables and it is sized at 24-gauge (diameter = 0.5106 mm) and the maximum allowable current of the wire is considered to be 3 A. The coil wire is made of copper whose relative permeability is assumed to be equal to that of free space, $\mu_c = 1$. It is noteworthy that the piston-shaft area is kept unchanged ($A_s = \pi R_s^2$, $R_s = 10$ mm) during the optimization process. In volume constrained optimization problem the radius of piston area is equal to valve radius R which is set as $R=30$ mm.

In this section the optimal design of MR valve to optimize damping force, valve ratio and inductive time constant are presented respectively. Since, the mathematical formulation and thus the corresponding optimization of valve ratio and dynamic range are the same, only the first one is studied in present study.

As discussed earlier in this chapter, in order to develop a comprehensive optimization of MR valve for vehicle suspension application, it is necessary to consider conflicting design objectives. Ride comfort and suspension travel are two most important conflicting performance indexes. A high damping force is required to reduce the suspension travel. To improve ride comfort a small valve ratio is desired because it results in low viscous damping. On the other hand, for improving controllability of the suspension system a fast time response is desired. Thus a multi- objective function must be formulated that considers all the three mentioned performance criteria. Considering this, a multi-objective functions which includes all concerned performance indexes may be established as follows:

$$OBJ = \alpha_F \frac{F_{MR,r}}{F_{MR}} + \alpha_d \frac{\lambda}{\lambda_r} + \alpha_T \frac{T}{T_r} \qquad (4.5)$$

The difference between this objective function with the one proposed in [18] which has been presented by Eq. (4.1), is that here the valve ratio λ is taken as objective function instead of dynamic range λ_d. It has been discussed in introduction part of this chapter that the values of weighting factors α_F, α_d and α_T are selected in optimization problem based on related application.

In this section, the optimal geometric dimensions of the MR damper to minimize the above mentioned multi-objective function with different weighting factors are obtained by both SQP and GA approaches. Six optimization design cases are investigated. First, the optimization design of MR valve considering damping force, valve ratio and inductive time constant are studied individually in each separate case. Then, the optimal design MR valves considering the multi- objective function defined in Eq. (4.5) are presented. Thus, the following optimal design case studies are accomplished:

Case 1: The objective of the optimization is to maximize the MR damping force

Case 2: The objective is to minimize the valve ratio of the MR valve

Case 3: The objective is to minimize the inductive time constant is solved

Case 4: The objective is to optimize the MR valve for suspension systems especially designed for uneven roads.

Case5: The objective function is to simultaneously optimize the damping force, valve ratio and inductive time constant.

Case 6: The objective is to optimize the MR valve in order to improve ride comfort.

4.4.1. Case 1

The mathematical presentation of the problem is as follow

$$Minimize \quad \frac{F_{MR,r}}{F_{MR}} \quad Subjected\ to\ B \leq 1.7T \qquad\qquad (4.6)$$

Lower and upper bonds on the design variables are defined in Eq. (4.4). The problem is solved with both SQP and GA. For the SQP approach, initial points must be given to optimization procedure. Since the optimal solution of the problem is depended on the location of chosen initial points, thus, in order to avoid trapping in local optima and as a result losing the potential global solution, 500 random initial points are generated and optimization is done for all these initial values and the best result is chosen as global solution. More discussion on the number of random points is given in following sections. In addition, the optimization problem is solved by GA to validate the solution. The GA solution is performed in MATLAB® Software. For choosing the proper number of population for GA to initiate the solving procedure, some numerical experiments have been done. According to our experiments, choosing 2000 and 5000 number of populations gives the same results. It is noted that raising the number of population increases the computation time drastically, but since the GA is a non-mathematical methods so in the developed program for GA, the population is taken as 5000 to enhance the probability of approaching to the global optimum results. It is noted that, the numbers of initial random points of SQP approach and initial population of GA are kept fixed in all optimization cases and the discussion regarding their values will be presented in Section 4.4.4 in detail. Moreover, the tolerances for both of feasibility with respect to nonlinear constrained and cumulative change in fitness function values are set to 1e-8. The results of both methods for Case 1 optimization are presented in Table 4-1.

71

Table 4-1: Optimal design of MR valve to maximize damping force

Design parameters (mm)			Damping force, valve ratio and inductive time		
Reference (mm)	Optimal(SQP) (mm)	Optimal (GA) (mm)	Reference	Optimal(SQP)	Optimal (GA)
$t=15$	$t=20$	$t=20$	$F_{MR}=821.78$ N	$F_{MR}=1392.34$N	$F_{MR}=1044.61$ N
$w=8$	$w=13.1719$	$w=14.3763$	$\lambda=0.0329$ N/N	$\lambda=0.0399$ N/N	$\lambda=0.0255$ N/N
$d_h=5$	$d_h=6.3563$	$d_h=4.7023$	$T=59.13$ ms	$T=81.39$ ms	$T=71.67$ ms
$d=1$	$d=0.8$	$d=1$	$OBJ=1.0000$	$OBJ=0.5902$	$OBJ=0.7867$

As it can be realized, although the results of GA is close to those of SQP, but the latter approach provides better results. To explain this, it is noted again that GA is a stochastic search optimization method which does not guarantee that the obtained result is a global solution; however, the results of GA are close to the global optimum point. While, SQP is a mathematical gradient based method and with 500 number of random initial points spread through the entire design space the true global solution has been caught. To validate this, the optimal geometrical dimensions found by GA were given to SQP program as an initial point. It is found that the SQP approaches to the same optimal results found before.

The optimal design of present work is also compared with similar study which has been done on the same class of MR damper which has $L=50mm$ and $R=30mm$. Nguyen et al. [16] studied the optimization of MR damper to maximize the yield stress pressure drop of the MR damper. It is well known that the pressure drop of the MR damper is related to the MR damper force as [16]:

$$F_{MR} = \left(A_p - A_s \right) \Delta P_y \qquad (4.7)$$

in which pressure drop due to the yield stress of MR damper is

$$\Delta P_y = \frac{2ct}{d}\tau_y \tag{4.8}$$

The above values in the obtained optimal design are $c=2.2498$, $t=20$ mm, $d=0.8$ mm and $\tau_y=49.27$ kPa which gives the pressure drop of $\Delta P_y=55.43$ bar. This value shows 48.60% increase in yield stress pressure drop compared with $\Delta P_y =37.30$ bar reported by Nguyen et al. [16]. Even the optimal design found by GA provides $c=2.1815$, $t=20$ mm, $d=1$ mm and $\tau_y=47.66$ kPa. Which yield $\Delta P=41.58$ bar. This value is also about 11.47% larger than the one reported in Ref. [16].

4.4.2. Case 2

The mathematical presentation of the optimization problem for this case can be stated as:

$$Minimize \ \ \frac{\lambda}{\lambda_r} \ \ Subjected \ to \ B \leq 1.7T \tag{4.9}$$

Again side constrains are those stated in Eq. (4.4). Here, also the optimization procedure has been conducted using both SQP and GA methods with the same considerations of optimal design Case 1. The result of the both optimization methods are presented in Table 4-2.

Table 4-2: Optimal design of MR valve to minimize valve ratio

Design parameters (mm)			Damping force, valve ratio and inductive time		
Reference (mm)	Optimal(SQP) (mm)	Optimal (GA) (mm)	Reference	Optimal(SQP)	Optimal (GA)
$t=15$	$t=20$	$t=20$	$F_{MR}=821.78$ N	$F_{MR}=850.43$ N	$F_{MR}=850.43$ N
$w=8$	$w=15$	$w=15$	$\lambda=0.0329$ N/N	$\lambda=0.0171$ N/N	$\lambda=0.0171$ N/N
$d_h=5$	$d_h=3$	$d_h=3$	$T=59.13$ ms	$T=70.01$ ms	$T=70.01$ ms
$d=1$	$d=1.2$	$d=1.2$	$OBJ=1.0000$	$OBJ=0.5190$	$OBJ=0.5190$

As it can be realized in this special case, both SQP and GA methods give exactly the same optimal results. The geometric optimal design of MR damper constrained in

H=50 mm and R=30 mm is also obtained by Nguyen et al. [15] to minimize valve ratio. The comparison of the results is provided in Table 4-3.

Table 4-3: Optimization results for Case 2

Optimal results of present work	Optimal results reported in Ref. [15]
$t=20$	$t=17.23$
$w=15$	$W=1.78$
$d_h=3$	$d_h=7.43$
$d=1.2$	$d=1$
$\lambda=0.0171$ N/N	$\lambda=0.033$ N/N

As Table 4-3 shows, the valve ratio based on our optimal design is 48% lower than the reported in Ref. [15].

The reason of such a difference may be attributed to the employment of different optimization approach. In Ref. [15], the optimization procedure is constructed by using golden section algorithms and local quadratic fitting techniques which are first order methods. Also in the optimization problem definition, for the w, the range of 5-15 mm has been considered while the reported optimal value for w in Ref. [15] is 1.78 mm which is out of the range.

4.4.3. Case 3

The mathematical presentation for this case is

$$Minimize \quad \frac{T}{T_r} \quad Subjected\ to\ B \leq 1.7T \tag{4.10}$$

where the same side constraints as Eq. (4.4) have been considered. Again, the optimization procedure is accomplished by both SQP and GA methods and results are provided in Table 4-4.

Table 4-4: Optimal Design of MR valve to Minimize Inductive Time Constant

Design parameters (mm)			Damping force, valve ratio and inductive time		
Reference (mm)	Optimal(SQP) (mm)	Optimal (GA) (mm)	Reference	Optimal(SQP)	Optimal (GA)
$t=15$	$t=20$	$t=20$	$F_{MR}=821.78$ N	$F_{MR}=438.21$ N	$F_{MR}=569.29$ N
$w=8$	$w=6.0417$	$w=5.8951$	$\lambda=0.0329$ N/N	$\lambda=0.0331$ N/N	$\lambda=0.0438$ N/N
$d_h=5$	$d_h=3$	$d_h=3$	$T=59.13$ ms	$T=17.61$ ms	$T=18.77$ ms
$d=1$	$d=1.1189$	$d=1$	$OBJ=1.0000$	$OBJ=0.2592$	$OBJ=0.3174$

As the Table 4-4 shows, there is minor difference between the optimal results of SQP and GA. As it was mentioned, although the GA can find the optimal solution close to the global optimum solution, but SQP method that utilizes 500 randomly initial points is most probably able to capture the true global optimal solution. This is due to proper numbers of initial points which are spread over the design domain. It is noted that the SQP approach guarantees to find global optima when the selected initial point is located in neighborhood of the global optima.

The only reported research on optimization of inductive time constant in this class of MR valve (which has $L=50$ mm and $R=30$ mm) is presented in Ref. [20] which reports inductive time constant of 40 ms at optimal configuration. This value is about 53% higher than $T\approx18$ ms obtained in this study.

4.4.4. Case 4

The optimization of MR valve utilized in suspension systems which are especially designed for uneven roads is performed in this case. Thus a multi objective function is in the form of Eq. (4.5) with weighting factors of $\alpha_F = 0.5$; $\alpha_d = 0.2$; $\alpha_T = 0.3$ as suggested by Ref. [17]. Again similar constrain function ($B\leq 1.7$) and design variable domain of previous cases have been considered.

As mentioned before, in SQP method the initial point may have a significant influence on the final answer of optimal variables. Figure 4-1 shows the trend of objective function in SQP approach starting with different initial points for this case of optimization.
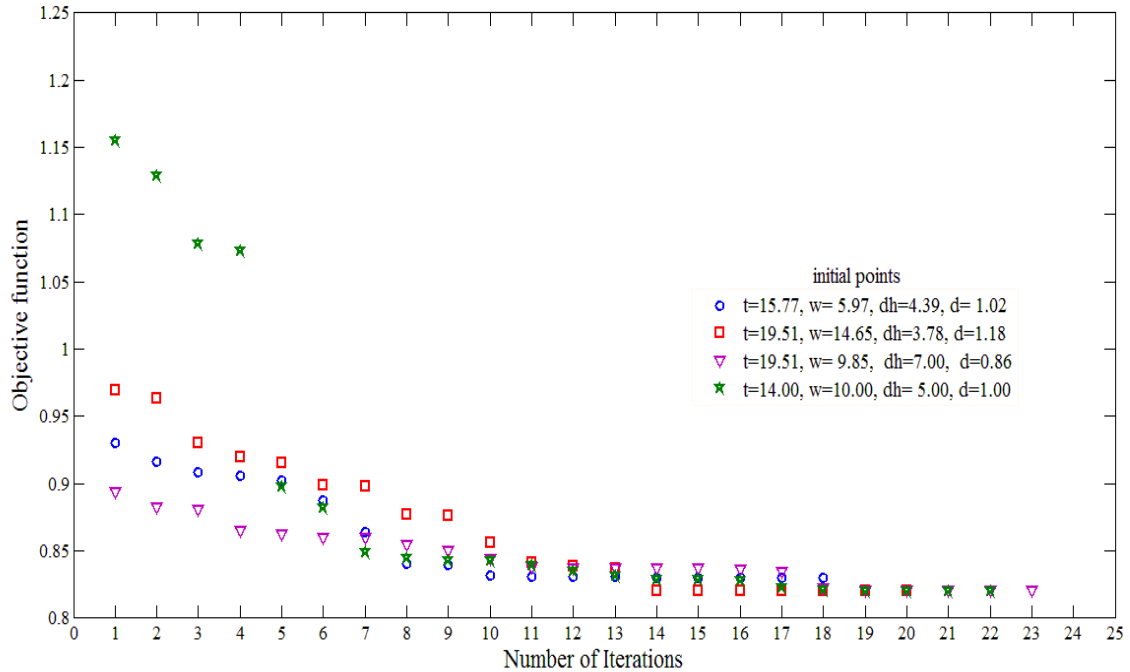

Figure 4-1: Iteration history for objective function in Case 4

As the figure shows, the optimal values are completely depend on the initial values. Thus selecting the initial vales which are in the vicinity of a locally optimal point prevents reaching the global optimal solution. To overcome this problem, a MATLAB® program has been developed to generate random points across the whole specified design space presented in Eq. (4.4). Then the optimization problem is solved for each generated initial points. Finally, the optimal objective functions obtained from each initial point are compared and minimum values with corresponding geometrics values are selected. Increasing the number of random points will increase the chance to catch the global optimal solution. It has been found that increasing the number of random points after

some limits does not change the accuracy of the obtained optimal solution. Therefore, the number of random points in SQP approach can be analyzed as a parameter. For better clarification, the optimal objective functions versus the number of random points are given in Table 4-5. As it can be realized, 500 initially generated random points provides the global optimal solution.

Table 4-5: The effect of the number of random points on the objective function value in SQP optimization

Number of Random points	1	10	100	500	1000
Objective Function	0.9708	0.8504	0.8258	0.8202	0.8202

To check the optimization result obtained by SQP approach, a genetic algorithms based optimization program is also developed in MATLAB to solve the optimization problem. As mentioned before, for the population of GA, same study has been done and found that 2000 population is enough to catch a result which is close enough to global optimal solution. The results of the numerical experiment on the population size of the GA are provided in Table 4-6. Since the GA is not a mathematic based solution, to increase the probability of finding the global optimal solution 5000 number of population is used.

Table 4-6 : The effect of the population size on the objective function value in GA

population size	1000	2000	5000
Objective Function	0.8732	0.8488	0.8488

It must be noted that the tolerance value of 1e-8 is selected for feasibility with respect to nonlinear constrains in the SQP method and cumulative change in the fitness function value in the GA method. It is noted that these parameters are assumed in optimization procedures of all six cases.

The obtained optimal values for Case 4 are presented in Table 4-7.

Table 4-7: Optimal design of MR valve for Case 4

Design parameters (mm)			Damping force, valve ratio and inductive time		
Reference (mm)	Optimal(SQP) (mm)	Optimal (GA) (mm)	Reference	Optimal(SQP)	Optimal (GA)
$t=15$	$t=20$	$t=20$	$F_{MR}=821.78$ N	$F_{MR}=1194.69$ N	$F_{MR}=925.12$ N
$w=8$	$w=9.5160$	$w=11.5843$	$\lambda=0.0329$ N/N	$\lambda=0.0406$ N/N	$\lambda=0.027$ N/N
$d_h=5$	$d_h=3$	$d_h=3$	$T=59.13$ ms	$T=45.10$ ms	$T=47.37$ ms
$d=1$	$d=0.806$	$d=1$	$OBJ=1.0000$	$OBJ=0.8202$	$OBJ=0.8488$

The results show that using randomly selected initial points; the SQP approach was able to catch the global optimum point while GA terminates prematurely at a point in the neighborhood of global optimum solution.

As it can be realized from Table 4-7, the optimal results obtained by GA and SQP for t and d_h are exactly the same. Figure 4-2 shows the variation of the objective function versus w and d assuming that t and d_h are fixed at their optimal values, 20 mm and 3 mm; respectively, according to Table 4-7.
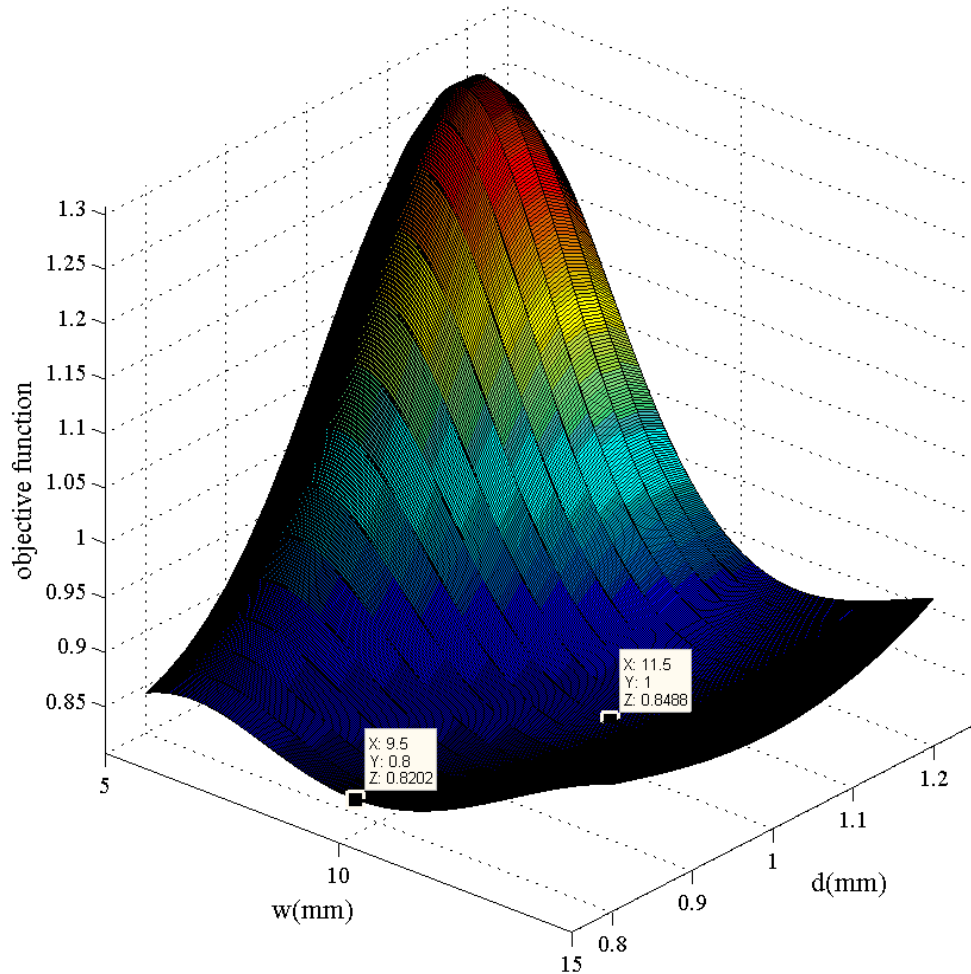
Figure 4-2: Objective function ($\alpha_F = 0.5$; $\alpha_d = 0.2$; $\alpha_T = 0.3$) versus d and w

It can be easily seen that at w=9.5 mm and d=0.8 mm, the objective function reaches to its global minimum value which is 0.8202. This exactly confirms the optimal results caught by the SQP approach. At w=11.5843 mm and d_h=3 mm, the objective function is 0.8488 with is the optimal results generated by GA.

The above observation, confirms that with adequate randomly generated points, SQP is capable to accurately capture the global minimum point while GA due to its stochastic nature is not really capable of that. In general GA approach terminates prematurely at true vicinity of global optimum solution.

4.4.5. Case 5

The design optimization of MR valve with considering a multi-objective function in the form of Eq. (4.9) with equal weighting factors of $\alpha_F = \alpha_d = \alpha_T = 1/3$ is studied in this case. Again similar constrain function ($B \leq 1.7$) and side constrains defined in Eq. (4.4) have been considered. The objective is to optimize the damping force, valve ratio and inductive time constant simultaneously. The optimal results fund by SQP and GA are presented in Table 4-8.

Table 4-8: Optimal design Case 5

Design parameters (mm)			Damping force, valve ratio and inductive time		
Reference (mm)	Optimal(SQP) (mm)	Optimal (GA) (mm)	Reference	Optimal(SQP)	Optimal (GA)
$t=15$	$t=20$	$t=20$	$F_{MR}=821.78$ N	$F_{MR}=742.90$ N	$F_{MR}=742.90$ N
$w=8$	$w=5$	$w=5$	$\lambda=0.0329$ N/N	$\lambda=0.022$ N/N	$\lambda=0.022$ N/N
$d_h=5$	$d_h=6.0908$	$d_h=6.0908$	$T=59.13$ ms	$T=39.51$ ms	$T=39.51$ ms
$d=1$	$d=1.2$	$d=1.2$	$OBJ=1.0000$	$OBJ=0.8157$	$OBJ=0.8157$

As it can be realized, both SQP and GA methods give exactly the same optimal results in this special case.

4.4.6. Case 6

In this case the optimization is conducted in order to design the MR valve to improve ride comfort. Thus, a multi-objective function with weighting factor of $\alpha_F = 0.2$; $\alpha_d = 0.4$; $\alpha_T = 0.4$ as suggested in Ref. [18] has been utilized. It is again noted that to improve ride comfort, the damping force due to MR fluid viscosity should be small. Therefore, a small value of valve ratio is desired. It is worth mentioning that the objective function is subjected to constrain function ($B \leq 1.7$) to avoid magnetic saturation along the valve

orifice gap. Again, the same side constrains given by Eq. (4.4) is considered. The results of optimal solution caught by SQP and GA are presented in Table 4-9.

Table 4-9: Optimal design of Case 6

Design parameters (mm)			Damping force, valve ratio and inductive time		
Reference (mm)	Optimal(SQP) (mm)	Optimal (GA) (mm)	Reference	Optimal(SQP)	Optimal (GA)
$t=15$	$t=20$	$t=20$	$F_{MR}=821.78$ N	$F_{MR}=658.58$ N	$F_{MR}=847.87$ N
$W=8$	$W=5$	$W=10.4522$	$\lambda=0.0329$ N/N	$\lambda=0.0231$ N/N	$\lambda=0.0295$ N/N
$d_h=5$	$d_h=5.1759$	$d_h=3$	$T=59.13$ ms	$T=33.89$ ms	$T=38.80$ ms
$d=1$	$d=1.2$	$d=1$	$OBJ=1.0000$	$OBJ=0.7496$	$OBJ=0.8147$

As it is realized, with adequate randomly generated points, SQP is capable to accurately capture the global minimum point. Although the results of GA is close to global optimal result found by SQP, the GA approach due to its stochastic nature terminates prematurely at true vicinity of the global optimum solution.

4.5. Sensitivity Analysis

Sensitivity analysis is conducted on the optimal design to investigate the sensitivity of the objective function with respect to perturbation on design variables of optimal solution. Sensitivity analysis is important in design to assign appropriate manufacturing tolerances for dimensions. Here, in the sensitivity analysis, the optimal design of MR valve for unpaved road design objective (Case 4) which has been provided in Table 4-7 is studied.

Figure 4-3, shows the variation of the objective function versus d in the specified design range, while $t=20$ mm, $w=9.51$mm and $d_h=3$ mm are kept constant at their optimal values.
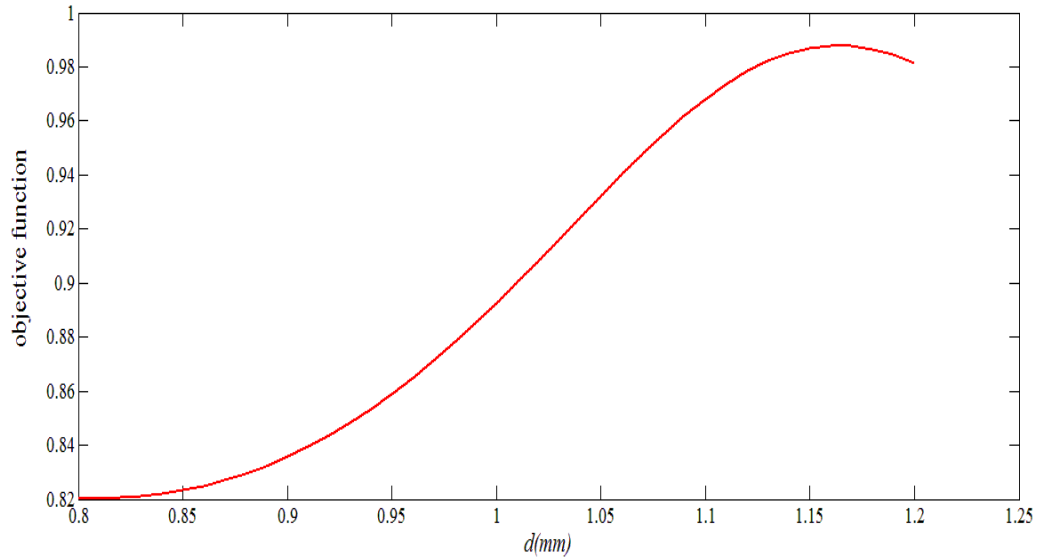
Figure 4-3: Objective function of optimal design Case 4 versus d

As it can been seen, the objective function takes its minimum values around the lower bound of design variable d which is 0.8 mm.

As mentioned earlier, for manufacturing process it is necessary to provide the allowable tolerances of each geoemtric parameter. To this end, the sensitivity analaysis of the performance function is done for each design variables. The sensitivity analysis for valve orifice gap, i.e. design variable d, has been done and it is shown in Figure 4-4. As it can be realized, in the vicinity of the optimal value (± 0.01 mm) the graph almost shows a nearly flat region. Thus considering range of ± 0.01 mm can be a good manufacturing tolerance for design variable d, as the optimal objective function is not really sensitive to the variation of d within that range.
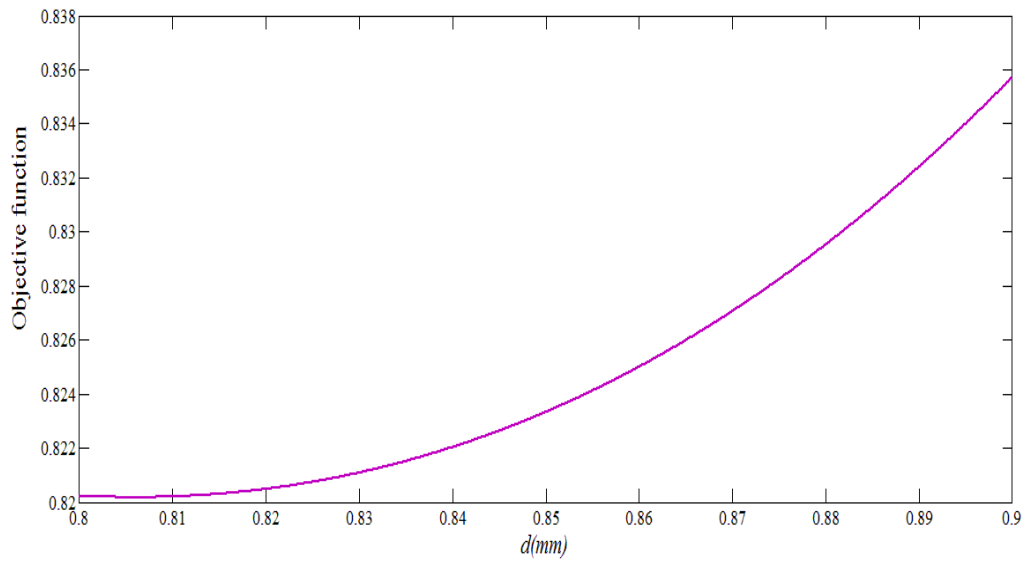
Figure 4-4: Sensitivity analysis of optimal design Case 4 for design variable d

Similarly the behavior of the objective function of optimal design Case 4 with respect to the variation of coil width w in the given design range while the other three parameters are kept constant at their optimal values (t=20 mm, d=0.8 mm and d_h=3 mm) is shown in Figure 4-5.

Figure 4-5: Objective function of optimal design Case 4 versus w

As it can be seen, the objective function takes its minimum value at around w=9.5 mm which is the optimum result predicted before by formal optimization procedure conducted by SQP and it has a smooth behavior in that vicinity.

To better visulalize the variation of the objective function with respect to the optimum solution for w, Figure 4-6 is redrawn for w varying in the range of 8-10 mm.
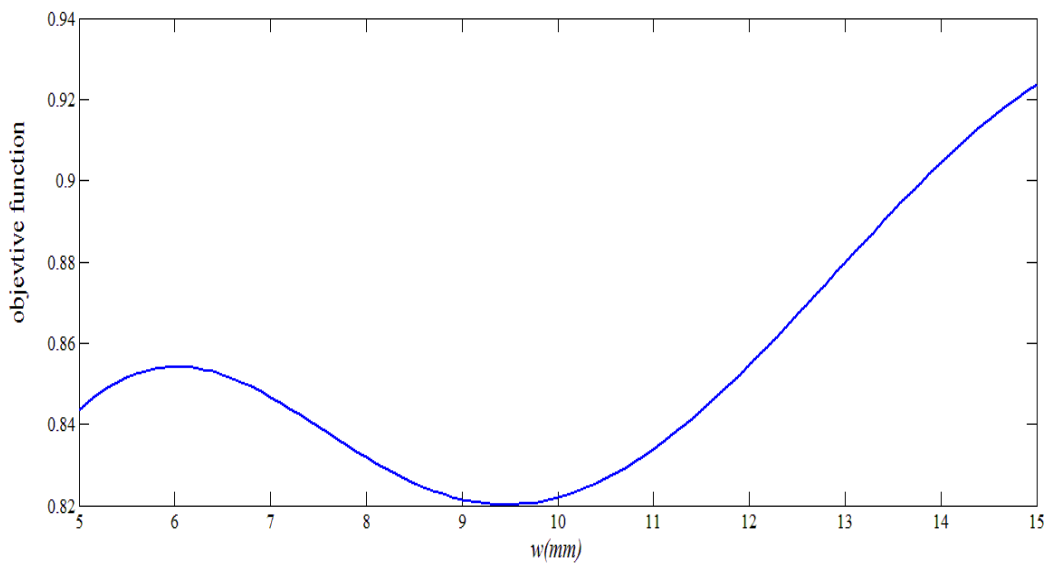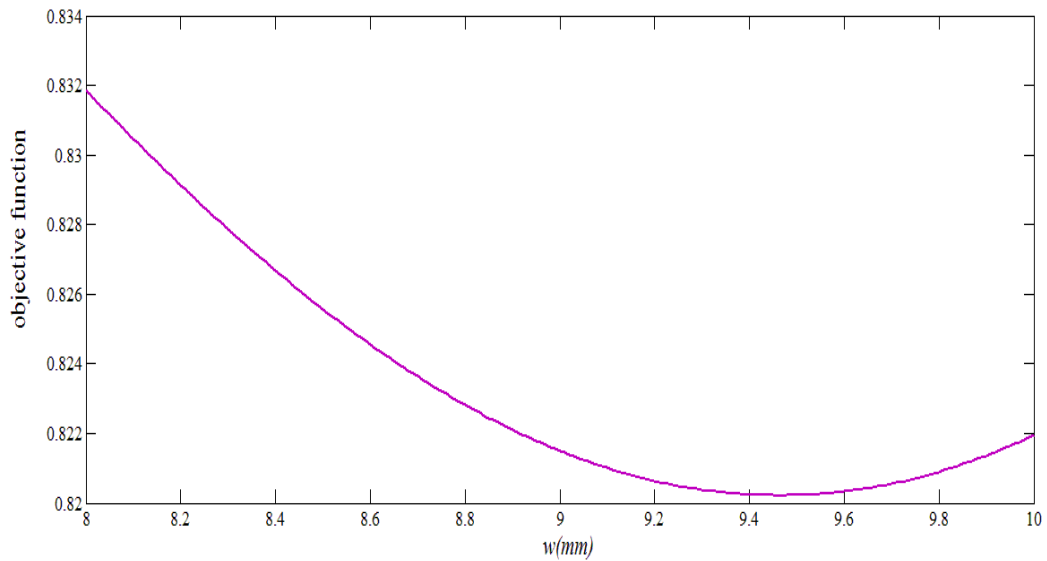

Figure 4-6: Sensitivity analysis of optimal design Case 4 for design variable w

It is clear that the objective function is not sensitive to the variation of w in the range between 9.4-9.6 mm. Thus considering tolerance of ±0.1 mm around the optimum value w=9.5 mm may be acceptable.

Similar investigation has also been done for design variables t and d_h and the results are shown in Figure 4-7 to Figure 4-10.
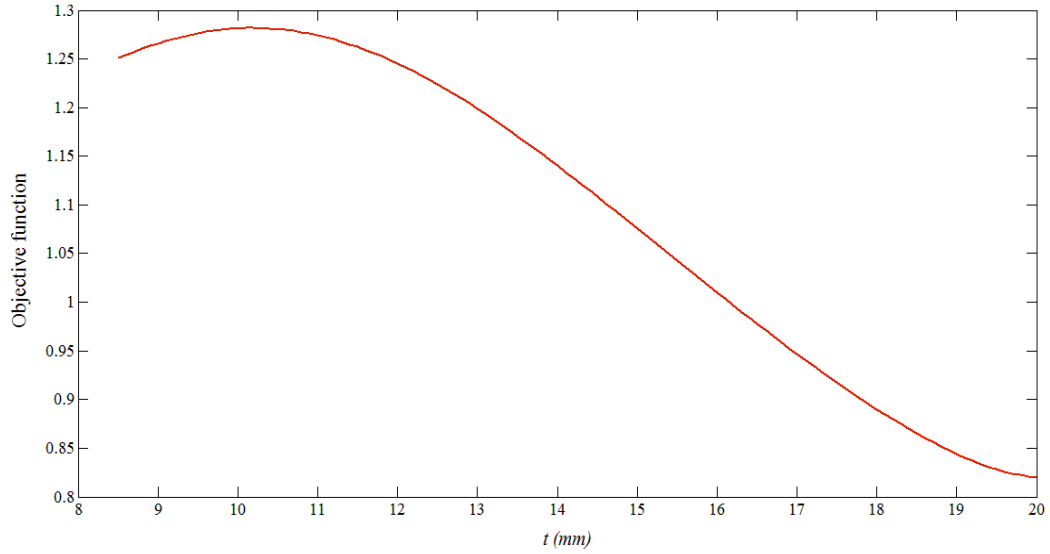
Figure 4-7: Objective function of optimal design Case 4 versus *t*

From the Figure 4-7, one can easily see that the optimal value for design variable *t* is 20 mm confirming the optimization results. Also considering the Figure 4-8, one may conclude that tolerance of ±0.05 mm may be suitable for *t* as no drastic change in objective function is visible in that neighborhood.
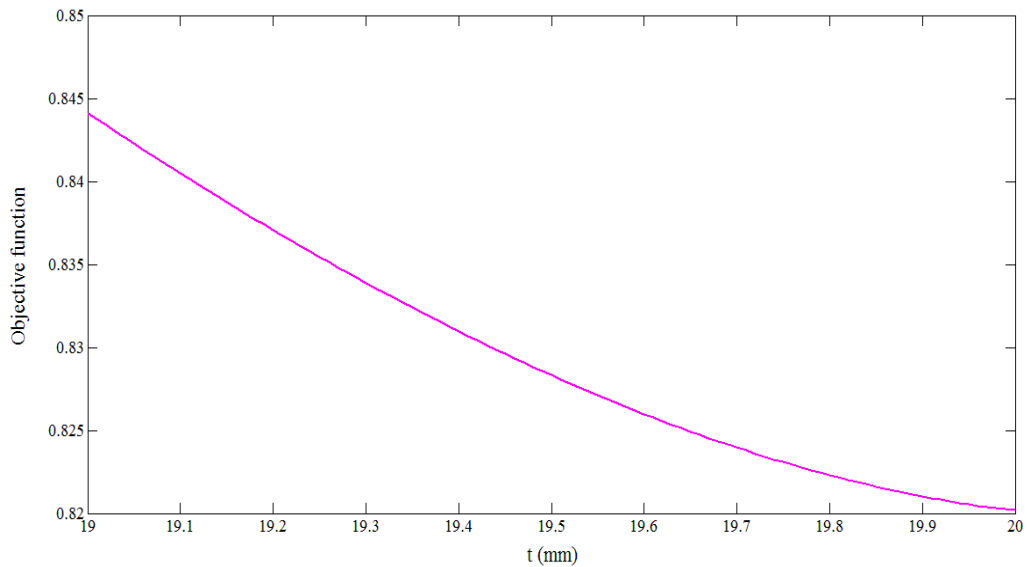
Figure 4-8: Sensitivity analysis of optimal design Case 4 for design variable *t*

Figure 4-9 and Figure 4-10 also show the variation of the same objective function with respect to design variable d_h in its entire range and in the range near its optimum solution, respectively while all other design variables are kept constant at their optimal values.
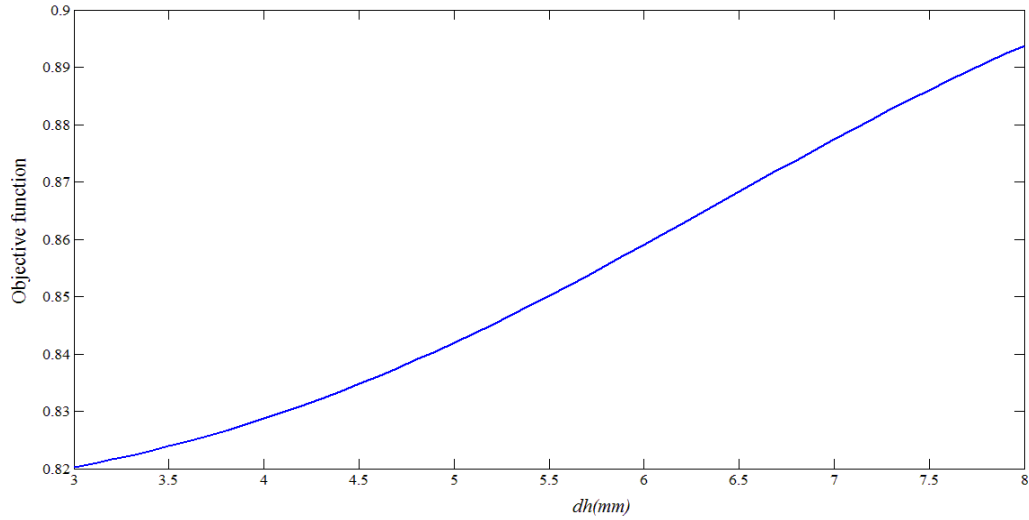

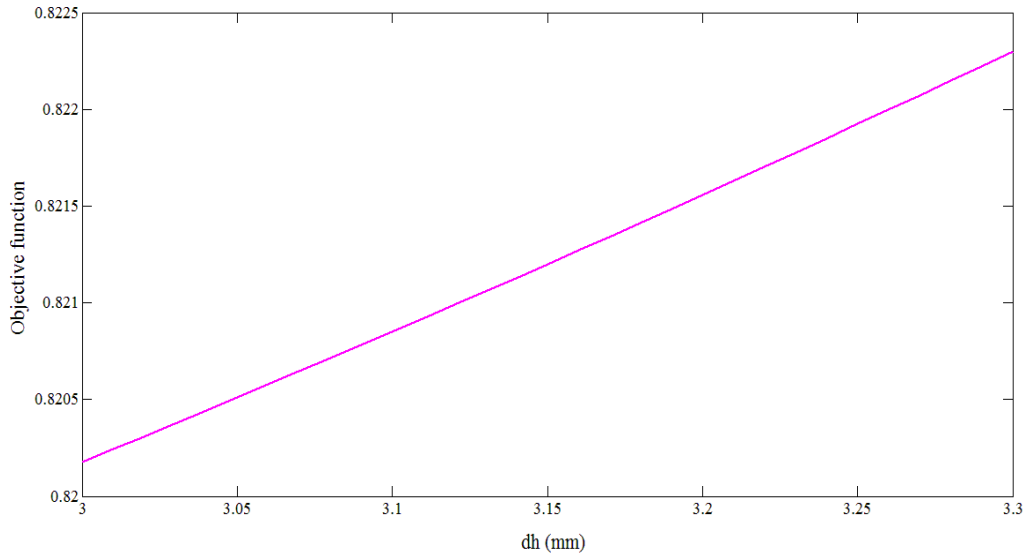Figure 4-9: Objective function of optimal design Case 4 versus t

Figure 4-10: Sensitivity analyses of optimal design Case 4 for design variable d_h

Figure 4-9 shows that minimum value for objective function occurs at d_h=3 mm. The Figure 4-10 reveals that the objective function is very sensitive to variation of d_h at its

optimal point, Thus the most precise available tolerance should be chosen for design and manufacturing with respect to this design variable.

The discussion regarding the sensitivity and suggested acceptable tolerances are summarized in Table 4-10.

Table 4-10: Design Variables Manufacturing Tolrance

Design Variable	Acceptable Tolerance
d	±0.01 mm
w	±0. 1 mm
t	±0.05 mm
d_h	Extremely sensitive to change

4.6. Conclusion

In this chapter formal design optimization approaches using both SQP and GA have been formulated to minimize the multi-objective function constructed by weighted summation of the damping force, valve ratio, and inductive time constant.

First, MR valve has been optimally designed to maximize damping force, to minimize the valve ratio, and to minimize the inductive time constant, individually. Then a multi-objective function has been established to simultaneously maximize the damping force and minimize both the valve ratio and inductive time constant for different weighting factors. It has been found that SQP can catch the global optimal solution if it has been executed on at least 500 randomly generated initial points.

One of the most important conclusions made by results is that the parameter t which presents the pole length of the MR valve is not an active design variable. It can be observed for all optimization cases the value of t is 20 mm which is the upper limit of this

design variable. This is completely in agreement with the physical perception of the problem. In fact, the magnetic field affects the MR fluid along the length of t. Thus increasing the value of t will allow the magnetic field to have more effect on the MR fluid. Therefore it is logical that in all of the optimization results, it takes the upper limit value. Also it is worth to point out that in some research works [19], pole length (t) has been also addressed as active length which shows the important role of this geometrical dimension.

The results show that the optimal values of the geometric design variables completely depend on the defined objective function. Optimal results presented in Table 4-7 to Table 4-9 reveal this fact that the weighting factors of the multi-objective functions have a great effect on the final optimal solution of the optimization problem. So designer should have a good knowledge of the vehicle dynamic as well as the road and application of the vehicle. Based on this information, proper values of weighting functions can be calculated and used in design.

The results from GA and SQP methods were presented and the values of objective functions were mentioned to compare the results of both. Although in some problems the results of the two approaches were exactly the same, it was proved that when the number of random initial points are sufficient, the SQP gives better results. Optimal results obtained by GA are typically in the neighborhood of the true optimal points.

Finally, the sensitivity analysis of optimal design of MR valve with application for uneven road ($\alpha_F=0.5; \alpha_d = 0.2; \alpha_T = 0.3$) was performed and manufacturing tolerances were presented for the design parameters.

Chapter 5 Semi-Active Control Performance of the Optimally Designed MR Damper

5.1. Introduction

Optimal design of the suspension system (optimal selection of the suspension dampers and stiffness parameters) of ground vehicles is an important practical and challenging problem which deserves special attention [31]. In this chapter semi-active control of previously optimally designed MR damper utilized in vehicle suspension system is investigated. A simple quarter-car model is considered to model the dynamic behavior of vehicle. The equation of motions are derived and then developed in state space model. A PID controller is designed for the semi-active suspension system featured by the optimally designed MR damper. The effect of the electrical current on the equivalent damping coefficient and saturation phenomenon in the MR valve is explored. In this chapter, we specifically study the optimally designed MR damper for unpaved road (optimal design Case 4) which has been optimized based on the multi-objective function with weighting coefficients of ($\alpha_F = 0.5;\ \alpha_d = 0.2;\ \alpha_T = 0.3$).

In fact, what this chapter aims at is to show the effectiveness of the optimally design damper and comparing it with the non-optimal damper. The study is performed by using

the MR damper on quarter-car models to verify the efficiency of the modeling and optimization method.

In this chapter, first the mechanical models and the corresponding equations of motion are derived for both the passive and semi-active suspension models. Industrial PID controlling system is utilized to control the vibration of system. For investigation of the active control of MR damper, the response of equivalent passive system and semi- active system are presented. To study the efficiency of the optimally designed MR damper to attenuate the vibration due to ground, its performance is compared with the performance of the initial design of MR damper.

5.2. Active Suspension Modeling

This section presents the mathematical model of a quarter car vehicle model with the MR damper. A typical active system model is first presented in which the MR damper is modeled as a force generator. Then, a nonlinear MR damper model is studied and the relationship between applied current to the damper and the generated force is described. Finally, the dynamic response of the system for equivalent passive system (when electrical current is equal to 1 Amp) and that of the semi-active one is studied.

5.2.1. Mechanical Modeling

In order to avoid dynamic complexity of the vehicle model, the ride model of the vehicle is simulated by a quarter-car model which has two degrees of freedom (DOFs) as shown in Figure 5-1.

Quarter-car model has two DOFs to define the position of the car body and the vibration caused by the wheel. Therefore, the effect of the car body orientation is eliminated. As a

result, this model may be used to study only the position of the car body and wheel in one direction. Quarter-car model is a simplified model commonly employed in many areas of the automotive industry research, including the prediction of dynamic response as well as the performance of parameter identification, optimization and control studies of ground vehicles [13, 14, 31-34, 36]. This model provides helpful information at the preliminary stage of design and creates a reliable basis for performing more accurate studies by employing more involved mechanical models [31]. The schematic view of the quarter-vehicle semi-active (AS) and passive suspension (PS) systems are shown in Figure 5-1.
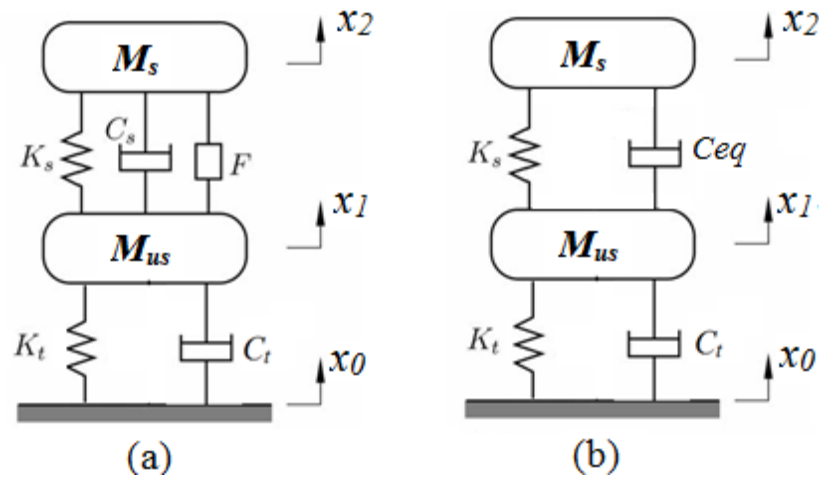

Figure 5-1: Diagram of quarter vehicle (a) semi-active suspension system and (b) equivalent passive suspension system

The definition of used parameter in the quarter car dynamic equation and their values are given in Table 5-1.

Table 5-1: Values of the parameters of quarter vehicle model

Parameters	values
Unsprung mass	M_{us}=50 kg
Sprung mass	M_s=350 kg
Tire stiffness	K_t=160000 N/m
Car spring stiffness	K_s =16000 N/m
Equivalent Damping Coefficient of AS C_{eq}	Ns/m
Passive Damping Coefficient	C_s Ns/m
Tire damping Coefficient	C_t=15 Ns/m

A force generator F represents the MR damper which is regulated by a controller to actively improve suspension performance. For a logical comparison with the passive system, the equivalent damping coefficient of the MR damper (when the applied current is 1 Amp) is used. The equivalent damping coefficient is calculated by means of Eq. (2.28) presented in Chapter 2.

5.2.2. State-Space Model

Linear differential equations are used to represent linear structural models in time domain. In order to describe the dynamic behavior of the system, the equilibrium equations could be written either in the form of degrees of freedom or in the form of the state-space system. Considering Figure 5-1, one can draw the free-body diagram for each sprung and unsprung mass and then derive the governing equation of the motions using second law of Newton as:

$$m_{us}\ddot{x}_1 + K_t(x_1 - x_0) + K_s(x_1 - x_2) + C_s(\dot{x}_1 - \dot{x}_2) + C_t(\dot{x}_1 - \dot{x}_0) + Fsgn(\dot{x}_1 - \dot{x}_2) = 0 \quad (5.1)$$

$$m_s\ddot{x}_2 + K_s(x_2 - x_1) + C_s(\dot{x}_2 - \dot{x}_1) + Fsgn(\dot{x}_2 - \dot{x}_1) = 0 \qquad (5.2)$$

where the *sgn* is the sign function which is defined as

$$sgn(\dot{x}_1 - \dot{x}_2) = \begin{cases} -1 & if\ (\dot{x}_1 - \dot{x}_2) < 0 \\ 0 & if\ (\dot{x}_1 - \dot{x}_2) = 0 \\ 1 & if\ (\dot{x}_1 - \dot{x}_2) > 0 \end{cases} \qquad (5.3)$$

In order to study the control and especially the dynamic of the system in the equivalent

passive models, it is better to describe the dynamic system in the state space. State space

is employed to reduce the order of differential equations to first order. To transform the

equations of motion of the quarter car model as defined in Eqs.(5.1) and (5.2) into a state

space format, the following state variables are introduced:

$$\begin{aligned} \tilde{x}_1 &= x_1 \\ \tilde{x}_2 &= x_2 \\ \tilde{x}_3 &= x_3 \\ \tilde{x}_4 &= x_4 \end{aligned} \qquad (5.4)$$

The state space form of the dynamic system can be written in the system of equations

described as:

$$\begin{aligned} \dot{\tilde{x}} &= A\tilde{x} + Bu + Wz \\ y &= C\tilde{x} + Du \end{aligned} \qquad (5.5)$$

in which z is utilized to define the disturbance due to the bumpy road and it is defined as

follows

$$z = \begin{Bmatrix} x_0 \\ \dot{x}_0 \end{Bmatrix} \qquad (5.6)$$

The matrix "*A*" defines the dynamic properties of the system. Matrix "*B*" represents the

actuator property which here is due to the MR damper force. The "*W*" defines the

imposing of road disturbance on the system. Matrix "*C*" is the sensor position and

properties in the vehicle. Finally, the matrix "*D*" is used to show the effect of constant force into the system which is zero in this study.

Finally considering Eqs.(5.1)-(5.6), the equations of motion of the quarter car model can be written in state space form as:

$$\dot{\tilde{x}} = \begin{bmatrix} 0 & 0 & 1 & 0 \\ 0 & 0 & 0 & 1 \\ \frac{-(K_s+K_t)}{M_1} & \frac{K_S}{M_1} & \frac{-C_S}{M_1} & \frac{C_S}{M_1} \\ \frac{-K_S}{M_2} & \frac{-K_S}{M_2} & \frac{C_S}{M_1} & \frac{-C_S}{M_1} \end{bmatrix} \tilde{x} + \begin{bmatrix} 0 \\ 0 \\ \frac{-1}{M_1} \\ \frac{1}{M_2} \end{bmatrix} F + \begin{bmatrix} 0 & 0 \\ 0 & 0 \\ \frac{-K_t}{M_1} & \frac{-C_t}{M_1} \\ 0 & 0 \end{bmatrix} z \tag{5.7}$$

Since we want to read the displacement and velocity of both masses in the output the matrix "*C*" is defined as

$$C = \begin{bmatrix} 1 & 0 & 0 & 0 \\ 0 & 1 & 0 & 0 \\ 0 & 0 & 1 & 0 \\ 0 & 0 & 0 & 1 \end{bmatrix} \tag{5.8}$$

These matrices are used to build up a program in MATLAB® to study the equivalent passive behavior of the system. Moreover, to employ the control toolbox of MATLAB® to tune the PID controller based on Ziegler-Nichols rules; it is necessary to define the system in the sate-space model.

The block diagram of the semi-active suspension system based on quarter-car model is presented in Figure 5-2, which can be use in MATLAB® control Toolbox for numerical solution.
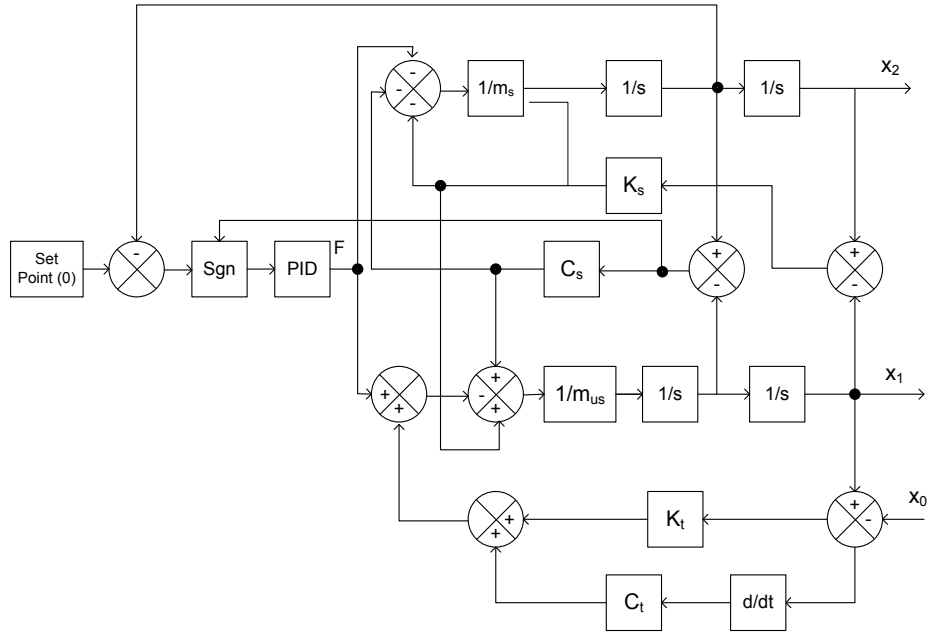
Figure 5-2: Block diagram of semi-active suspension system

Input of the system is the road displacement signal which is assumed as a pulse function. For monitoring of responses, the displacement and velocity response of unsprung and sprung masses are observed as output variables.

To generate the input force, displacement due to the road profile and its derivative are first multiplied by tire stiffness K_t and tire damping rate C_t, respectively, and then added together.

5.3. Active Control of Quarter-car Model by Using PID Controller

According to Kirchhoff's law for magnetic circuits as presented by Eq.(3.1), the magnetic field intensity is proportional to the applied electrical current I. Considering this fact, the finite element results and consequently the RSM based functions have been determined for unit current i.e. I=1 Amp. Therefore, the magnetic field intensity at any current is proportional to the result of FEM. In other words, the magnetic field intensity can be easily determined by multiplying the value of the electrical current by the results of RSM.

95

Afterward, substituting the optimal values of design variables of Case 4 in Eq. (3.21) and then substituting the result in Eq.(2.6), the shear yield stress developed in the optimal MR damper can be written as:

$$\tau = 0.3 + 67.09\,I - 29.60I^2 + 4.28I^3 \qquad (5.9)$$

Subsequently, considering Eq. (5.9) into Eq. (2.13) in Chapter 2, the MR damping force for the Case 4 optimally designed MR valve is derived as:

$$
\begin{aligned}
F_{MR} = &\left(\frac{0.0045}{0.2096\,I^3 - 1.450\,I^2 + 3.286\,I + 0.01502} + 28.4065 \right) \\
&\times \left(4.281I^3 - 29.603I^2 + 67.09I + 0.3 \right)
\end{aligned}
\qquad (5.10)
$$

It can be realized that when the current is zero, H becomes zero and F_{MR} takes its passive mode value which is the off state force of MR damper and it is equal to 8.6 N. Since the damping force presented by Eq. (5.10) is derived based on the presented geometrical dimensions of optimal design Case 4, for every other valve which has different dimensions, a similar function should be derived that exclusively expresses the damping force of that valve as a function of the applied electrical current. In other words, the coefficients of Eq. (5.10) will be changed by changing the dimensions of the valve.

Eq. (5.10) can be effectively used in the active control system in the present case. According to Eq. (5.10), the MR damper force is highly nonlinear function with respect to the applied electrical current I. As nonlinear control methods are too complicated, non model based approach is employed in present study. This means that the controller is designed based on the closed loop feedback of the dynamic system. In the considered case studies, the dynamic force is caused by the base excitation from the ground.

It is well known that the state space approach is just applicable to solve linear differential equations. Since the active system is nonlinear due to nonlinear damping force, the Simulink block diagram in MATLAB® software is directly utilized to simulate and solve the dynamic problem. The block diagram of semi-active system is shown in Figure 5-3. It is worth noting that MATLAB Simulink® solves the nonlinear problem with "*Runge Kutta*" numerical method.

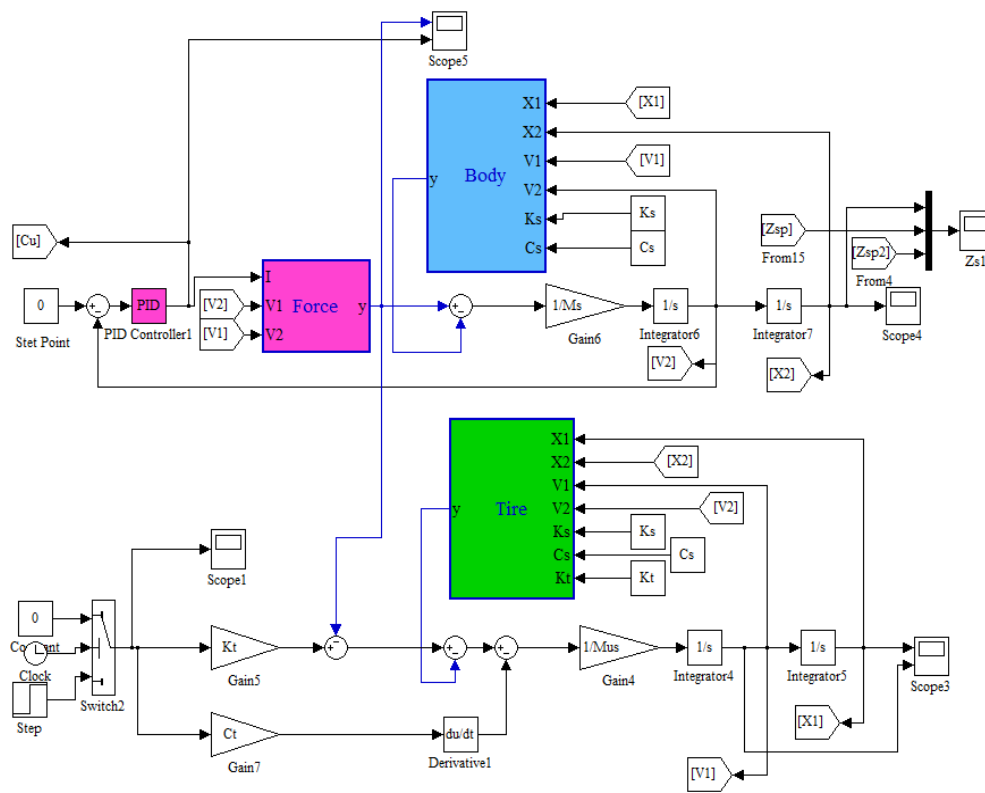Figure 5-3: Block diagram of semi-active system in MATLAB Simulink

The blue and green blocks define dynamic characteristics of body and wheel respectively. The main function of the active system is to efficiently damp the vibrations caused by road irregularities. So the closed loop controller applied electrical current to change the rate of energy dissipation of the system to make velocity of the car body oscillation

toward zero value (set point of controller). The criterion for the closed loop design is to make velocity of the sprung mass zero. It is noted that the damping force is imposed to the system by F_{MR} as an embedded function in MATLAB Simulink$^®$.

In current study PID control strategy is applied to the active system. Ziegler-Nichols rules [58] are experimentally employed to tune and determine the proportional gain K_p, integral time T_i ,and derivative time T_d of the PID controller. In this method, first the values of integral time and derivative are set as $T_i=\infty$ and $T_d=0$, respectively. Then K_p is increased from zero to a critical value K_{cr} where the output first shows sustained oscillations to a unit-step input. Thus the critical gain K_{cr} and corresponding critical period P_{cr} are found experimentally. Ziegler-Nichols recommended $K_p=0.6K_{cr}$, $T_i=0.5P_{cr}$ and $T_d=0.125$ P_{cr} for PID controller [58]. Following the mentioned instructions, the $K_{cr}=0.6$ and $P_{cr}=1s$ are found for the optimal active system. Thus K_p , T_i and T_d are determined to be 1.5, 0.5 and 0.125, respectively.

Response of the passive and semi-active systems due to the step base excitation shown in Figure 5-4 has been obtained and shown in Figure 5-5 and Figure 5-6.
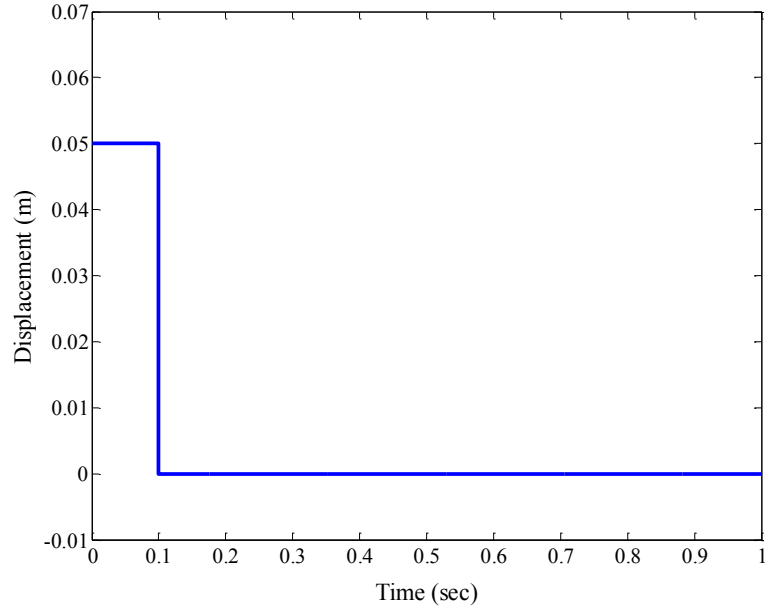
Figure 5-4: Step Base Excitation

Figure 5-5 shows the response of sprung mass of the equivalent passive system (when applied current is set to 1 Amp) and semi-active system featured by optimal MR damper.
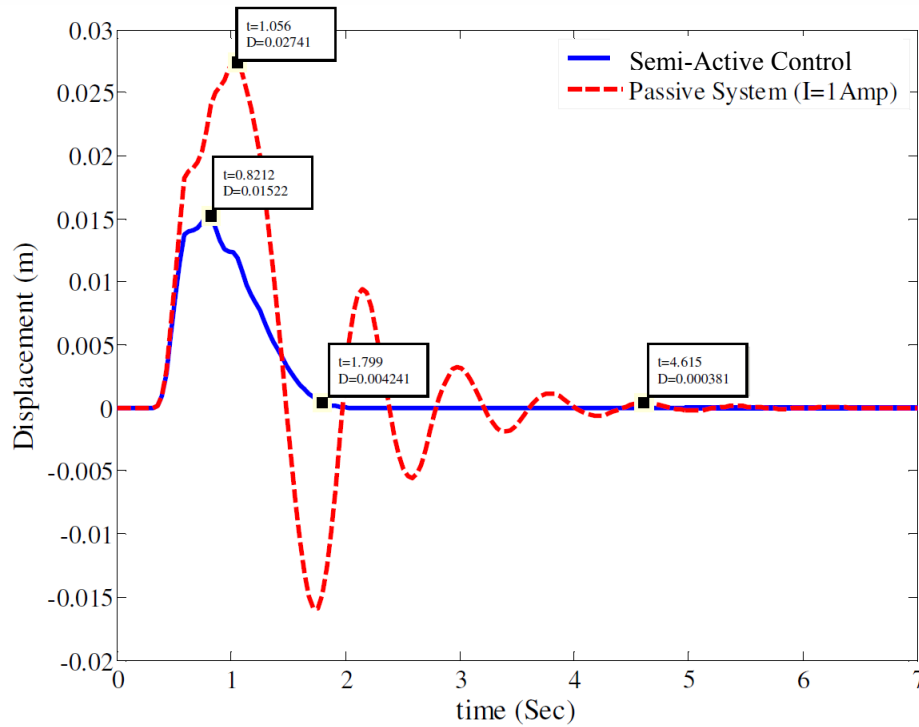

Figure 5-5: Displacement response of sprung mass for equivalent passive and semi-active systems

The most important parameters to study are overshoot (D_0) and settling time of the response. Here, the settling time (t_s) of 2% steady state error is taken as criterion. To evaluate the performance of the designed controller, the values of both parameters are demonstrated on the plot. The overshoot and settling time of the passive and semi-active responses are summarized in Table 5-2.

Table 5-2: Results of dispalcement responses of quarter vehicle model

Parameters	Passive System	Semi-Active System	Improvement
Overshoot (m)	0.02741	0.01522	44.47%
Settling Time (Sec)	4.615	1.799	61.01%

As the results show, by using a well tuned PID controller with optimally designed MR damper, a significant improvement in overshoot and settling time has been achieved. Thus, optimally designed MR damper can efficiently suppress the vibration of the sprung mass. Figure 5-6 compares the velocity response of semi-active suspension system featured by optimal MR damper and the response of the passive system.
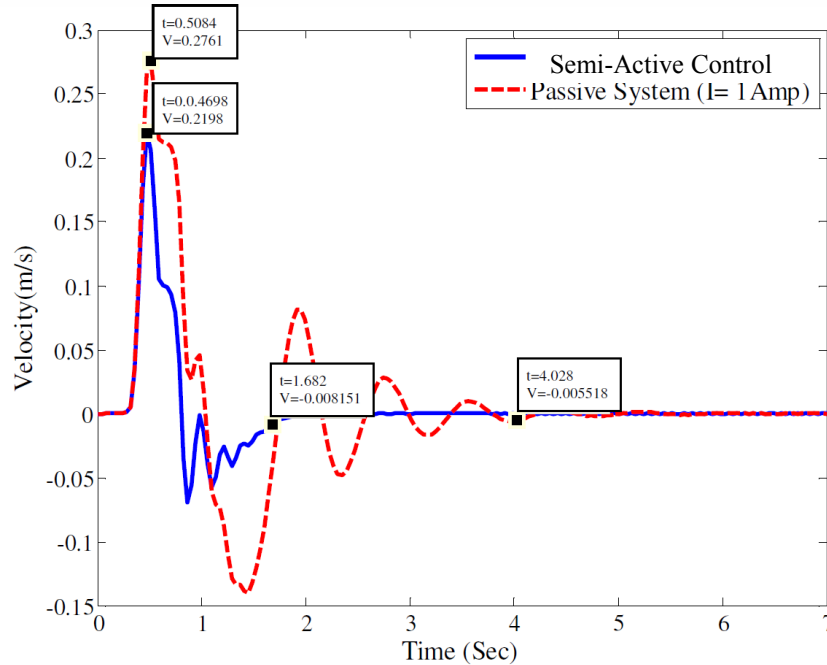
Figure 5-6: Velocity response of sprung mass for equivalent passive and semi-active systems

The overshoot and settling time of the velocity response for both passive and semi-active systems are also compaerd and presented in Table 5-3.

Table 5-3: Results of velocity responses of quarter vehicle model

Parameters	Passive System	Semi-Active System	Improvement
Overshoot (m)	0.5084	0.4693	7.69%
Settling Time (Sec)	4.028	1.682	58.24%

Results show a good improvement in the settling time of velocity of the sprung mass which is an important parameter in ride comfort and controllability. The responses follow the same trends as Karnoop [59] presented for the responses of a semi-active suspension system.

It is clearly observed that the displacement and velocity of the sprung mass are significantly reduced by employing the PID controller for the MR shock absorber. It is

101

noteworthy that for the passive system study, the equivalent passive system of the optimally designed MR damper has been used when the applied current is equal to 1 Amp. At this current, the equivalent damping coefficient is equal to 1.8092e4 Ns/m which is larger (an order of magnitude) than common damping coefficients. Force and corresponding applied electrical current of optimal MR damper subjected to the defined step function versus time are plotted in Figure 5-7 and Figure 5-8, respectively. The maximum value of force is found to be 730 N which is correlated to the electrical current of 0.33 *Amp* which is well below the saturation current of the valve.
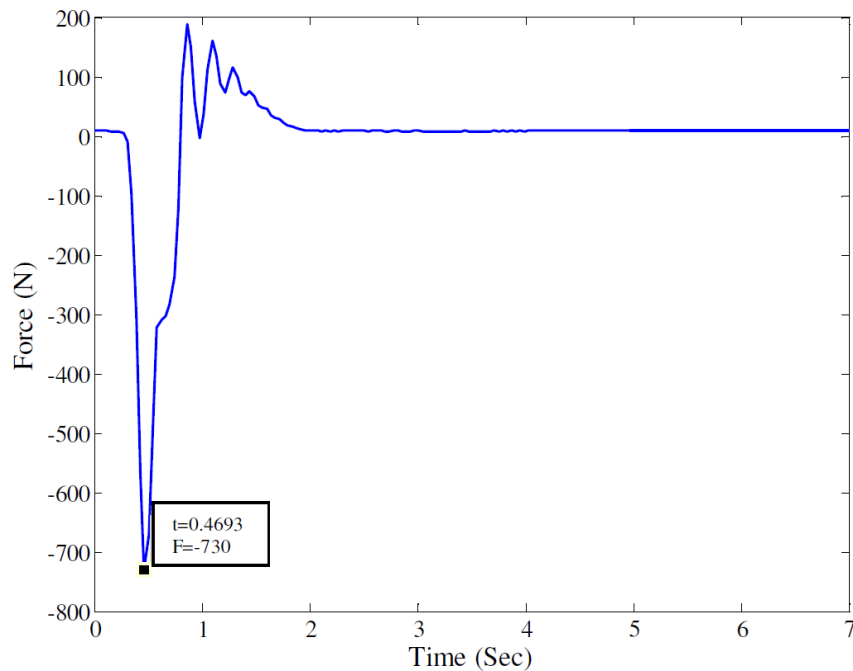
Figure 5-7: Force of optimal MR damper versus time
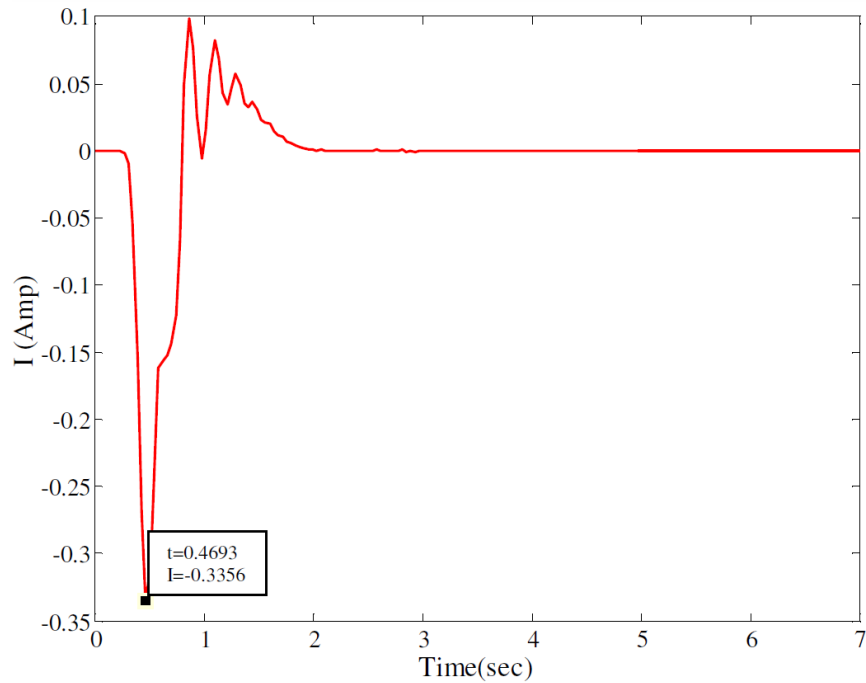
Figure 5-8: Applied electrical current to optimal MR damper versus time

5.4. Equivalent Damping Coefficient Approach

This approach is a method to compare the performance of systems with different damping characteristics. This is well-known that this approach is derived based on equal energy dissipation in the system and it is not able to simulate the actual response of the systems. The equivalent damping coefficient has been presented by Eq. (2.28) for MR dampers. In this section first the effect of the applied electrical current on the equivalent damping coefficient MR valves is studied. Then, this approach is used to compare the responses of the two types of the optimally designed and initial designed dampers.

5.4.1. Effect of the Electrical Current on the Equivalent Damping Coefficient

The equivalent damping coefficient of optimally designed and initial design MR valve as a function of applied current are calculated by Eq. (2.28) and results are plotted in Figure 5-9.
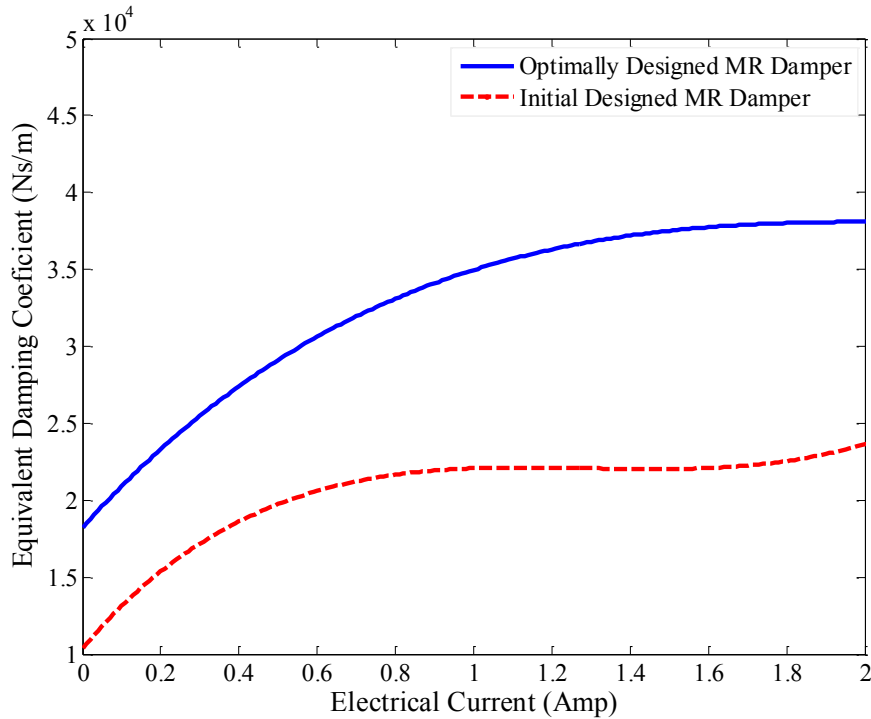
Figure 5-9: Equivalent Damping Coefficient versus Electrical Current

This figure clearly depicts the effect of saturation phenomenon on the performance of the MR valve. As it can be seen, further increase of applied electrical current than a specific value does not considerably change the equivalent damping coefficient. This is due to the magnetic saturation phenomenon in the MR fluid. Thus in design, it is recommended to design an MR valve far away from saturation point to have the maximum controllability. Figure 5-9 also shows that the saturation of initial MR valve is happened at around 1.05 Amp while the saturation of optimally designed MR valve is around 1.90 Amp. Thus, the optimized geometry of MR valve provides wider range of performance. Moreover, in all

range of allowable applied electrical current, the optimally designed MR valve gives considerably larger damping coefficients.

5.4.2. Comparison of Optimal and Non-optimal MR dampers

As stated before, the PID controller is experimentally designed based on the response of the dynamic model where the MR damper force which is formulated by nonlinear function Eq. (5.10) has a significant effect on its tuned parameters. In other words, comparing the results of two semi-active controllers, one featured by optimal MR damper and the other one with initial design, is not a proper evaluation of their performance. As each system has different dynamic model and needs different controller to actively control it, for a comparative study the effect of the controller must be eliminate.

To overcome this problem, the equivalent passive systems of the two semi-active systems are introduced and compared. In this order, first the equivalent damping coefficients given by Eq. (2.28) are calculated for both systems and then the response of two equivalent passive systems are plotted and compared. Equivalent passive systems of optimally designed and initial design MR damper when they are exposed to current excitation 1 Amp are determined and the equivalent damping coefficients are obtained. The results are provided in Table 5-4.

Table 5-4: Shear Stress and Equivalent Damping Coeficients of the MR valves

Parameters	Initial Design	Optimal Design
Magnetic Filed Intensity (kA/m)	284.72	159.75
Yield Stress Shear (kPa)	50.08	42.07
Equivalent Damping Coefficient (Ns/m)	1.2005e4	2.0194e4

The presented results in Table 5-4 show the significant effects of the optimal geometrical dimensions of the valve on the equivalent damping coefficient. Although the value of

magnetic field intensity and as a result the yield stress of MR fluid is higher in initial design MR damper, the equivalent damping coefficient of the optimally designed MR damper is 40% more.

Having the values of equivalent damping coefficients for both systems, we can now find their time responses. The result of such analysis will be more unbiased because the effects of PID controller on the results have not been imposed to the responses. Displacement and velocity responses of sprung mass for equivalent passive systems of semi-active systems with current of 1 Amp featured by optimal and non-optimal MR dampers are plotted in Figure 5-10 and Figure 5-11, respectively.
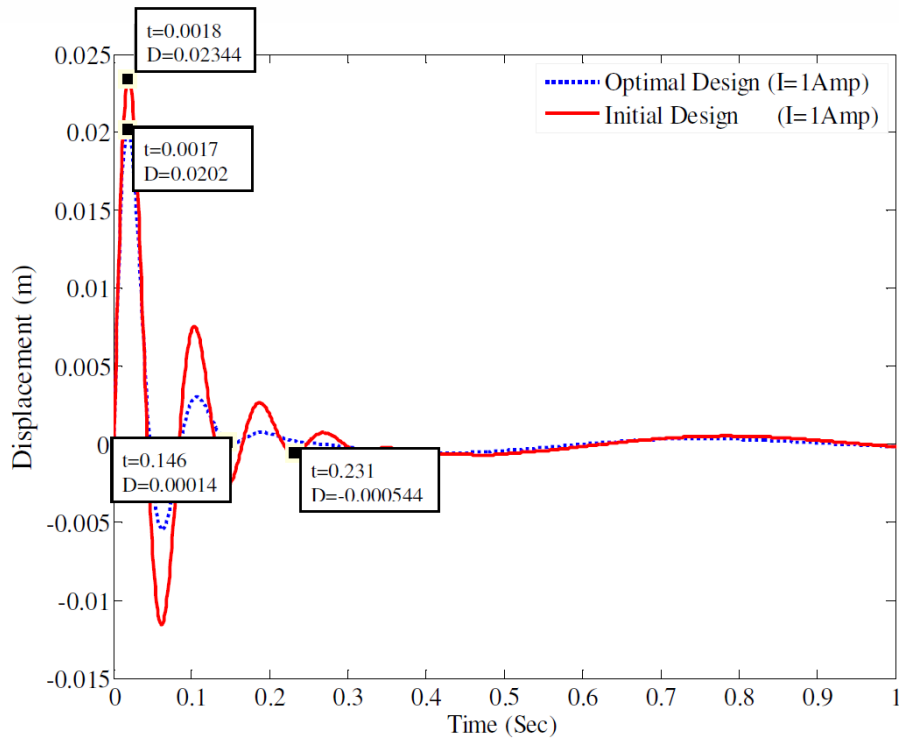
Figure 5-10: Displacement response of sprung mass for equivalent passive systems
(I =1Amp)
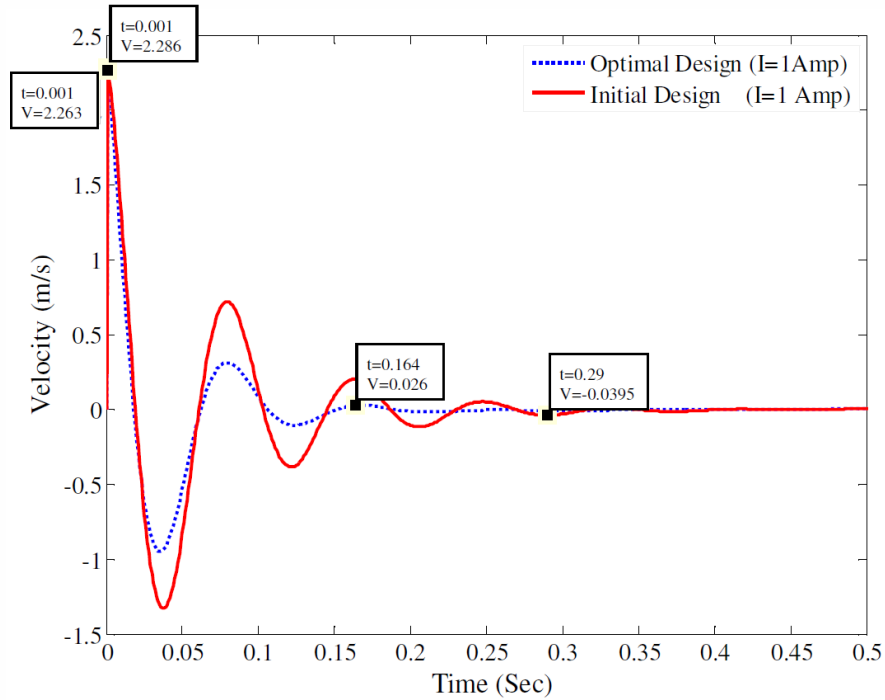
Figure 5-11: Velocity response of sprung mass for equivalent passive systems (I=1Amp)

Results for overshoot and settling time of the displacement and velocity responses are summarized in Table 5-5.

Table 5-5: Displacement and velosity responses of equivalent passive systems

Parameters	Displacement Response			Velocity Response		
	Initial	Optimal	Difference	Initial	Optimal	Difference
Overshoot(m)	0.0234	0.0170	27.3%	2.286	2.263	1.0%
Settling Time(Sec)	0.231	0.146	36.8%	0.164	0.290	43.4%

As results show, the overshoot of optimal design is significantly less than non-optimal design while the settling time is less. The results show that the vibration of the sprung mass is better suppressed by employing the optimized shock absorber than using the initial one.

107

5.5. Conclusion

In this chapter, a PID controller was designed for the chosen optimal MR damper. It was shown that optimal MR damper controlled by PID controller can reduce the displacement overshoot of sprung mass by 44.47%; and the settling time of the system by 61.01% comparing to equivalent passive damper. Applied current to MR valve and corresponding force were plotted versus time. Maximum value of applied electrical current is 0.33 Amp for actively control of optimal MR damper which is far away from the maximum allowable electrical current.

It was discussed that comparing two MR dampers with PID controllers is not possible because the performance of the controllers also affects the results. Therefore, to compare the performance of the optimal MR damper with a non-optimal one, equivalent passive systems have been developed.

It was shown that the optimal designed MR valve has higher damping coefficients and the saturation of the magnetic flux density is occurred at higher electrical current.

Finally, it has been investigated that the optimally designed MR damper can suppress the vibration of the sprung mass more effectively than the initial designed MR damper.

Chapter 6 Conclusion and Future Works

6.1. Introduction

In this thesis a comprehensive study of MR valve and dampers has been presented. Sets of design variables were selected by I-optimal design of experiments. In each designed set the design variables were determined.

Finite Element Method in commercial software ANSYS has been utilized to solve the magnetic field intensity along the valve orifice gap for geometries defined by each set of design variables. Since the magnetic field intensity and magnetic flux density are not constant along the length of the orifice, the average values have been calculated by integration on a line through the path. Then the Analytical functions were mapped to the results of FEM analysis using the response surface method.

The analytical expressions of the magnetic field intensity and magnetic flux density for any design option in the defined design space were presented. These analytical equations provide a unique tool to define objective functions of performance indexes of MR dampers analytically. Thus, SQP and GA optimization methods can be conducted effectively to find optimal values of geometric parameters for various objective functions.

Finally choosing one of the optimal designs, a PID controller has been designed to evaluate the performance of the optimally designed MR damper. Displacement and

velocity responses of passive system as well as optimal and initial semi-active systems were presented.

6.2. Contributions and Conclusions

The main important contributions of the current study can be mentioned as

- Develop a comprehensive finite element model to calculate Magnetic Field Intensity and Magnetic Flux Density in MR valves.

- Design of experiments and finding analytical functions for Magnetic Field Intensity and Magnetic Flux Density in MR valves. Thus there is no need to run FEM code for large number of points in the defined design space and only by substituting design variables in the derived analytical functions; the magnetic parameters can be calculated.

- Conduct more advanced and reliable optimization methods to solve the optimal design problem in MR valve. The results of this projects shows that our design is more optimal than the optimal designs proposed by other research groups before.

- Determine the manufacturing tolerances of design parameters based on sensitivity analysis of the objective functions.

- Design PID controller for the proposed optimal design and discuss on the valve performance indexes

6.3. Future Works

Although optimal design of single coil annular duct MR valve with application as shock absorber has been accomplished successfully in this thesis, other important interesting subjects for future works are identified as

110

- Optimal design of other kinds of MR valves

- Analysis of the performance evaluation of the proposed MR damper in a full model car with seven degrees of freedom

- Implementing different controllers and compare their performance

- Extending the optimization to both material selection and geometry optimization of the MR valve.

References

1. N.M.Wereley and L.Pang, "Nondimensional analysis of semi-active electrorheological and magnetorheological dampers using approximate parallel plate models," *Smart Materials and Structures*, 1998. 7: p. 732–743.

2. D.Y.Lee and N.M.Wereley, "Quasi-steady Herschel-Bulkley analysis of electro and magneto-rheological flow mode dampers," *Journal of intelligent material systems and structures*, 1999. 10(10): p. 761-769.

3. A.Dominguez, R.Sedaghati, and I.Stiharu, "A new dynamic hysteresis model for magnetorheological dampers," *Smart Materials and Structures*, 2006. 15: p. 1179–1189.

4. S.Guo, S.Yang, and C.Pan, "Dynamic modeling of magnetorheological damper behaviors," *Journal of Intelligent Material Systems and Structures*, 2006. 17(1): p. 3-14.

5. B.F.Spencer, S.J.Dyke, M.K.Sain, and J.D.Carlson, "Phenomenological model for magnetorheological dampers," *Journal of engineering mechanics*, 1997. 123(3): p. 230-238.

6. Q.H.Nguyen and S.B.Choi, "Dynamic modeling of an electrorheological damper considering the unsteady behavior of electrorheological fluid flow," *Smart Materials and Structures*, 2009. 18: p. 055016-24.

7. D.Xiao-min, Y.U.Miao, L.Chang-rong, and C.Wei-min, "Adaptive Fuzzy Sliding Mode Control for Magneto-rheological Suspension System Considering Nonlinearity and Time Delay," *Journal of Vibration and Shock*, 2009: p. 1-12.

8. C.Y.Lai and W.H.Liao, "Vibration control of a suspension system via a magnetorheological fluid damper," *Journal of Vibration and Control*, 2002. 8(4): p. 527-547.

9. Y.Miao, D.Xiao-min, L.Chang-rong, and C.Wei-min, "Adaptive Fuzzy-Neural Network Control for Magneto-Rheological Suspension," *International Journal of Computer Science and Network Security*, 2006. 6(10): p. 66-71.

10. C.Park and D.Jeon, "Semiactive vibration control of a smart seat with an MR fluid damper considering its time delay," *Journal of Intelligent Material Systems and Structures*, 2002. 13(7-8): p. 521-524.

11. M.M.Rashid, N.A.Rahim, M.A.Hussain, F.Mohamed, and M.A.Rahman, "Development and Testing of Hybrid Fuzzy Logic Controller for Car Suspension System Using Magneto-Rheological Damper". 2008: *IEEE*.

12. C.Spelta, F.Previdi, S.M.Savaresi, G.Fraternale, and N.Gaudiano, "Control of magnetorheological dampers for vibration reduction in a washing machine," *Mechatronics*, 2009. 19(3): p. 410-421.

13. A.Turnip, K.S.Hong, and S.Park, "Control of a Semi-Active MR-Damper Suspension System: A New Polynomial Model, " in *Proceedings of the 17th World Congress, The International Federation of Automatic Control*. 2008: Seoul, Korea. p. 4683-4688.

14. J.Wang, C., Dong, Y.Shen, and J.Wei, "Robust modelling and control of vehicle active suspension with MR damper," *Vehicle System Dynamics*, 2008. 46: p. 509-520.

15. Q.H.Nguyen, Y.M.Han, S.B.Choi, and N.M. Wereley, "Geometry optimization of MR valves constrained in a specific volume using the finite element method," *Smart Materials and Structures*, 2007. 16: p. 2242–2252.

16. Q. H.Nguyen, S.B.Choi, Y.S.Lee, and M.S.Han, "An analytical method for optimal design of MR valve structures," *Smart Materials and Structures,* 2009. 18: p. 095032-44.

17. Q.H.Nguyen and S.B.Choi, "Optimal design of a vehicle magnetorheological damper considering the damping force and dynamic range," *Smart Materials and Structures*, 2009. 18: p. 015013-22.

18. Q.H.Nguyen and S.B.Choi, "Optimal design of MR shock absorber and application to vehicle suspension," *Smart Materials and Structures*, 2009. 18: p. 035012-22.

19. N.C.Rosenfeld and N.M.Wereley, "Volume-constrained optimization of magnetorheological and electrorheological valves and dampers," *Smart Materials and Structures*, 2004. 13: p. 1303–1313.

20.   Q.H.Nguyen,   S.B.Choi,   and   N.M.Wereley,   "Optimal   design   of magnetorheological valves via a finite element method considering control energy and a time constant," *Smart Materials and Structures*, 2008. 17: p. 025024-36.

21.   G.Z.Yao, F.F.Yap, G.Chen, W.H.Li, and S.H.Yeo, "MR damper and its application for semi-active control of vehicle suspension system," *Mechatronics,* 2002. 12(7): p. 963-973.

22.   F.Gordaninejad and S. P.Kelso," Fail-safe magneto-rheological fluid dampers for off-highway, high-payload vehicles," *Journal of Intelligent Material Systems and Structures*, 2000. 11(5): p. 395-406.

23.   M.R.Jolly,   J.W.Bender,   and   J.D.Carlson,   "Properties   and   applications   of commercial magnetorheological fluids," 1998, Thomas Lord Research Center, Lord Corporation. p. 262-275.

24.   G.Yang and B.F.Spencer, "Large-scale MR fluid dampers: modeling and dynamic performance considerations," *Engineering structures*, 2002. 24(3): p. 309-323.

25.   J.H.Koo, F.D.Goncalves, and M.Ahmadian, "A comprehensive analysis of the response time of MR dampers," *Smart Materials and Structures,* 2006. 15: p. 351–358.

26.   H.S.Lee and S.B.Choi, "Control and response characteristics of a magneto-rheological fluid damper for passenger vehicles," *Journal of Intelligent Material Systems and Structures*, 2000. 11(1): p. 80-87

27.   A.Grunwald and A.G.Olabi, "Design of magneto-rheological (MR) valve," *Sensors and Actuators A: Physical*, 2008. 148(1): p. 211-223.

28. J.C.Poynor, *Innovative designs for magneto-rheological dampers*. 2001, Virginia Polytechnic Institute and State University.

29. J.H.Yoo and N.M.Wereley, "Design of a high-efficiency magnetorheological valve," J*ournal of Intelligent Material Systems and Structures,* 2002. 13(10): p. 679-685.

30. A.G.Olabi and A.Grunwald, "Design and application of magneto-rheological fluid," *Materials & Design*, 2007. 28(10): p. 2658-2664.

31. G.Georgiou, G.Verros , and S.Natsiavas, "Multi-objective optimization of quarter-car models with a passive or semi-active suspension system," *Vehicle System Dynamics*, 2007. 45(1): p. 77-92.

32. A.M.Tusset, M.Rafikov, and J.M.Balthazar," An Intelligent Controller Design for Magnetorheological Damper Based on a Quarter-car Model," *Journal of Vibration and Control*, 2009. 15(12): p. 1-14.

33. K.Kim and D.Jeon, "Vibration suppression in an MR fluid damper suspension system," *Journal of Intelligent Material Systems and Structures*, 1999. 10(10): p. 779-786

34. M.M.Rashid, N.A.Rahim, M.A.Hussain, and M.A.Rahman, "Analysis and experimental study of magnetorheological-based damper for semiactive suspension system using fuzzy hybrids," I*EEE Transactions on Industry Applications,* 2011. 47(2): p. 1051-1059.

35. V. S.Atray and P. N.Roschke, "Neuro Fuzzy Control of Railcar Vibrations Using Semiactive Dampers," *Computer Aided Civil and Infrastructure Engineering*, 2004. 19(2): p. 81-92.

36. X.Dong, M.Yu, C.Liao, and W.Chen, "Comparative research on semi-active control strategies for magneto-rheological suspension," *Nonlinear dynamics*, 2010. 59(3): p. 433-453.

37. G.U.C.Rahmi, "Active control of seat vibrations of a vehicle model using various suspension alternatives," *Turkish J. Eng. Env. Sci*, 2003. 27: p. 361-373.

38. H.Gavin, J.Hoagg, and M.Dobossy. "Optimal design of MR dampers," in *Proc. U.S.-Japan Workshop on Smart Structures for Improved Seismic Performance in Urban Regions*. 2001.

39. N.Q.Guo, H.Du, and W.H.Li, "Finite element analysis and simulation evaluation of a magnetorheological valve," *The international journal of advanced manufacturing technology*, 2003. 21(6): p. 438-445.

40. L.Yang, F.Duan, and A.Eriksson, "Analysis of the optimal design strategy of a magnetorheological smart structure," *Smart Materials and Structures*, 2008. 17: p. 015047(8pp).

41. J.D.Carlson and M.R.Jolly, "MR fluid, foam and elastomer devices," *Mechatronics*, 2000. 10(4-5): p. 555-569.

42. J.D.Carlson, D.M.Catanzarite, and K.A.S.Clair, "Commercial magnetorheological fluid devices*," International Journal of Modern Physics B*, 1996. 10(23): p. 2857-2866.

43.   A.Chaudhuri, N.M.Wereley, R.Radhakrishnan, and S.B.Choi, "Rheological parameter estimation for a ferrous nanoparticle-based magnetorheological fluid using genetic algorithms," *Journal of intelligent material systems and structures*, 2006. 17(3): p. 261.

44.   W.Thomson, *Theory of vibration with applications*. 2004: Taylor & Francis.

45.   D.C.Montgomery, *Design and Analysis of Experiments*. 5 ed. 2008: John Wiley & Sons Inc.

46.   *ANSYS Help*

47.   K.Ibrahim, *Design optimization of vehicle structures for crashworthiness improvement*, in *Mechanical Engineering*. PhD Thesis, 2009 , CONCORDIA UNIVERSITY.

48.   W.J.Hill and W.G.Hunter, "A review of response surface methodology: a literature survey," *Technometrics*, 1966. 8(4): p. 571-590.

49.   Y.B.Gianchandani and S.B.Crary, "Parametric modeling of a microaccelerometer: comparing I-and D-optimal design of experiments for finite-element analysis," *Journal of Microelectromechanical Systems*, 1998. 7(2): p. 274-282.

50.   P.Tobias, *NIST/SEMATECH e-Handbook of Statistical Methods*.

51.   W.Adams, *Handbook for Experimenters, Version 7.3, Stat-Ease.* Inc., Minneapolis, MN, USA, 2006.

52.   W.D.Kappele, "Using I-Optimal Designs for Narrower Confidence Limits," *IASI conference*. 1998: Orlando, FL,USA.

53.   P.Sheth, S.Ensari, "Applying Modern Design of Experiments to Mass Transfer Characterization in Bioreactors," *BioProcessing Journal*, 2009. 8(3): p. 38-43.

54.   J.P.Sall, C.M.Fladung., "Trees, Neural Nets, PLS, I-Optimal Designs and other New JMP$^{®}$ Version 5 Novelties," *SUGI27* 2002: Orlando, Florida, USA.

55.   K. M.Carley, *Response surface methodology*. 2004, DTIC Document.

56.   J.Nocedal, S.J.Wright, *Numerical Optimization, Series in Operations Research and Financial Engineering,* 2006: Springer, New York.

57.   J.S.Arora, *Introduction to optimum design*. 2004: Academic Press.

58.   K.Ogata, *Modern control engineering*. 2001: Prentice Hall PTR.

59.   D.Karnopp, "Active damping in road vehicle suspension systems," *Vehicle System Dynamics*, 1983. 12(6): p. 291-311.